Current state of modeling the photochemistry of Titan's mutually dependent atmosphere and ionosphere

E. H. Wilson
NASA/Jet Propulsion Laboratory, Pasadena, California, USA

S. K. Atreya
Department of Atmospheric, Oceanic, and Space Sciences, University of Michigan at Ann Arbor, Ann Arbor, Michigan, USA

Received 16 September 2003; revised 28 November 2003; accepted 12 February 2004; published 4 June 2004.

[1] In the context of recent observations, microphysical models, and laboratory data, a photochemical model of Titan's atmosphere, including updated chemistry focusing on rate coefficients and cross sections measured under appropriate conditions, has been developed to increase understanding of these processes and improve upon previous Titan photochemical models. The model employs a two-stream discrete ordinates method to characterize the transfer of solar radiation, and the effects of electron-impact, cosmic-ray deposition, and aerosol opacities from fractal and Mie particles are analyzed. Sensitivity studies demonstrate that an eddy diffusion profile with a homopause level of 850 km and a methane stratospheric mole fraction of 2.2% provides the best fit of stratospheric and upper atmosphere observations and an improved fit over previous Titan photochemical models. Lack of fits for C_3H_8, HC_3N, and possibly C_2H_3CN can be resolved with adjustments in aerosol opacity. The model presents a benzene profile consistent with its detection in Titan's stratosphere [*Coustenis et al.*, 2003], which may play an important role in the formation of Titan hazes. An electron peak concentration of 4200 cm^{-3} is calculated, which exceeds observations by 20%, considerably lower than previous ionosphere models. With adjustments in aerosol opacities and surface fluxes the model illustrates that reasonable fits to existing observations are possible with a single eddy diffusion profile, contrary to the conclusions of previous Titan models. These results will aid in the receipt and interpretation of data from Cassini-Huygens, which will arrive at Titan in 2004 and deploy a probe into Titan's atmosphere in January 2005. *INDEX TERMS:* 5405 Planetology: Solid Surface Planets: Atmospheres—composition and chemistry; 6280 Planetology: Solar System Objects: Saturnian satellites; 5435 Planetology: Solid Surface Planets: Ionospheres (2459); 0335 Atmospheric Composition and Structure: Ion chemistry of the atmosphere (2419, 2427); 0305 Atmospheric Composition and Structure: Aerosols and particles (0345, 4801); *KEYWORDS:* Titan, photochemistry, composition, haze, ion chemistry, planetary atmospheres

Citation: Wilson, E. H., and S. K. Atreya (2004), Current state of modeling the photochemistry of Titan's mutually dependent atmosphere and ionosphere, *J. Geophys. Res.*, *109*, E06002, doi:10.1029/2003JE002181.

1. Introduction

[2] Titan, the only satellite in the Solar System with an extensive atmosphere, has been an object of considerable scrutiny for some time. Titan has a largely N_2 atmosphere (90–98%) [*Lindal et al.*, 1983; *Broadfoot et al.*, 1981] with methane (2–6%) [*Samuelson et al.*, 1997; *Hanel et al.*, 1981] being the most abundant minor constituent. Methane is dissociated through the transfer of UV solar radiation, photoelectrons, and magnetospheric electrons, which produce highly reactive radical species. These species along with the nitrogen atoms produced through N_2 dissociation react to form a bevy of hydrocarbons and nitriles that characterize Titan's atmosphere. The presence of CO along with the likely influx of micrometeorites into Titan's atmosphere contributes to the collection of oxygen-bearing species that exist in Titan's atmosphere, as well.

[3] A brief historical perspective of relevant observations and previous modeling studies is given first in order to place the present work in proper perspective. The presence of most of the species known to exist in Titan's atmosphere was revealed by the Voyager flybys, which unveiled an object covered with orange-brown hazes. Beneath the haze region the surface was found to have a temperature of 94 K at a pressure of 1.5 bars and a radius of 2575 km [*Lindal et al.*, 1983]. Through these radio occultation measurements, *Lindal et al.* [1983] were able to infer the temperature profile up to 200 km, which included a tropopause region near 42 km with a temperature of 71 K and a stratospheric

0148-0227/04/2003JE002181

Table 1. List of Neutral and Ionic Compounds Used in the Model

Neutrals		Ions
H	atomic hydrogen	H^+
H_2	molecular hydrogen	H_2^+
C	atomic carbon	H_3^+
CH	methylidyne	H_2O^+
$^1CH_2$	excited-state methylene	H_3O^+
$^3CH_2$	ground-state methylene	HCO^+
CH_3	methyl radical	CH_3^+
CH_4	methane	CH_4^+
C_2	molecular carbon	CH_5^+
C_2H	ethynyl radical	$C_2H_2^+$
C_2H_2	acetylene	$C_2H_3^+$
C_2H_3	vinyl radical	$C_2H_4^+$
C_2H_4	ethylene	$C_2H_5^+$
C_2H_5	ethyl radical	$C_2H_6^+$
C_2H_6	ethane	c-$C_3H_3^+$
C_3H_2	propadienylidene	$C_3H_5^+$
C_3H_3	propargyl radical	$C_4H_2^+$
CH_3C_2H	methylacetylene	$C_4H_3^+$
CH_2CCH_2	allene	$C_6H_7^+$
C_3H_5	allyl radical	N^+
C_3H_6	propylene	N_2^+
C_3H_7	isopropyl radical	NH^+
C_3H_8	propane	N_2H^+
C_4H		NH_2^+
C_4H_2	diacetylene	NH_3^+
C_4H_2*	excited-state diacetylene	NH_4^+
C_4H_3		CN^+
C_4H_4	vinylacetylene	HCN^+
C_4H_5	1-butyn-3-yl radical	H_2CN^+
C_4H_6	1,3-butadiene	$C_xH_y^+$
C_4H_8	1-butene	$C_xH_yN_z^+$
C_4H_{10}	n-butane	$C_xH_yO_z^+$
C_6H		N_x^+
C_6H_2	triacetylene	
C_6H_4	benzyne	
n-C_6H_4	linear-C_6H_4	
C_6H_5	phenyl radical	
n-C_6H_5	linear-C_6H_5	
C_6H_6	benzene	
n-C_6H_6	linear-C_6H_6	
C_6H_7	cyclized-C_6H_7	
n-C_6H_7	linear-C_6H_7	
C_8H_2	tetraacetylene	
N^{4s}	ground-state atomic nitrogen	
N^{2d}	excited-state atomic nitrogen	
N_2	molecular nitrogen	
NH	imidogen	
NH_2	amino radical	
NH_3	ammonia	
N_2H_2	diimide	
N_2H_3	hydrazinyl radical	
N_2H_4	hydrazine	
CN	cyano radical	
HCN	hydrogen cyanide	
H_2CN	methylene-amidogen radical	
CHCN		
CH_2CN	cyanomethyl radical	
CH_3CN	acetonitrile	
C_2N_2	cyanogen	
HC_2N_2		
C_3N	cyanoethynyl radical	
HC_3N	cyanoacetylene	
H_2C_3N	cyanovinyl radical	
C_2H_3CN	acrylonitrile	
C_4N_2	dicyanoacetylene	
O^{3p}	ground-state atomic oxygen	
O^{1d}	excited-state atomic oxygen	
OH	hydroxyl radical	
H_2O	water	
CO	carbon monoxide	
CO_2	carbon dioxide	
HCO	formyl radical	
H_2CO	formaldehyde	
CH_2OH	hydroxymethyl radical	
CH_3O	methoxy radical	
CH_3OH	methanol	
CH_2CO	ketene	
CH_3CO	acetyl radical	
CH_3CHO	ethylene oxide	
C_2H_4O	oxirane	

inversion layer, increasing temperatures to 170 K at 200 km. Further analysis of Voyager Infrared Spectrometer (IRIS) and Voyager Ultraviolet Spectrometer (UVS) data yielded much of what is known about the distribution of constituents in Titan's atmosphere listed as shown in Table 1. However, Voyager did not uncover much about the middle and upper atmosphere. An exospheric temperature of 186 K was obtained by *Smith et al.* [1982]. But, beyond some observations of CH_4 and C_2H_2 [*Smith et al.*, 1982], little is known about the vertical distribution of Titan's constituents throughout the atmosphere, largely due to the opacity provided by CH_4 and Titan's hazes. In fact, the hazes themselves remain largely a mystery. Voyager revealed an opaque haze region consisting of a main haze layer around 220 km and a detached haze layer at 300–350 km [*Rages and Pollack*, 1983]. However, the precise source of this region and its composition is left to speculation.

[4] In the upper atmosphere the absorption of solar EUV radiation produces an ionosphere that interacts with Saturn's magnetosphere and the solar wind. This interaction is not constant as variations in solar wind pressure cause a compression of the magnetosphere, resulting in Titan being outside of the magnetosphere part of the time. However, upon Voyager 1's arrival, Titan was inside Saturn's magnetosphere, and Voyager observed a Venus-like interaction between Titan and the magnetosphere with no bow shock [*Neubauer et al.*, 1984; *McNutt and Richardson*, 1988], allowing Titan to mainly interact with precipitating magnetospheric electrons along with photoelectrons produced within Titan's ionosphere. Early analysis revealed a variation in electron peak concentration with derived upper limits of 3000 cm^{-3} at the evening terminator and 5000 cm^{-3} at the morning terminator [*Lindal et al.*, 1983]. *Bird et al.* [1997] reanalyzed Voyager data to obtain an electron peak density of 2400 ± 1100 cm^{-3} at 1180 ± 150 km at the evening terminator at a solar zenith angle near 90°.

[5] The data presented by the Voyager flybys provided the impetus for the construction of photochemical models that have attempted to investigate how chemical species are distributed in Titan's atmosphere. The first extensive photochemical model after the Voyager flybys was developed by *Yung et al.* [1984], which made use of a large reaction set and early analyses of Voyager data [*Hanel et al.*, 1981; *Maguire et al.*, 1981; *Kunde et al.*, 1981; *Samuelson et al.*, 1983]. *Toublanc et al.* [1995] and *Lara et al.* [1996] took advantage of improved analysis of Voyager observations [*Coustenis et al.*, 1989, 1991] and subsequent ground-based millimeter observations [*Tanguy et al.*, 1990; *Hidayat et al.*, 1997] to infer different profiles of the eddy diffusion coefficient. *Toublanc et al.* [1995] included a Monte Carlo treatment of the transfer of solar radiation in the atmosphere, while *Lara et al.* [1996] included physically based water ablation profiles to account for the oxygen source from micrometeor-

ites. *Keller et al.* [1992] and *Fox and Yelle* [1997] used neutral photochemical models as a basis for the construction of ionosphere models. *Galand et al.* [1999] used the *Toublanc et al.* [1995] photochemical model to investigate diurnal effects on Titan's ionosphere, while *Banaszkiewicz et al.* [2000] combined the *Lara et al.* [1996] model with an investigation of charged particle chemistry to construct a coupled model of Titan's atmosphere and ionosphere.

[6] Despite these investigations many questions regarding Titan chemistry still remain unanswered. Photochemical models have been unable to simultaneously fit the vertical profiles of observed species. Furthermore, although many microphysical models have been developed [e.g., *Rannou et al.*, 1995], the chemical sources of Titan's haze layer are still quite unknown.

[7] The low temperatures which characterize outer planetary atmospheres, and Titan, in particular, have prompted many measurements of reaction rates and cross sections at low temperatures which were not included in previous Titan photochemical models. Microphysical modeling and analysis of Voyager photometric and polarimetric observations and albedo data have suggested the fractal nature of Titan haze whose scattering effects differ than those considered in previous one-dimensional Titan photochemical models (the two-dimensional model of *Lebonnois et al.* [2001] does consider fractal haze particles). With this in mind and in the context of preparation for the retrieval and interpretation of data from the upcoming Cassini-Huygens investigation of Titan, a one-dimensional steady state photochemical model has been constructed. This model computes the mole fraction for 80 neutrals and 33 ions, shown in Table 2, from the surface to 1600 km, while self-consistently calculating the total number density as a function of the mean molecular weight. The model incorporates a two-stream discrete ordinates scattering model, differing from the scattering treatment of previous Titan models, and includes dissociation via photoelectrons from 15–1000 eV, magnetospheric electrons, and cosmic rays, along with solar radiation from 50–3000 Å. A multicomponent treatment of molecular diffusion is included along with sensitivity studies of various eddy diffusion profiles. The sensitivity studies include the analysis of constituent profiles generated by 100 eddy diffusion profiles, increasing through the stratosphere in varying degrees, with homopause levels ranging from 600 km to 1150 km.

[8] This paper discusses the details of the photochemical model, including the equations and inputs used to calculate constituent densities in sections 2 and 3. A discussion of the important free parameter of eddy diffusion is provided, detailing the basis for the profiles used in the sensitivity studies regarding Titan's homopause level. The chemical mechanisms, which govern the distribution of hydrocarbon, oxygen, and nitrile neutrals as well as ions in Titan's atmosphere, are discussed in section 4. Sensitivity studies regarding eddy diffusion and aerosol opacity are examined in section 5, along with a discussion on constituent profiles. Finally, conclusions are detailed in section 6.

2. Model Description

[9] To examine the physical and chemical processes that shape the distribution of constituents with altitude in Titan's atmosphere, a one-dimensional photochemical model is developed. This photochemical model solves the steady state altitude-dependent continuity-diffusion equation in spherical coordinates

$$P_i - L_i = \frac{1}{r^2}\frac{\partial(r^2\Phi_i)}{\partial r} \tag{1}$$

where P_i is the chemical production rate of species i, L_i is the chemical loss rate, the radius $r = (R_0 + z)$, where R_0 is the radius of Titan and z is the altitude, and Φ_i is the vertical flux, which can be expressed as

$$\Phi_i(z) = -D_i\left[n\frac{\partial \xi_i}{\partial z} + \xi_i\frac{\partial n}{\partial z} + [1 + [1-\xi_i]\alpha_i]\frac{n\xi_i}{T}\frac{\partial T}{\partial z} + \frac{n\xi_i}{H_i}\right] - Kn\frac{\partial \xi_i}{\partial z} \tag{2}$$

where n is the total number density, ξ_i is the mole fraction, D_i is the molecular diffusion coefficient, K is the eddy diffusion coefficient, α_i is the thermal diffusion coefficient, T is the temperature, and H_i is the scale height

$$H_i = \frac{RT}{m_i g}, g = \frac{GM}{r^2} \tag{3}$$

with R as the gas constant, m_i as the molecular weight of species i, g as the gravity, G as the gravitational constant, and M representing Titan's mass. The total number density as a function of mean molecular weight can be determined from the equation of hydrostatic equilibrium,

$$\frac{dp}{dz} = -\rho g \tag{4}$$

where p is the pressure and ρ is the mass density = nm, where $m = \sum_i m_i\xi_i(z)$, the mean molecular weight at altitude z, and the gas law

$$p[f+1] = nkT, \tag{5}$$

where k is Boltzmann's constant and f is a factor marking the departure from gas ideality, as Titan's atmosphere exhibits non-ideal characteristics near its surface [*Lindal et al.*, 1983]. Atmospheric parameters that are inputs into the model are the surface pressure p_0 = 1496 mb [*Lindal et al.*, 1983] and the non-ideality profile and temperature profile (Figure 1a), modeled by *Yelle et al.* [1997] and used for all studies related to the Huygens probe.

[10] These equations are finite differenced (see Appendix A) and solved through the reduced Jacobian solver method [*Sandilands and McConnell*, 1997] where the species in Table 2 are divided into two families, representing the neutrals and the ions. The structure of the model is laid out in Figure 2. The primary input parameters - the solar flux and cross sections combined with the thermal profile - are used to calculate the next group of parameters located in the first box. The calculation of the radiation field then follows, producing photolysis rates for absorbing species. The continuity-diffusion equation is then inverted

Table 2. Observations of Constituents in Titan's Atmosphere

Species	Altitude, km	Instrument	Observation	References
CH_4[a]	1400	Voyager UVS	$20 \pm 2\%$	*Strobel et al.* [1992]
	1130		$8 \pm 3\%$	*Smith et al.* [1982]
	1000		$6 \pm 1\%$	*Smith et al.* [1982]
	>825		$1-2\%$	*Smith et al.* [1982]
	725		$0.1-0.3\%$	
C_2H_2[a,b]	300^{+80}_{-60}	Voyager IRIS	NP[b]:$4.7^{+3.5}_{-2.1} \times 10^{-6}$	*Coustenis et al.* [1991]
	180^{+50}_{-30}		NP[b]:$2.3^{+1.6}_{-1} \times 10^{-6}$	
	125^{+50}_{-40}		EQ[b]:$2.2^{+0.7}_{-0.9} \times 10^{-6}$	*Coustenis et al.* [1989]
C_2H_4[a]	180^{+50}_{-30}	Voyager IRIS	NP[b]:$3.0^{+2.8}_{-2.1} \times 10^{-6}$	*Coustenis et al.* [1991]
	125^{+55}_{-35}		EQ[b]:$9.0^{+3}_{-5} \times 10^{-8}$	*Coustenis et al.* [1989]
C_2H_6[a]	300^{+80}_{-60}	Voyager IRIS	NP[b]:$1.5^{+2.6}_{-0.9} \times 10^{-5}$	*Coustenis et al.* [1991]
	180^{+50}_{-30}		NP[b]:$1.0^{+1.4}_{-0.6} \times 10^{-5}$	
	125^{+50}_{-40}		EQ[b]:$1.3^{+0.5}_{-0.7} \times 10^{-5}$	*Coustenis et al.* [1989]
CH_3C_2H	105–300	IRHS-IRTF	$8.8 \pm 2.2 \times 10^{-6}$	*Livengood et al.* [2002]
	300^{+80}_{-60}	Voyager IRIS	NP[b]:$6.2^{+4}_{-2.5} \times 10^{-8}$	*Coustenis et al.* [1991]
	180^{+50}_{-30}		NP[b]:$2.0^{+1.1}_{-0.8} \times 10^{-8}$	
	105^{+55}_{-30}		EQ[b]:$4.4^{+1.7}_{-2.1} \times 10^{-9}$	*Coustenis et al.* [1989]
C_3H_8	180^{+50}_{-30}	Voyager IRIS	NP[b]:$5.0^{+4}_{-3.5} \times 10^{-7}$	*Coustenis et al.* [1991]
	105^{+55}_{-30}		EQ[b]:$7.0^{+4}_{-4} \times 10^{-7}$	*Coustenis et al.* [1989]
	90–250	TEXES-IRTF	$6.2 \pm 1.2 \times 10^{-7}$	*Roe et al.* [2003]
C_4H_2[a]	300^{+80}_{-60}	Voyager IRIS	NP[b]:$4.2^{+3.3}_{-2.1} \times 10^{-8}$	*Coustenis et al.* [1991]
	180^{+50}_{-30}		NP[b]:$2.7^{+2}_{-1.2} \times 10^{-8}$	
	105^{+55}_{-30}		EQ[b]:$1.4^{+0.6}_{-0.7} \times 10^{-9}$	*Coustenis et al.* [1989]
H_2O	400	ISO	$8.0^{+6}_{-4} \times 10^{-9}$[c]	*Coustenis et al.* [1998]
	>40		4.0×10^{-10}	
CO	350	IRAM – Pico Veleta, Spain	$4.8^{+3.8}_{-1.5} \times 10^{-6}$	*Hidayat et al.* [1998]
	175		$2.4^{+0.5}_{-0.5} \times 10^{-5}$	
	60		$2.9^{+0.9}_{-0.5} \times 10^{-5}$	
	200–300	Owens Valley millimeter array	$5.2 \pm 1.2 \times 10^{-5}$	*Gurwell and Muhleman* [2000]
	40–200		$5.2 \pm 0.6 \times 10^{-5}$	
CO_2	180^{+50}_{-30}	Voyager IRIS	NP[b]: $\leq 7.0 \times 10^{-9}$	*Coustenis et al.* [1991]
	~180		EQ[b,c]:1.4×10^{-8}	*Coustenis et al.* [1989]
	105^{+55}_{-30}		EQ[b]:$1.4^{+0.3}_{-0.5} \times 10^{-8}$	
	300^{+80}_{-60}	Voyager IRIS	NP[b]:$2.3^{+1.8}_{-1.4} \times 10^{-7}$	*Coustenis et al.* [1991]
	180^{+50}_{-30}		NP[b]:$4.0^{+2.8}_{-2.2} \times 10^{-7}$	
	125^{+55}_{-40}		EQ[b]:$1.6^{+0.4}_{-0.6} \times 10^{-7}$	*Coustenis et al.* [1989]
HCN[a]	350	IRAM – Pico Veleta, Spain	$3.7^{+1.8}_{-1.2} \times 10^{-7}$	*Hidayat et al.* [1997]
	300		$5.2^{+6.6}_{-3.9} \times 10^{-6}$	*Tanguy et al.* [1990]
	200		$3.5^{+1.2}_{-1.1} \times 10^{-7}/6.2^{+1.9}_{-2.1} \times 10^{-7}$	*Hidayat et al.* [1997]/*Tanguy et al.* [1990]
	170		$2.0^{+0.3}_{-0.4} \times 10^{-7}/3.3^{+0.9}_{-0.8} \times 10^{-7}$	
	110		$5.0^{+1.1}_{-0.9} \times 10^{-8}$	*Hidayat et al.* [1997]
	100		$7.5^{+8.0}_{-3.0} \times 10^{-8}$	*Tanguy et al.* [1990]
CH_3CN	320	IRAM – Pico Veleta, Spain	1.0×10^{-8}[c]	*Bézard et al.* [1993]
	250		3.5×10^{-9}[c]	
	180		1.5×10^{-9}[c]	
HC_3N[a]	300^{+80}_{-60}	Voyager IRIS	NP[b]: $2.5^{+1.1}_{-1} \times 10^{-7}$	*Coustenis et al.* [1991]
	180^{+50}_{-30}		NP[b]:$8.4^{+3}_{-3.5} \times 10^{-8}$	
	105^{+55}_{-30}		EQ[b]: $\leq 1.5 \times 10^{-9}$	*Coustenis et al.* [1989]
C_2N_2[a]	300^{+80}_{-60}	Voyager IRIS	NP: $1.6^{+2.6}_{-1} \times 10^{-8}$	*Coustenis et al.* [1991]
	180^{+50}_{-30}		NP: $5.5^{+5}_{-2.2} \times 10^{-9}$	
	105^{+55}_{-30}		EQ[b]: $\leq 1.5 \times 10^{-9}$	*Coustenis et al.* [1989]

[a] *Vervack* [1997] and *Vervack et al.* [2003] conducted Voyager UVS reanalysis of upper atmosphere observations for these constituents. See text.
[b] Voyager IRIS observations taken at NP: north polar region, EQ: equatorial region.
[c] Value obtained by linear fitting of a model-calculated density profile.

for a given chemical family before proceeding back to the recalculation of box 1 parameters with the new abundance values. This cycle continues until a solution is reached, defined by the convergence level

$$(\Delta\xi, \Delta n)_{conv} = \begin{cases} \dfrac{\Delta\xi}{\xi} < 10^{-4} \\ \dfrac{\Delta n}{n} < 10^{-4} \end{cases}.$$

The resultant nominal total number density profile is shown in Figure 1b.

3. Model Parameters

3.1. Radiation Field

3.1.1. Solar Flux Input

[11] During the Voyager 1 flyby of Titan in November 1980, the solar flux output was near the maximum of its 11-year cycle, amplifying the effect of solar radiation on the

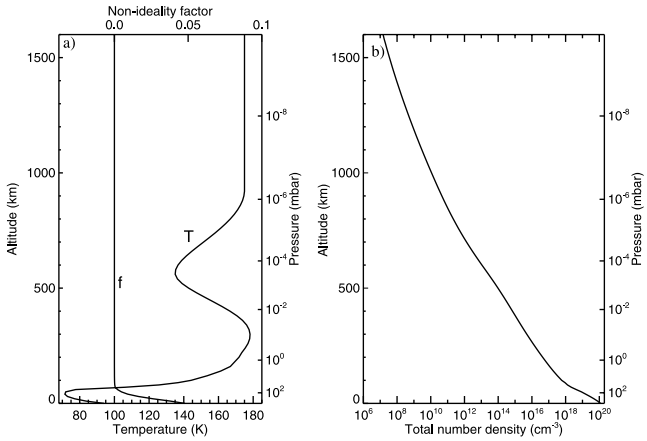

Figure 1. a) Temperature profile and non-ideality factor from *Yelle et al.* [1997]. b) Calculated total number density in Titan's atmosphere.

atmosphere. However, most of the stable constituents in Titan's atmosphere have lifetimes longer than one solar cycle in the stratosphere and are thus less sensitive to the changes in solar flux over the course of that cycle in that region. Thus the solar flux for moderate solar conditions obtained by The Solar-Stellar Irradiance Comparison Experiment (SOLSTICE) [*Woods et al.*, 1996] on the Upper Atmosphere Research Satellite (UARS) from 1150–3000 Å and an EUV flux, calculated using the EUVAC model [*Richards et al.*, 1994] for solar conditions associated with a 10.7 cm radio solar flux of 130 ($\times$ 10^{-22} W m^{-2} Hz^{-1}), is used to calculate neutral densities in the nominal model. However, in the upper atmosphere above $\sim$0.01 μbar, lifetimes for most constituents are considerably shorter. Sensitivity to solar flux for many of these constituents is discussed in section 5.2, in which simulations are run for solar minimum, solar maximum, and moderate solar conditions. Due to the short ion chemical lifetimes, profiles for charged particles in the solar maximum case are considered for the nominal model. In the solar maximum case, an EUV flux for F10.7 = 233 and the 81-day average 10.7 cm radio solar flux (F10.7A) equal to 211.9, which matches the solar conditions during the Voyager flyby, is used to calculate the distribution of species. The incident solar flux is calculated with a zenith angle of 58°, corresponding to the zenith angle representing a globally averaged incident flux in November 1980.

[12] The scattering contribution to the solar flux is calculated through a two-stream discrete ordinates algorithm detailed by *Edgington et al.* [1998]. The contributions of solar radiation, direct and scattered flux, for three characteristic wavelengths are shown in Figure 3. In the EUV region, scattering does not play a major role, shown in the 800 Å example, as nitrogen absorption prevents the penetration of photons to deeper regions where scattering would have a larger effect. In the 1700 Å example, radiation penetrates further into the atmosphere, allowing some backscattering to take place. In the denser regions, the effect

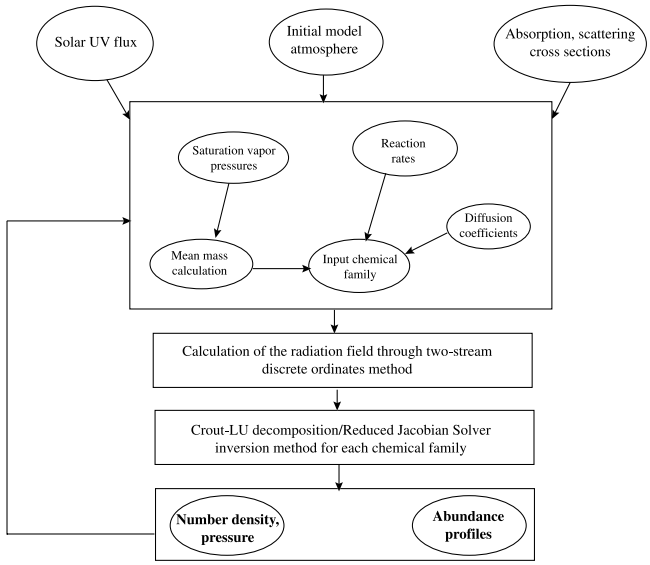

Figure 2. Layout of the structure of the model.

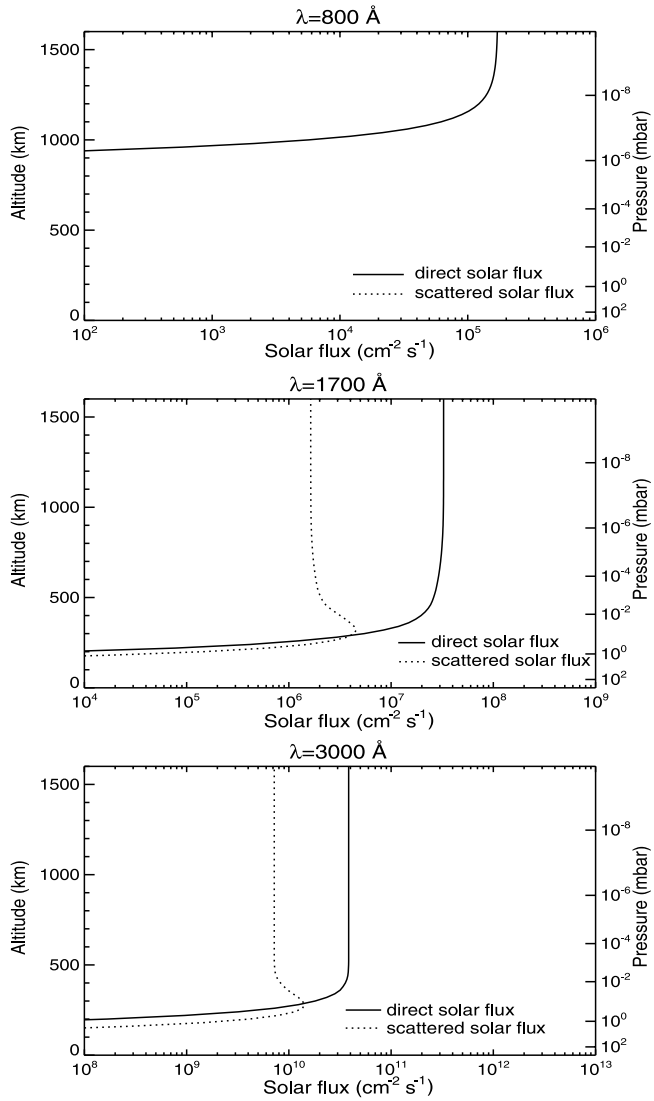

Figure 3. The direct solar flux and diffuse contribution as a function of altitude for 800 Å, 1700 Å, and 3000 Å intensities.

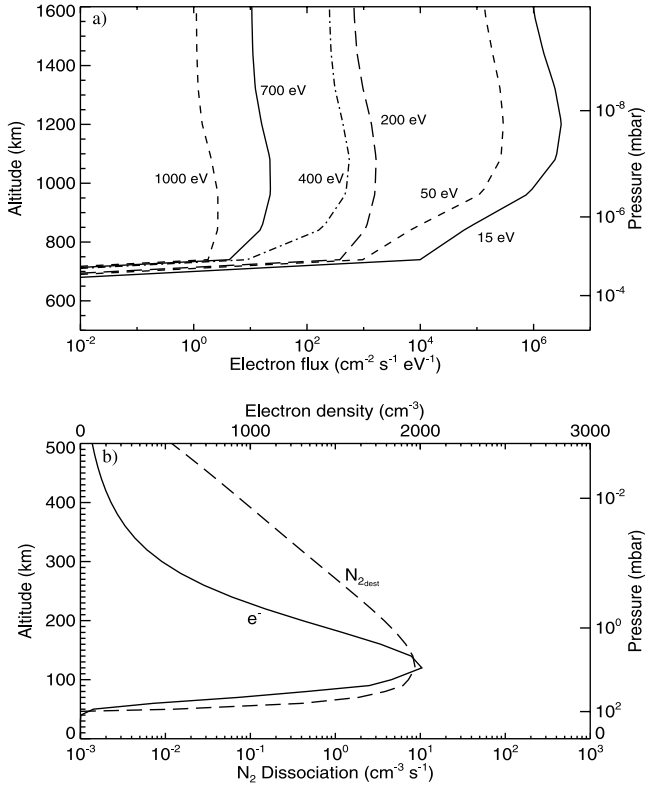

Figure 4. a) Radial electron fluxes from T. Cravens (personal communication, 1998) for various electron energies. b) Electron density profile in Titan's stratosphere (solid line) and molecular nitrogen dissociation as a result of cosmic ray deposition (long dashed line).

of scattering increases. At 3000 Å, the high single scattering albedo results in similar levels of direct and diffuse radiation throughout the atmosphere, with scattering dominating the solar input below 300 km.

3.1.2. Electron Input

[13] The solar flux while ionizing molecules also creates photoelectrons in the process. These photoelectrons play a significant role in the radiation field by providing an additional source of energy through which chemistry is induced. In their study of Titan's ionosphere, *Gan et al.* [1992] calculated photoelectron fluxes through Titan's atmosphere as a function of electron energy. On the basis of this study, the radial fluxes of photoelectrons from 15–100 eV, for a solar zenith angle of 60 degrees is adopted for altitudes from 725–1600 km (T. Cravens, personal communication, 1998). The radial fluxes for some of these electrons are shown in Figure 4a. Considering the input from Saturn's magnetosphere, *Keller et al.* [1992] calculated the ion production rates of N_2^+, N^+, and CH_4^+, the ions that begin Titan ion chemistry, due to magnetospheric electron impact. These rates are also considered in the model.

3.1.3. Cosmic Rays

[14] The deposition of cosmic rays in Titan's stratosphere can be an important source of nitrile formation through cosmic ray-induced N_2 dissociation. Cosmic ray input in Titan's atmosphere is treated using the model of local energy deposition described by *Atreya et al.* [1995], assuming zero magnetic rigidity for Titan, under moderate solar conditions. The cascading penetration of energy deposition analyzed by *Capone et al.* [1983] is neglected, amounting to a possible underprediction of N_2 dissociation of a factor $\sim$2, according to *Lellouch et al.* [1994]. The total ionization rate calculated is assumed to equal the N_2 ionization rate and is scaled for the dissociation and ionization rate of N_2 and other species by a factor relating the peak absorption cross section via electron impact of that species with the N_2 absorption cross section at that wavelength. Thus, for $X + e^- \rightarrow j^{(+)}$, where j is a neutral or ion,

$$P_j^X = \frac{\sigma_X\left(E_j^{peak}\right)q_j}{\sigma_{N_2}\left(E_j^{peak}\right)q_{ion}^{N_2}} Q_{N_2}\xi_X = J_j n \xi_X \tag{6}$$

where, P_j^X is the production rate of species j from destruction of X, σ_j is the electron impact absorption cross section of species j, E_j^{peak} is the electron energy of peak absorption for species j, q_j is the quantum yield of species j from destruction of X, $q_{ion}^{N_2}$ is the total ionization quantum yield of N_2 for electron impact, Q_{N_2} is the calculated total ionization rate of N_2 from cosmic ray impact, and J_j is the coefficient of production from destruction of X.

3.2. Photochemistry

[15] The chemical production term in the continuity equation (1) is given by

$$P_i = \sum_j \sum_k k_{jk} n^2 \xi_j \xi_k + \sum_l J_l^i n \xi_l \tag{7}$$

where k_{jk} is the rate coefficient of the reaction in which species j and species k react to form species i, while

$$J_l^i(z) = \int_\lambda \sigma_l^{abs} I(z,\lambda) q_i(\lambda) d\lambda \tag{8}$$

where $q_i(\lambda)$ is the quantum yield, representing the probability that the photolysis of l will produce i. The expression $k_{jk}n^2\xi_j\xi_k$ represents the production rate of i resulting from the two-body reaction of j and k, and $J_l n \xi_l$ is the production rate of i resulting from the photolysis of l. The chemical term for species i, on the other hand, is dependent on the mixing ratio of i, as the loss rate of a species is affected by its abundance

$$L_i = \sum_j k_{ij} n^2 \xi_i \xi_j + J_i n \xi_i. \tag{9}$$

k_{ij} is the rate coefficient of the reaction of reactant i with some reactant j, with $k_{ij}n^2\xi_i\xi_j$ expressing the reaction rate of i and j. The photolysis rate of i is $J_i n \xi_i$.

[16] For three-body pressure dependent reactions, where the two reactants react with the background atmosphere, k_{jk} is often given in terms of a low-pressure rate k_0 and a high-pressure rate k_∞ where

$$k_{jk} = \frac{k_0 k_\infty n}{(k_0 n + k_\infty)}. \tag{10}$$

Meanwhile, the production rate due to the deexcitation of an excited constituent is $k_j n \xi_j$, where k_j is the deexcitation rate of constituent j.

[17] The set of reactions used in the model is displayed in Table 3. The reaction rates chosen are the rates calculated or measured under the conditions most representative of Titan's atmosphere. The most important of these conditions is temperature. The rate of a reaction can vary by many orders of magnitude over the span of 100 K in temperature, which can have a large effect on the overall chemistry of the atmosphere. The bulk of chemistry in Titan's atmosphere occurs in the region where atmospheric temperatures range between about 130 K and 180 K. So, rate coefficient measurements that are applicable at or near these temperatures are favored over rate measurements that are applicable at room temperature, for example. The pressure at which the rate was measured and the bath gas used is also taken into consideration.

[18] The absorption cross sections and quantum yields which are used in (7) to calculate photolysis rates are referenced in Table 4. Many of these cross sections can also vary significantly with temperature, and thus low temperature cross sections, where available, are used. For Rayleigh scattering, the cross section is

$$\sigma_i^{Ray} = \frac{32\pi^3 \alpha_i^2 \left[\frac{6+3\delta_i}{6-7\delta_i}\right]}{3\lambda^4}, \tag{11}$$

where $\alpha_{CH_4} = 25.6 \times 10^{-25}$, $\delta_{CH_4} = 0$, $\alpha_{N_2} = 3.96 \times 10^{-25}$, and $\delta_{N_2} = 0.03$ [*Allen*, 1976].

[19] Microphysical models matched with geometric albedo observations [e.g., *McGrath et al.*, 1998] have suggested that Titan aerosols in the main haze layer are likely fractal in nature. Aerosol opacities for fractal particles were taken from *Lebonnois et al.* [2001], assuming aerosol single scattering albedos calculated from scattering and extinction efficiency factors from *Rannou et al.* [1995]. Haze opacity profiles for Mie particles from *Rannou et al.* [1995] were also tested.

[20] Charged particles are assumed to be governed solely through chemical processes with the assumption of charge neutrality. The electron temperature is taken from *Keller et al.* [1992] model A.

3.3. Condensation

[21] Due to the very low temperatures reached in Titan's tropopause and lower stratosphere, many gases become saturated and proceed to condense according to their saturation vapor pressures. The saturation laws governing condensing species are taken from *Allen and Nelson* [1998] for CH_4 above 90 K, C_2H_2, and C_2H_4, *Moses et al.* [1992] for other hydrocarbons, *Washburn* [1924] for H_2O, and *Sagan and Thompson* [1984] for HC_3N. Vapor pressures for other compounds are determined by fitting the lowest two points in the vapor pressure table from *Weast et al.* [1987] for the expression $\ln p(z) = A + \frac{B}{T(z)}$. This process is taken into account in the chemical side of equation (1) where for condensing species,

$$P_i - L_i - \gamma_i = \frac{1}{r^2}\frac{\partial(r^2\Phi_i)}{\partial r} \tag{12}$$

where γ_i is the condensation factor of species i. The condensation factor is assumed to dominate in regions of condensation, forcing the constituent mixing ratio profile to follow the profile associated with its saturation vapor pressure. This is done by setting the condensation factor

$$\gamma_i = \left[An\left[\xi_i - \xi_i^{sat}\right]\right]^p \tag{13}$$

where ξ_i^{sat} equals the saturation mole fraction, $A \gg P_i$, L_i, and p is a constant ≈ 1 to smooth the transition between condensation and non-condensation regions.

[22] As evident in equation (4) the total number density is dependent on the mean mass of the atmosphere, which will be affected by the distribution of the most abundant constituents. Thus condensation must be taken into account in the mean mass calculation in a similar fashion as the mole fractions in equation (13), by forcing $m(z) = m^{sat}(z)$ in condensing regions, where

$$m^{sat}(z) = \sum_i m_i \min\left(\xi_i, \xi_i^{sat}\right). \tag{14}$$

3.4. Boundary Conditions

[23] The boundary conditions for the model are presented in Table 5. At the lower boundary, the mole fractions for H_2 and CO are set to their observed quantities in the stratosphere, while CH_4 assumes a mixing ratio profile consistent with the saturation model of *Samuelson et al.* [1997], with a surface mole fraction of 5.6% and a supersaturation of 1.37. ξ_{N_2} follows as $1 - \sum \xi_i$, $i \neq N_2$ throughout the model. The total number density is set to 1.2×10^{20} cm^{-3} at the lower boundary, associated with a pressure of 1496 mb, a temperature of 94 K, and a non-ideality factor of 0.0347. At the upper boundary, $\Phi_i = 0$ is assumed for most species, although $\Phi_{H_2O} = -5.0 \times 10^6$ molecules cm^{-2} s^{-1} is adopted for H_2O, accounting for the influx of water molecules arising from micrometeorites [*Feuchtgruber et al.*, 1997]. For H and H_2, the escape flux is dependent on the density of these constituents that are being solved. Thus the boundary condition accounting for escape of H, H_2 is expressed in terms of velocity

$$w_i(\tilde{r}_N) = -D_i\left[\frac{1}{\xi_i}\frac{\partial \xi_i}{\partial z} + \frac{1}{n}\frac{\partial n}{\partial z} + [1+\alpha_i]\frac{1}{T}\frac{\partial T}{\partial z} + \frac{1}{H_i}\right] - K\frac{1}{\xi_i}\frac{\partial \xi_i}{\partial z}. \tag{15}$$

The top of the model is assumed to be the exobase, where the effusion velocity from Jeans escape is given as

$$w_e = \sqrt{\frac{kT}{2\pi m}}[1+E_e]e^{-E_e} \tag{16}$$

where $E_e = \frac{r_e}{H_e}$. Thus $w_H = 2.72 \times 10^4$ cm s^{-1} and $w_{H_2} = 7000$ cm s^{-1}.

3.5. Vertical Transport

3.5.1. Molecular Diffusion

[24] Molecular diffusion coefficients are often provided as measurements of diffusivity in a medium consisting of two constituents. Atmospheres, however, are not binary

Table 3 (Representative Sample). Rate Coefficients Used in the Model (The full Table 3 is available in the HTML version of this article)

Rxn	Reactions	Rate Coefficients	References and Comments
1	$H + H + M \rightarrow H_2 + M$	$1.5 \times 10^{-29}\ T^{-1.3}$	*Tsang and Hampson* [1986]; bath gas N_2
2	$C + C_2H_2 \rightarrow$ products	2.6×10^{-10}	*Guadagnini et al.* [1998]
3	$CH + H_2 + M \rightarrow CH_3 + M$	$k_0 = 4.7 \times 10^{-26}\ T^{-1.6}$ $k_\infty = 2.5 \times 10^{-10}\ T^{-0.08}$	*Brownsword et al.* [1997]
	$CH + H_2 \rightarrow {}^3CH_2 + H$	$3.1 \times 10^{-10}\ e^{-1650/T}$	
4	$CH + H \rightarrow C + H_2$	1.4×10^{-11}	*Becker et al.* [1989]
5	$CH + CH_4 \rightarrow C_2H_4 + H$	$3.96 \times 10^{-8}\ T^{-1.04}\ e^{-36.1/T}$	*Canosa et al.* [1997]
6	$CH + C_2H_2 \rightarrow C_3H_2 + H$	$1.59 \times 10^{-9}\ T^{-0233}\ e^{-16/T}$	*Canosa et al.* [1997]
7	$CH + C_2H_4 \rightarrow CH_3C_2H + H$	$3.87 \times 10^{-9}\ T^{-0.546}\ e^{-29.6/T}$	*Canosa et al.* [1997]
	$CH + C_2H_4 \rightarrow CH_2CCH_2 + H$	$3.87 \times 10^{-9}\ T^{-0.546}\ e^{-29.6/T}$	
8	$CH + C_2H_6 \rightarrow C_2H_4 + CH_3$	$1.9 \times 10^{-8}\ T^{-0.859}\ e^{-53.2/T}$	*Canosa et al.* [1997]
	$CH + C_2H_6 \rightarrow C_3H_6 + H$	$1.9 \times 10^{-8}\ T^{-0.859}\ e^{-53.2/T}$	
9	$CH + C_4H_8 \rightarrow$ products	$8.78 \times 10^{-9}\ T^{-0.529}\ e^{-33.5/T}$	*Canosa et al.* [1997]
10	${}^3CH_2 + H + M \rightarrow CH_3 + M$	$k_0 = 3.1 \times 10^{-30}\ e^{457/T}$ $k_\infty = 1.5 \times 10^{-10}$	*Gladstone* [1983]
	${}^3CH_2 + H \rightarrow CH + H_2$	$4.7 \times 10^{-10}\ e^{-370/T}$	*Zabarnick et al.* [1986]
11	${}^3CH_2 + {}^3CH_2 \rightarrow C_2H_2 + H_2$	$2.0 \times 10^{-11}\ e^{-400/T}$	*Baulch et al.* [1992]
	${}^3CH_2 + {}^3CH_2 \rightarrow C_2H_2 + 2H$	$1.8 \times 10^{-11}\ e^{-400/T}$	
12	${}^3CH_2 + CH_3 \rightarrow C_2H_4 + H$	7.0×10^{-11}	*Tsang and Hampson* [1986]
13	${}^3CH_2 + C_2H_2 \rightarrow C_3H_3 + H$	$1.5 \times 10^{-11}\ e^{-3332/T}$	*Bohland et al.* [1986]
14	${}^3CH_2 + C_2H_3 \rightarrow CH_3 + C_2H_2$	3.0×10^{-11}	*Tsang and Hampson* [1986]
15	${}^3CH_2 + C_2H_5 \rightarrow CH_3 + C_2H_4$	3.0×10^{-11}	*Tsang and Hampson* [1986]
16	${}^1CH_2 + H_2 \rightarrow {}^3CH_2 + H_2$	1.26×10^{-11}	*Langford et al.* [1983]
	${}^1CH_2 + H_2 \rightarrow CH_3 + H$	9.24×10^{-11}	
17	${}^1CH_2 + CH_4 \rightarrow {}^3CH_2 + CH_4$	1.2×10^{-11}	*Bohland et al.* [1985]
	${}^1CH_2 + CH_4 \rightarrow CH_3 + CH_3$	6.0×10^{-11}	
18	${}^1CH_2 + C_2H_2 \rightarrow C_3H_3 + H$	3.6×10^{-10}	*Guadagnini et al.* [1998]
19	${}^1CH_2 + N_2 \rightarrow {}^3CH_2 + N_2$	$2.36 \times 10^{-14}T$	*Ashfold et al.* [1981]
20	$CH_3 + H + M \rightarrow CH_4 + M$	$k_0 = 4.0 \times 10^{-29}$ $k_\infty = 4.7 \times 10^{-10}$ $F_c = 0.902 - 1.03 \times 10^{-3}T$	*Brouard et al.* [1989]
21	$CH_3 + CH_3 + M \rightarrow C_2H_6 + M$	$k_0 = 8.76 \times 10^{-6}\ T^{-7.03}\ e^{-1390/T}$ $k_\infty = 1.5 \times 10^{-6}\ T^{-1.18}\ e^{-329/T}$ $F_c = 0.381\ e^{-T/37.2} - 0.619\ e^{-T/1180}$	*Slagle et al.* [1988]; Rate used is 10 × measured rate - see text
22	$CH_4 + C_2 \rightarrow C_2H + CH_3$	$5.05 \times 10^{-11}\ e^{-297/T}$	*Pitts et al.* [1982]
23	$CH_4 + C_2H \rightarrow C_2H_2 + CH_3$	$1.2 \times 10^{-11}\ e^{-491/T}$	*Opansky and Leone* [1996a]
24	$CH_4 + C_4H \rightarrow C_4H_2 + CH_3$	$1.2 \times 10^{-11}\ e^{-491/T}$	estimating that C_4H reaction rates are equal to their C_2H analogues; *Kiefer and von Drasek* [1990]
25	$CH_4 + C_6H \rightarrow C_6H_2 + CH_3$	$1.2 \times 10^{-11}\ e^{-491/T}$	estimating that C_6H reaction rates are equal to their C_2H analogues; *Kiefer and von Drasek* [1990]
26	$C_2 + H_2 \rightarrow C_2H + H$	$1.77 \times 10^{-12}\ e^{-1469/T}$	*Pitts et al.* [1982]
27	$C_2H + H + M \rightarrow C_2H_2 + M$	$k_0 = 1.26 \times 10^{-18}\ T^{-3.1}\ e^{-721/T}$ $k_\infty = 3.0 \times 10^{-10}$	*Tsang and Hampson* [1986]
28	$C_2H + H_2 \rightarrow C_2H_2 + H$	$9.2 \times 10^{-18}\ T^{2.17}\ e^{-478/T}$	*Opansky and Leone* [1996b]
29	$C_2H + C_2H_2 \rightarrow C_4H_2 + H$	$9.53 \times 10^{-11}\ e^{30.8/T}$	*Chastaing et al.* [1998]
30	$C_2H + C_2H_4 \rightarrow C_4H_4 + H$	$4.6 \times 10^{-11}\ e^{24.6/T}$	*Opansky and Leone* [1996b], *Chastaing et al.* [1998]
	$C_2H + C_2H_4 \rightarrow C_2H_2 + C_2H_3$	$4.6 \times 10^{-11}\ e^{24.6/T}$	
31	$C_2H + C_2H_6 \rightarrow C_2H_2 + C_2H_5$	$3.5 \times 10^{-11}\ e^{2.9/T}$	*Opansky and Leone* [1996b]
32	$C_2H + C_3H_6 \rightarrow$ products	$1.47 \times 10^{-10}\ e^{65.3/T}$	*Chastaing et al.* [1998]
33	$C_2H + C_3H_8 \rightarrow C_2H_2 + C_3H_7$	$7.8 \times 10^{-11}\ e^{3/T}$	*Hoobler et al.* [1997]
34	$C_2H + C_4H_2 \rightarrow C_6H_2 + H$	$9.53 \times 10^{-11}\ e^{30.8/T}$	*Chastaing et al.* [1998]; estimated from *Kiefer and von Drasek* [1990]
35	$C_2H + C_6H_2 \rightarrow C_8H_2 + H$	$9.53 \times 10^{-11}\ e^{30.8/T}$	*Chastaing et al.* [1998]; estimated from *Kiefer and von Drasek* [1990]
36	$C_2H + C_8H_2 \rightarrow$ *polymer*	$9.53 \times 10^{-11}\ e^{30.8/T}$	*Chastaing et al.* [1998]; estimated from *Kiefer and von Drasek* [1990]
37	$C_2H_2 + H + M \rightarrow C_2H_3 + M$	$k_0 = 3.3 \times 10^{-30}\ e^{-740/T}$ $k_\infty = 1.4 \times 10^{-11}\ e^{-1300/T}$	*Baulch et al.* [1992]
38	$C_2H_2 + C_4H \rightarrow C_6H_2 + H$	$9.53 \times 10^{-11}\ e^{30.8/T}$	*Chastaing et al.* [1998]; estimated from *Kiefer and von Drasek* [1990]
39	$C_2H_2 + C_6H \rightarrow C_8H_2 + H$	$9.53 \times 10^{-11}\ e^{30.8/T}$	*Chastaing et al.* [1998]; estimated from *Kiefer and von Drasek* [1990]
40	$C_2H_3 + H \rightarrow C_2H_2 + H_2$	7.6×10^{-11}	k_0 estimate; *Monks et al.* [1995]
	$C_2H_3 + H + M \rightarrow C_2H_4 + M$	$k_0 = 5.76 \times 10^{-24}\ T^{-1.3}$ $k_\infty = 8.0 \times 10^{-11}$	
41	$C_2H_3 + H_2 \rightarrow C_2H_4 + H$	$5.01 \times 10^{-20}\ T^{2.63}\ e^{-4298/T}$ $k_{min} = 1.0 \times 10^{-23}$	*Tsang and Hampson* [1986]
42	$C_2H_3 + CH_3 \rightarrow C_2H_2 + CH_4$	3.4×10^{-11}	*Fahr et al.* [1991]
	$C_2H_3 + CH_3 + M \rightarrow C_3H_6 + M$	$k_0 = 8.76 \times 10^{-6}\ T^{-7.03}\ e^{-1390/T}$ $k_\infty = 1.2 \times 10^{-10}$	k_0 estimated from $k_0(CH_3 + CH_3)$; *Fahr et al.* [1991]
43	$C_2H_3 + CH_4 \rightarrow CH_3 + C_2H_4$	$2.4 \times 10^{-24}\ T^{4.02}\ e^{-2754/T}$	*Tsang and Hampson* [1986]
44	$C_2H_3 + C_2H_2 \rightarrow C_4H_4 + H$	$3.32 \times 10^{-12}\ e^{-2516/T}$	*Fahr and Stein* [1988]
	$C_2H_3 + C_2H_2 + M \rightarrow C_4H_5 + M$	$k_0 = 3.3 \times 10^{-29}\ e^{-740/T}$ $k_\infty = 4.17 \times 10^{-19}\ T^{1.9}\ e^{-1058/T}$	k_0 estimated as 10 × $k_0(C_2H_3 + H)$; *Weissman and Benson* [1988]
45	$C_2H_3 + C_2H_3 \rightarrow C_2H_4 + C_2H_2$	2.4×10^{-11}	*Fahr et al.* [1991]

Table 4. Absorption Cross Sections and Quantum Yields Used in the Model

Pathways	Branching Ratios	Cross Sections	Quantum Yields
[J1] $H + h\nu \rightarrow H^+ + e^-$	1.0		*Palenius et al.* [1976]
[J2] $H_2 + h\nu \rightarrow$ a) $H_2^+ + e^-$	see Quantum Yields	*Chan et al.* [1992]; *Samson and Haddad* [1994]	*Ford et al.* [1975]
b) $H^+ + H + e^-$			
[J3] $CH_3 + h\nu \rightarrow {}^1CH_2 + H$	1.0 (2160 Å)		*Parkes et al.* [1973]
[J4] $CH_4 + h\nu \rightarrow$ a) $CH_3 + H$	q_{neu}[a] (<950 Å); 1.0 (>950 Å); 0.41 (Ly α)	*Au et al.* [1993]; *Mount et al.* [1977],	*Au et al.* [1993]; *Romani* [1996];
b) $^1CH_2 + H_2$	0.28 (Ly α)	*Mount and Moos* [1978] at 200 K	*Samson et al.* [1989]; see text
c) $^1CH_2 + 2H$	0.0		
d) $^3CH_2 + 2H$	0.21 (Ly α)		
e) $CH + H_2 + H$	0.10 (Ly α)		
f) $CH_4^+ + e^-$	see Quantum Yields; *Au et al.* [1993]		
g) $CH_3^+ + H + e^-$			
h) $H^+ + H + e^- + \ldots$			
[J5] $C_2H_2 + h\nu \rightarrow$ a) $C_2H + H$	0.3 × q_{neu}[a] (<1100 Å); 0.3 (1100–1660 Å); 0.06 (1660–1900 Å); 0.3 (1900–2400 Å)	*Wu and Judge* [1985]; *Cooper et al.* [1995];	50–1100 Å quantum yields are taken from electron
b) $C_2 + H_2$	0.1 × q_{neu}[a] (<1100 Å); 0.1 (1100–1660 Å); 0.1 (1660–1900 Å); 0.1 (1900–2400 Å)	*Wu et al.* [2001] at 150 K; *Seki and Okabe* [1993]	impact quantum yields *Zheng and Srivastava* [1996];
c) $C_2H_2^* \rightarrow C_2H_2$	0.6 × q_{neu}[a] (<1100 Å); 0.6 (1100–1660 Å);		*Okabe* [1981, 1983]; *Seki and Okabe* [1993]
d) $C_2H_2^+ + e^-$	0.84 (1660–1900 Å); 0.6 (1900–2400 Å)		
e) $C_2H + H^+ + e^-$	see Quantum Yields; *Zheng and Srivastava* [1996]		
[J6] $C_2H_3 + h\nu \rightarrow C_2H_2 + H$	1.0		*Fahr et al.* [1998]
[J7] $C_2H_4 + h\nu \rightarrow$			
a) $C_2H_2 + H_2$	0.58 × q_{neu}[a] (<1180 Å); 0.58 (1180–1750 Å); 0.73 (1750–2100 Å)	*Holland et al.* [1997]; *Zelikoff and Watanabe* [1953];	500–1200 Å quantum yields are taken from electron
b) $C_2H_2 + 2H$	0.42 × q_{neu}[a] (<1180 Å); 0.42 (1180–1750 Å); 0.27 (1750–2100 Å)	*Schmitt and Brehm* [1966];	impact quantum yields *Tian and*
c) $C_2H_4^+ + e^-$	see Quantum Yields; *Tian and Vidal* [1998a]	F. Raulin (personal communication, 1995)	*Vidal* [1998a];
d) $C_2H_3^+ + H + e^-$			*Holland et al* [1997]; *Chang et al.* [1998]
e) $C_2H_2^+ + e^- + ..$			
f) $H_2^+ + e^- + ..$			
[J8] $C_2H_5 + h\nu \rightarrow CH_3 + {}^1CH_2$	1.0		*Adachi et al.* [1979]
[J9] $C_2H_6 + h\nu \rightarrow$ a) $C_2H_4 + H_2$	0.56 × q_{neu}[a] (<1130 Å); 0.56 (1130–1700 Å); 0.12 (Ly α)	*Au et al.* [1993]; *Mount and Moos* [1978] at 200 K	60–1200 Å taken from electron impact quantum yields
b) $C_2H_4 + 2H$	0.14 × q_{neu}[a] (<1130 Å); 0.14 (1130–1700 Å); 0.30 (Ly α)		*Tian and Vidal* [1998b]; *Kameta et al.* [1996];
c) $C_2H_2 + 2H_2$	0.27 × q_{neu}[a] (<1130 Å); 0.27 (1130–1700 Å); 0.25 (Ly α)		*Mount et al.* [1977]
d) $CH_4 + {}^1CH_2$	0.02 × q_{neu}[a] (<1130 Å); 0.02 (1130–1700 Å); 0.25 (Ly α)		
e) $2CH_3$	0.01 × q_{neu}[a] (<1130 Å); 0.01 (1130–1700 Å); 0.08 (Ly α)		
f) $C_2H_6^+ + e^-$	see Quantum Yields; *Tian and Vidal* [1998b]		
g) $C_2H_5^+ + H + e^-$			
h) $C_2H_4^+ + e^- + \ldots$			
i) $C_2H_3^+ + e^- + \ldots$			
j) $C_2H_2^+ + e^- + \ldots$			
k) $H^+ + e^- + \ldots$			
l) $H_2^+ + e^- + \ldots$			
m) $H_3^+ + e^- + \ldots$			
n) $CH_3^+ + e^- + \ldots$			

Table 4. (continued)

Pathways	Branching Ratios	Cross Sections	Quantum Yields
[J10] $C_3H_3 + h\nu \rightarrow$ a) $C_3H_2 + H$	0.96	*Fahr et al.* [1997]	*Jackson et al.* [1991]
b) $C_3H + H_2$	0.04		
[J11] $CH_3C_2H + h\nu \rightarrow$ a) $C_3H_3 + H$	0.56 × q_{neu}[a] (<1200 Å); 0.56 (1200–2200 Å)	*Ho et al.* [1998]; *Chen et al.* [2000] at 200 K	*Sun et al.* [1999]; *Ho et al.* [1998]
b) $C_3H_2 + H_2$	0.44 × q_{neu}[a] (<1200 Å); 0.44 (1200–2200 Å)		
[J12] $CH_2CCH_2 + h\nu \rightarrow$ a) $C_3H_3 + H$	0.64	*Rabalais et al.* [1971]; *Chen et al.* [2000] at 200 K	*Rabalais et al.* [1971]
b) $C_3H_2 + H_2$	0.36		
[J13] $C_3H_5 + h\nu \rightarrow$ a) $C_2H_2 + CH_3$	0.79	*Jenkin et al.* [1993]	*Gierczak et al.* [1988]
b) $CH_3C_2H + H$	0.16		
c) $CH_2CCH_2 + H$	0.01		
[J14] $C_3H_6 + h\nu \rightarrow$ a) $C_3H_5 + H$	0.0 (1000–1350 Å); 0.0 (1350–1550 Å); 0.565 (1550–1750 Å); 0.41 (1750–1950 Å)	*Samson et al.* [1962]; *Fahr and Nayak* [1996] at 223 K	*Collin* [1988]
b) $CH_3C_2H + H_2$	0.11 (1000–1350 Å); 0.11 (1350–1550 Å); 0.01 (1550–1750 Å); 0.01 (1750–1950 Å)		
c) $CH_2CCH_2 + H_2$	0.17 (1000–1350 Å); 0.22 (1350–1550 Å); 0.01 (1550–1750 Å); 0.01 (1750–1950 Å)		
d) $C_2H_4 + {}^1CH_2$	0.06 (1000–1350 Å); 0.04 (1350–1550 Å); 0.02 (1550–1750 Å); 0.03 (1750–1950 Å)		
e) $C_2H_3 + CH_3$	0.21 (1000–1350 Å); 0.27 (1350–1550 Å); 0.335 (1550–1750 Å); 0.4 (1750–1950 Å)		
f) $C_2H_2 + CH_4$	0.05 (1000–1350 Å); 0.03 (1350–1550 Å); 0.05 (1550–1750 Å); 0.04 (1750–1950 Å)		
[J15]$C_3H_8 + h\nu \rightarrow$ a) $C_3H_6 + H_2$	0.19 (1000–1150 Å); 0.34 (1150–1350 Å); 0.66 (1350–1540 Å); 0.94 (1540–1630 Å)	*Koch and Skibowski* [1971]; *Okabe and Becker* [1963]	*Johnston et al.* [1978]
b) $C_2H_6 + {}^1CH_2$	0.09 (1000–1150 Å); 0.09 (1150–1350 Å); 0.04 (1350–1540 Å); 0.00 (1540–1630 Å)		
c) $C_2H_5^+ + CH_3$	0.40 (1000–1150 Å); 0.35 (1150–1350 Å); 0.19 (1350–1540 Å); 0.00 (1540–1630 Å)		
d) $C_2H_4 + CH_4$	0.32 (1000–1150 Å); 0.22 (1150–1350 Å); 0.11 (1350–1540 Å); 0.06 (1540–1630 Å)		
[J16] $C_4H_2 + h\nu \rightarrow$ a) $C_4H + H$	0.20 (1200–1640 Å); 0.00 (1640–2640 Å)	*Okabe* [1981]; *Fahr and Nayak* [1994] at 223 K; *Smith et al.* [1998] at 193 K.	*Glicker and Okabe* [1987]
b) $2C_2H$	0.03 (1200–1640 Å); 0.01 (1640–2640 Å)		
c) $C_2H_2 + C_2$	0.10 (1200–1640 Å); 0.06 (1640–2640 Å)		
d) $C_4H_2^*$	0.67 (1200–1640 Å); 0.93 (1640–2640 Å)		
[J17] $C_4H_4 + h\nu \rightarrow$ a) $C_4H_2 + H_2$	0.8	*Fahr and Nayak* [1996] at 233 K.	*Gladstone et al.* [1996]
b) $2C_2H_2$	0.2		
[J18] $C_4H_6 + h\nu \rightarrow$ a) $C_4H_4 + H_2$	0.05	*Samson et al.* [1962]	*Bergmann and Demtröder* [1968]
b) $2C_2H_3$	0.10		
c) $C_2H_4 + C_2H_2$	0.17		
d) $C_3H_3 + CH_3$	0.40		
e) $C_4H_5 + H$	0.28		

Table 4. (continued)

Pathways	Branching Ratios	Cross Sections	Quantum Yields
[J19] $C_4H_8 + h\nu \rightarrow$ a) $C_4H_6 + 2H$	0.23 (1050–1350 Å); 0.14 (1350–1600 Å); 0.06 (1600–1980 Å)	*Samson et al.* [1962]	*Niedzielski et al.* [1978, 1979]; *Collin and Wieckowski* [1978]
b) $C_3H_5 + CH_3$	0.12 (1050–1350 Å); 0.39 (1350–1600 Å); 0.66 (1600–1980 Å)		
c) $CH_3C_2H + CH_4$	0.03 (1050–1350 Å); 0.02 (1350–1600 Å); 0.00 (1600–1980 Å)		
d) $CH_2CCH_2 + CH_4$	0.14 (1050–1350 Å); 0.10 (1350–1600 Å); 0.00 (1600–1980 Å)		
e) $C_2H_5 + C_2H_3$	0.25 (1050–1350 Å); 0.14 (1350–1600 Å); 0.04 (1600–1980 Å)		
f) $2C_2H_4$	0.02 (1050–1350 Å); 0.04 (1350–1600 Å); 0.05 (1600–1980 Å)		
g) $C_2H_2 + 2CH_3$	0.02 (1050–1350 Å); 0.00 (1350–1600 Å); 0.04 (1600–1980 Å)		
h) $C_3H_6 + {}^1CH_2$	0.02 (1050–1350 Å); 0.02 (1350–1600 Å); 0.00 (1600–1980 Å)		
[J20] $C_4H_{10} + h\nu \rightarrow$ a) $C_4H_8 + H_2$	0.48 (1000–1350 Å); 0.31 (1350–1650 Å)	*Koch and Skibowski* [1971]; *Okabe and Becker* [1963]	*Obi et al.* [1971]
b) $C_2H_6 + C_2H_4$	0.15 (1000–1350 Å); 0.17 (1350–1650 Å)		
c) $C_3H_6 + CH_3 + H$	0.28 (1000–1350 Å); 0.41 (1350–1650 Å)		
d) $C_2H_5 + C_2H_4 + H$	0.09 (1000–1350 Å); 0.11 (1350–1650 Å)		
[J21] $C_6H_2 + h\nu \rightarrow$ a) $C_6H + H$	0.20 (1150–1640 Å); 0.00 (1640–3000 Å)	*Kloster-Jensen et al.* [1974]; *Bénilan et al.* [1995] at 233 K	*Wilson and Atreya* [2003]
b) $C_4H + C_2H$	0.13 (1150–1640 Å); 0.07 (1640–3000 Å)		
[J22] $C_8H_2 + h\nu \rightarrow$ a) $2C_4H$	0.20 (1150–1640 Å); 0.00 (1640–3000 Å)	Assumed same as $C_6H_2 + h\nu$	*Wilson and Atreya* [2003]
b) $C_6H + C_2H$	0.13 (1150–1640 Å); 0.07 (1640–3000 Å)		
[J23] $C_6H_6 + h\nu \rightarrow$ a) $C_6H_5 + H$	0.8 × q_{neu}[a] (<1300 Å); 0.8 (1300–2200 Å); 0.0 (2200–2700 Å)	*Rennie et al.* [1998]; *Pantos et al.* [1978]	*Yokoyama et al.* [1990]; *Rennie et al.* [1998]
b) $C_6H_4 + H_2$	0.16 × q_{neu}[a] (<1300 Å); 0.16 (1300–2200 Å); 0.96 (2200–2700 Å)		
c) $C_5H_3 + CH_3$	0.04 × q_{neu}[a] (<1300 Å); 0.04 (1300–2200 Å); 0.04 (2200–2700 Å)		
[J24] $N + h\nu \rightarrow N^+ + e^-$	1.0		*Fennelly and Torr* [1992]
[J25] $N_2 + h\nu \rightarrow$ a) $N^{4s} + N^{2d}$	see Quantum Yields	*Chan et al.* [1993]	*Shaw et al.* [1992]; *Zipf and McLaughlin* [1978]; *Gallagher et al.* [1988]
b) $N_2^+ + e^-$			
c) $N^+ + N^{4s} + e^-$			
[J26] $HCN + h\nu \rightarrow$ a) $CN + H$	q_{neu}[a] see Quantum Yields; *Kreile et al.* [1982]	180–620 Å assumed equal to C_2H_2; *Nuth and Glicker* [1982]; F. Raulin (personal communication, 1995)	*Kreile et al.* [1982]; *Nuth and Glicker* [1982]
b) $HCN + e^-$			
c) $CN^+ + H + e^-$			
d) $H^+ + e^- + \ldots$			
[J27] $HC_3N + h\nu \rightarrow$ a) $C_3N + H$	0.09	*Connors et al.* [1974]; *Clarke and Ferris* [1996]; *Andrieux et al.* [1995]; *Bénilan et al.* [1994]; *Bruston et al.* [1989]	*Clarke and Ferris* [1995]; *Halpern et al.* [1988]; see text
b) $CN + C_2H$	0.05		
c) HC_3N^*	0.24		
[J28] $CH_3CN + h\nu \rightarrow CN + CH_3$	1.0	*Nuth and Glicker* [1982]; *Suto and Lee* [1985]	
[J29] $C_2H_3CN + h\nu \rightarrow$ a) $CN + C_2H_3$	0.01	F. Raulin (personal communication, 1995), *Derecskei-Kovacs and North* [1999]	
b) $HCN + C_2H_2$	0.15	*Wilson and Atreya* [2003]	
c) $HC_3N + H_2$	0.59		
d) $H_2C_3N + H$	0.25		
[J30] $C_2N_2 + h\nu \rightarrow 2CN$	1.0	*Nuth and Glicker* [1982]; F. Raulin (personal communication, 1995)	
[J31] $C_4N_2 + h\nu \rightarrow C_3N + CN$	1.0	*Connors et al.* [1974]; *Bénilan et al.* [1996] at 233 K	

Table 4. (continued)

Pathways	Branching Ratios	Cross Sections	Quantum Yields
[J32] $CO + h\nu \rightarrow C + O^{3p}$	q_{neu}[a]	*Wight et al.* [1976]; *Gallagher et al.* [1988]	*Wight et al.* [1976]; *Okabe* [1978]
[J33] $CO_2 + h\nu \rightarrow$ a) $CO + O^{3p}$	1.0 (1000–1670 Å); 0.0 (1670–2150 Å)	*Nakata et al.* [1965]; *Ogawa* [1971]; *Lewis and Carver* [1983] at 200 K	*Okabe* [1978]
b) $CO + O^{1d}$	0.0 (1000–1670 Å); 1.0 (1670–2150 Å)		
[J34] $H_2O + h\nu \rightarrow$ a) $OH + H$	$0.78 \times q_{neu}$[a] (<990 Å); 0.78 (990–1450 Å); 1.0 (1450–1980 Å)	*Haddad and Samson* [1986]; *Watanabe and Jursa* [1964]; *Watanabe et al.* [1953]; *Thompson et al.* [1963]	*Haddad and Samson* [1986]; *Stief et al.* [1975]; *Mordaunt et al.* [1994]
b) $O^{1d} + H_2$			
c) $O^{3p} + H_2$	$0.11 \times q_{neu}$[a] (<990 Å); 0.11 (990–1450 Å); 0.0 (1450–1980 Å)		
d) $H_2O^+ + e^-$			
e) $H^+ + e^- + \ldots$	$0.11 \times q_{neu}$[a] (<990 Å); 0.11 (990–1450 Å); 0.0 (1450–1980 Å)		
	see Quantum Yields; *Haddad and Samson* [1986]		
[J35] $H_2CO + h\nu \rightarrow$ a) $CO + H_2$	0.5	*Gentieu and Mentall* [1970]; *Suto et al.* [1985]	*Glicker and Stief* [1971]; *Moortgat et al.* [1983]
b) $CO + 2H$	0.5		
[J36] $CH_2CO + h\nu \rightarrow CO + {}^1CH_2$	1.0	*Braun et al.* [1970]; *Rabalais et al.* [1971]	
[J37] $CH_3OH + h\nu \rightarrow$ a) $CH_3O + H$	0.83	*Harich et al.* [1999]	
b) $H_2CO + H_2$	0.17		
[E1] $H + e^- \rightarrow H^+ + 2\,e^-$	1.0	*Shah et al.* [1987]	
[E2] $H_2 + e^- \rightarrow$ a) $H_2 + 2\,e^-$	see Quantum Yields	*Backx et al.* [1976]	
b) $H^+ + H + 2\,e^-$			
c) $2H + e^-$			
[E3] $CH_4 + e^- \rightarrow$ a) $CH_4^+ + 2\,e^-$	see Quantum Yields	*Orient and Srivastava* [1987]	
b) $CH_3^+ + H + 2\,e^-$			
[E4] $C_2H_2 + e^- \rightarrow$ a) $C_2H_2^+ + 2\,e^-$	see Quantum Yields	*Zheng and Srivastava* [1996]	
b) $C_2H + H^+ + 2\,e^-$			
[E5] $C_2H_4 + e^- \rightarrow$ a) $C_2H_4^+ + 2\,e^-$	see Quantum Yields	*Tian and Vidal* [1998a]	
b) $C_2H_3^+ + H + 2\,e^-$			
c) $C_2H_2^+ + 2\,e^- + \ldots$			
d) $H^+ + 2\,e^- + \ldots$			
e) $H_2^+ + 2\,e^- + \ldots$			
f) $H_3^+ + 2\,e^- + \ldots$			
g) $CH_3^+ + 2\,e^- + \ldots$			
[E6] $C_2H_6 + e^- \rightarrow$ a) $C_2H_6^+ + 2\,e^-$	see Quantum Yields	*Tian and Vidal* [1998b]	
b) $C_2H_5^+ + H + 2\,e^-$			
c) $C_2H_4^+ + 2\,e^- + \ldots$			
d) $C_2H_3^+ + 2\,e^- + \ldots$			
e) $C_2H_2^+ + 2\,e^- + \ldots$			
f) $H^+ + 2\,e^- + \ldots$			
g) $H_2^+ + 2\,e^- + \ldots$			
h) $H_3^+ + 2\,e^- + \ldots$			
i) $CH_3^+ + 2\,e^- + \ldots$			
[E7] $N + e^- \rightarrow N^+ + 2\,e^-$	1.0	*Brook et al.* [1978]	
[E8] $N_2 + e^- \rightarrow$ a) $N^{4s} + N^{4s} + e^-$	see Quantum Yields	*Zipf et al.* [1980]; *Itikawa et al.* [1986]	
b) $N^{4s} + N^{2d} + e^-$			
c) $N^{2d} + N^{2d} + e^-$			
d) $N_2^+ + 2\,e^-$			
e) $N^+ + N^{4s} + 2\,e^-$			
[E9] $H_2O + e^- \rightarrow$ a) $H_2O^+ + 2\,e^-$	see Quantum Yields	*Rao et al.* [1995]	
b) $H^+ + 2\,e^- + \ldots$			

[a] q_{neu} is the neutral quantum yield.

Table 5. Boundary Conditions Used in the Model

Physical Quantity	Boundary Constraint
Lower Boundary Conditions	
Pressure	$p_0 = 1496$ mb
Methane mole fraction	$\xi_{CH_4} = 5.6\%$
Methane supersaturation	1.37
Molecular hydrogen mole fraction	$\xi_{H_2} = 1.1 \times 10^{-3}$
Carbon monoxide mole fraction	$\xi_{CO} = 5.0 \times 10^{-5}$
Upper Boundary Conditions	
Atomic hydrogen escape velocity	$H_{vel}^{esc} = 2.7 \times 10^4$ cm s^{-1}
Molecular hydrogen escape velocity	$H_2^{esc} = 7 \times 10^3$ cm s^{-1}
Water influx from micrometeorites	$\Phi_{H_2O}^{a} = 5 \times 10^6$ cm^{-2} s^{-1}

[a]Flux referred to the surface.

mixtures of gases, but rather are composed of many constituents. For an atmosphere dominated by one constituent, binary coefficients involving that major constituent and a minor constituent are sufficient for calculating the molecular diffusion coefficient of that given minor constituent. However, an atmosphere with a minor constituent that makes up a significant portion of the bulk gas requires a multicomponent treatment. *Wilke* [1950] provides a convenient approximation for the diffusion of gas in a multicomponent mixture of J gases

$$D_i = \frac{1 - \xi_i}{\sum_{j=1, j\neq i}^{J} \frac{\xi_j}{D_{ij}}} \tag{17}$$

where D_{ij} are the binary diffusion coefficients and ξ_i is the mole fraction for species i. This formulation, which is good to about 10% for multicomponent systems where the individual diffusion coefficients are not sensitive to composition changes [*Wilke*, 1950], is useful for Titan where methane increases, due to diffusive separation, in the heterosphere, exceeding 20% above 1400 km [*Strobel et al.*, 1992]. Unfortunately, the measurements of binary coefficients have been conducted for only a select group of molecules. The diffusion coefficient follows the form of

$$D = \frac{AT^s}{n} \tag{18}$$

where T = temperature and n = bulk gas density. The binary gas mixtures pertinent to Titan that have been measured or empirically calculated are shown in Table 6. In the absence of measurements, empirical correlations are often used, on the basis of the physical parameters of the given molecules.

[25] Thermal diffusion, which typically affects light gases, is given by the term in equation (2)

$$[1 - \xi_i]\alpha_i \frac{n\xi_i}{T} \frac{\partial T}{\partial z},$$

where α_i is the thermal diffusion coefficient. In the model, $\alpha_H = \alpha_{H_2} = -0.38$ is adopted [*Banks and Kockarts*, 1973], while for all other species $\alpha = 0$.

3.5.2. Eddy Diffusion

[26] Owing to the complexity involved in relating microscopic turbulent processes to macroscopic transport, the eddy diffusion coefficient acts as a free parameter that must be estimated to match constituent observations. This task is relatively trivial for a completely inert species (e.g., argon), as the point where the constituent profile changes from well-mixed to diffusively separated marks the homopause where the eddy diffusion coefficient is equal to the molecular diffusion coefficient of the constituent. Unfortunately, there is no known vertical profile of such a species for Titan. Methane, however, is largely inert and is distributed largely through diffusive processes, as shown in Figure 5a. Thus the methane distribution can be used as a proxy for the determination of the homopause level. In the lower atmosphere, chemistry plays a major role for many species. However, HCN is largely formed in the upper atmosphere and transported to lower altitudes. In much of the lower regions of the atmosphere the eddy diffusion time constant is much smaller than the HCN chemical time constant (Figure 5b), and the millimeter observations of *Tanguy et al.* [1990] and *Hidayat et al.* [1997] provide a vertical

Table 6. Binary Molecular Diffusion Coefficients Used in the Model

Binary Mixture	A, cm^{-1} K^{-s}	s	References
N_2-N_2	5.09×10^{16}	0.810	*Massman* [1998]
CH_4-N_2	7.34×10^{16}	0.750	*Banks and Kockarts* [1973]
H-N_2	4.87×10^{17}	0.698	*Banks and Kockarts* [1973]
H_2-N_2	1.88×10^{17}	0.820	*Mason and Marrero* [1970]
N-N_2	9.69×10^{16}	0.774	*Mason and Marrero* [1970]
O-N_2	9.69×10^{16}	0.774	*Banks and Kockarts* [1973]
CO-N_2	5.15×10^{16}	0.810	*Massman* [1998]
CO_2-N_2	4.08×10^{16}	0.810	*Massman* [1998]
H_2O-N_2	6.26×10^{16}	0.810	*Massman* [1998]
C_2H_6-N_2	7.64×10^{16}	0.730	*Wakeham and Slater* [1973]
C_3H_8-N_2	6.54×10^{16}	0.660	*Wakeham and Slater* [1973]
C_4H_{10}-N_2	7.34×10^{16}	0.610	*Wakeham and Slater* [1973]
CH_4-CH_4	5.73×10^{16}	0.500	estimated from Lennard-Jones correlation; *Reid et al.* [1987]
H_2-CH_4	2.30×10^{17}	0.765	*Mason and Marrero* [1970]

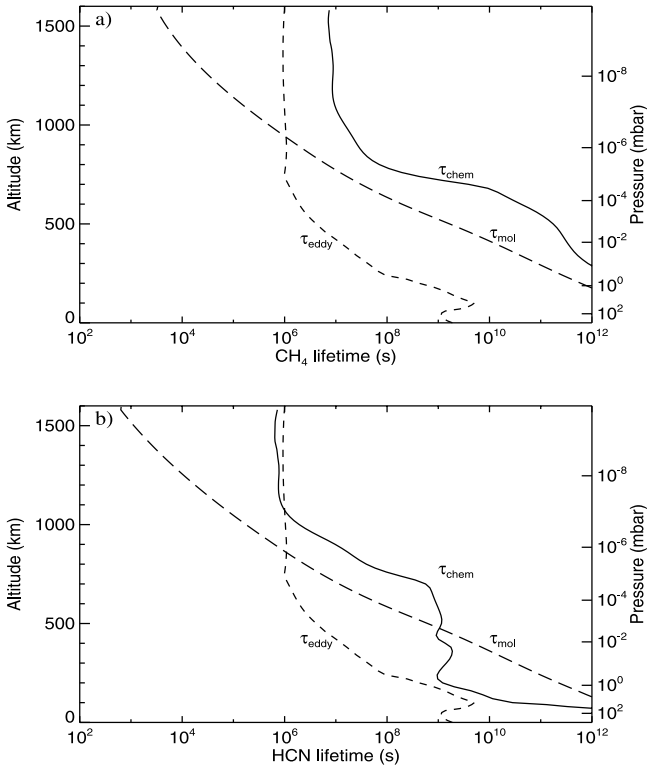

Figure 5. Local chemical, eddy, and molecular diffusive time constants for a) CH_4 and b) HCN.

profile for HCN in this region. These factors make HCN a good candidate for constraining the eddy diffusion profile in the lower atmosphere.

[27] Observations of CH_4 in the upper atmosphere were provided by *Smith et al.* [1982], who analyzed the Voyager ultraviolet spectrometer (UVS) observations and obtained mole fractions of 6 ± 1% at 1000 km and 8 ± 3% at 1130 km. However, the reanalysis of Voyager data by R. J. Vervack et al. (New perspectives on Titan's upper atmosphere from a reanalysis of the Voyager 1 UVS solar occultations, submitted to *Icarus*, 2003) (hereinafter referred to as Vervack et al., submitted manuscript, 2003) suggested a methane mixing ratio profile that might decrease with altitude, contrary to what would be expected from diffusive separation. Such a profile might be possible through a large chemical sink for CH_4, as suggested by *Lara et al.* [1999], but such a sink would most likely require much larger electron densities that what has been observed, as discussed in section 5.7. The authors argue that this profile may be the result of misassignment of CH_4 absorption to other species above 1050 km. With the large error bars and lack of coverage below the nanobar region, these results are unable to yield any firm conclusions about the homopause level, although the authors favor a high homopause level. *Strobel et al.* [1992], in their analysis of Voyager UVS solar occultation and airglow data, also infer a high homopause level around 1000 km. However, *Steiner and Bauer* [1990] in their study of diffusive processes on Titan, presented an analytical eddy profile corresponding to a homopause level of 660 km.

[28] The UVS reanalysis also points out a discrepancy with the *Smith et al.* [1982] C_2H_2 observations, retrieving up to three orders of magnitude less acetylene in the upper atmosphere than was suggested by the *Smith et al.* [1982] observations. This finding is supported by photochemical models, which have not determined a mechanism to form upper atmospheric C_2H_2 at such high densities as suggested by *Smith et al.* [1982].

[29] The millimeter observations of *Hidayat et al.* [1997] and *Tanguy et al.* [1990] are in decent agreement with each other over the lower 200 km of the atmosphere. However, above this level they diverge, with *Hidayat et al.* [1997] observing an approximately uniform HCN mixing ratio profile while *Tanguy et al.* [1990] observed a profile increasing with altitude. The recent *Marten et al.* [2002] observations corroborate the finding of *Tanguy et al.* [1990] that HCN increases in mole fraction throughout the stratosphere. To determine the nominal eddy diffusion profile, the fitting of the *Smith et al.* [1982] CH_4 observations in the upper atmosphere and the HCN observations of *Hidayat et al.* [1997] and *Tanguy et al.* [1990] are used as a guideline. Considering this set of observations, 100 monotonically increasing, randomly generated eddy diffusion coefficients are used to determine the best fits for the CH_4 and HCN observations. These profiles are generated by obtaining diffusion coefficients at 12 altitude levels, determined by calculating a randomly generated positive slope from the previous altitude level within a predetermined range. The eddy diffusion coefficient at the lower boundary is randomly chosen between 100–10000 $cm^2\ s^{-1}$. The results of the best-fit profiles are then compared to determine which profile fits the remaining observational constraints, with slight adjustments made to achieve a better fit. The resulting nominal profile (NOM) along with the *Steiner and Bauer* [1990] profile (SB) is shown in Figure 6a, corresponding to a homopause level of 850 km. This process was repeated, replacing the *Smith et al.* [1982] results with those from the Vervack et al. (submitted manuscript, 2003) nominal CH_4 profiles up to 1050 km, to determine the best-fit high homopause eddy profile (HI), which is also displayed in Figure 6b.

[30] The nominal profile allows for more mixing in the middle atmosphere than previous models, with a larger eddy coefficient from 250–700 km (Figure 6c). The homopause level of 850 km is higher than the *Yung et al.* [1984], *Toublanc et al.* [1995], and *Lara et al.* [1996] profiles, although considerably lower than the *Lara et al.* [2002] model, which counteracts the result of a smaller methane upper atmosphere mole fraction from the higher homopause level by assuming a larger methane surface density.

4. Chemical Mechanisms

4.1. Hydrocarbons

[31] The formation of hydrocarbons begins with the photodissociation of CH_4, which proceeds through the following channels:

(J4a) $$CH_4 + h\nu \rightarrow CH_3 + H$$

(J4b) $$\rightarrow {}^1CH_2 + H_2$$

(J4c) $$\rightarrow {}^1CH_2 + 2H$$

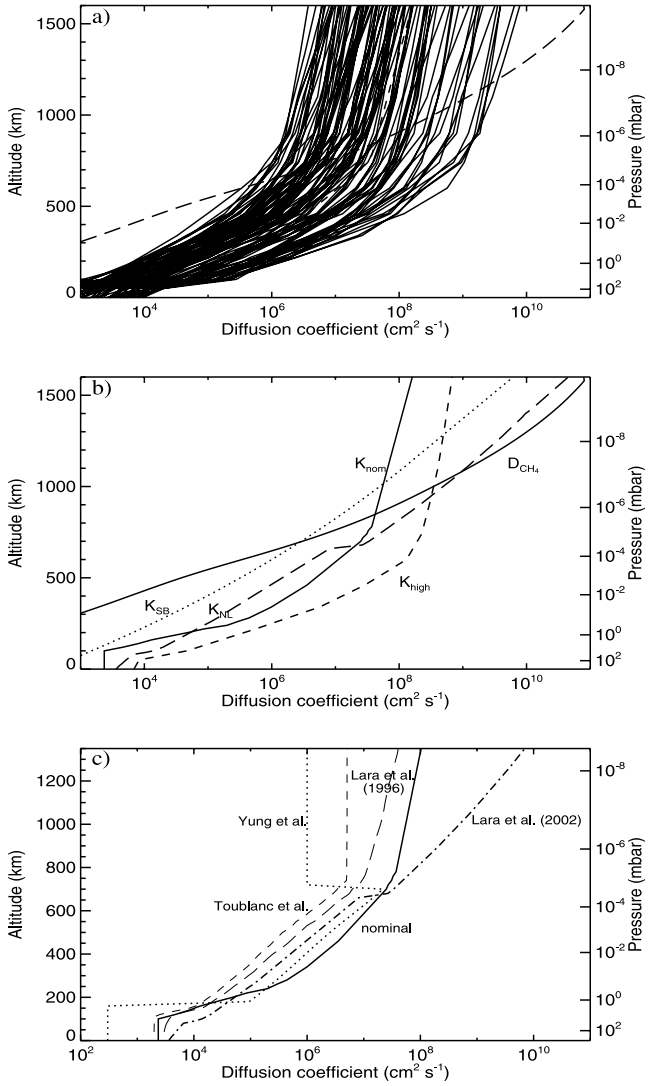

Figure 6. a) Randomly generated eddy diffusion profiles used to determine best fitting profile to constituent observations. b) Plots of tested eddy diffusion profiles - nominal profile (solid line), *Steiner and Bauer* [1990] profile (dotted line), the best-fit high homopause profile (short dashed line), and the *Lara et al.* [2002] profile (long dashed line). Also included in the methane molecular diffusion coefficient profile c) Eddy diffusion profiles from various photochemical models - nominal profile (solid line), *Yung et al.* [1984] profile (dotted line), *Toublanc et al.* [1995] profile (short dashed line), *Lara et al.* [1996] profile (long dashed line), and *Lara et al.* [2002] profile (dot dashed line).

(J4d) $$\rightarrow {}^3CH_2 + 2H$$

(J4e) $$\rightarrow CH + H_2 + H.$$

The branching ratios for this process, particularly at Lyman α, which accounts for 75% of methane photodissociation above 700 km, are still unsettled. *Toublanc et al.* [1995] used the *Mordaunt et al.* [1993] model 1 scheme, which places half of methane dissociation into (J4a) while splitting the other half between (J4b) and (J4d), and *Lara et al.* [1996] chose the *Mordaunt et al.* [1993] model 2 scheme, splitting methane dissociation into (J4a) and (J4e). The scheme adopted for this model is the *Romani* [1996] scheme where the quantum yields at Lyman α are as follows: q(J4a) = 0.41, q(J4b) = 0.28, q(J4c) = 0.0, q(J4d) = 0.21, q(J4e) = 0.10. At wavelengths other than Lyman α, methane is assumed to dissociate into the (J4a) channel. *Wilson and Atreya* [2000b] examined and compared these methane photolytic schemes along with that provided by *Smith and Raulin* [1999] and determined that there was little impact in the distribution of C_2-hydrocarbons, while there was considerable difference in the profiles of the C_3H_4 isomers and C_3H_6, mainly arising from the differences in CH yield among the schemes. The progression of hydrocarbon chemistry follows with reactions involving the radicals produced from methane dissociation.

[32] Ethylene is created in the upper atmosphere through two different addition/decomposition mechanisms - radical/radical association

(R12) $$^3CH_2 + CH_3 \rightarrow C_2H_4 + H,$$

and the CH-insertion-H-elimination process involving methane

(R5) $$CH + CH_4 \rightarrow C_2H_4 + H$$

to yield the net reaction $2CH_4 \rightarrow C_2H_4 + H_2 + 2H$, as well as through ion chemistry in the scheme

(S1)
$$\begin{array}{c} N_2 + h\nu \rightarrow N_2^+ + e^- \\ CH_4 + N_2^+ \rightarrow CH_3^+ + N_2 + H \\ CH_4 + CH_3^+ \rightarrow C_2H_5^+ + H_2 \\ HCN + C_2H_5^+ \rightarrow H_2CN^+ + C_2H_4 \\ e^- + H_2CN^+ \rightarrow HCN + H \\ \hline 2CH_4 \rightarrow C_2H_4 + H_2 + 2H \end{array}.$$

The ion contribution through (S1) controls ethylene production near the model-calculated ionospheric peak at 1060 km. However, the peak of ethylene production corresponds with the peak of methane dissociation near 800 km, controlled by processes (R12) and (R5) which accounts for 56% and 42%, respectively, of ethylene production above 600 km [*Wilson and Atreya*, 2000b]. Once ethylene is formed, it serves as the major source of acetylene above 500 km through photolysis (J7), responsible for 75% of the total acetylene column production rate above 500 km. This differs from the *Toublanc et al.* [1995] and *Yung et al.* [1984] models where recombination of methylene radicals plays a larger role due to the authors' choice of methane photolytic scheme and the larger $^3CH_2$ recombination rate coefficient. Most of this acetylene is diffused into the lower atmosphere where it is polymerized to form higher-order hydrocarbons (e.g., C_4H_2)

(S2)
$$\begin{array}{c} C_2H_2 + h\nu \rightarrow C_2H + H \\ \hline C_2H + C_2H_2 \rightarrow C_4H_2 + H \\ 2C_2H_2 \rightarrow C_4H_2 + 2H \end{array},$$

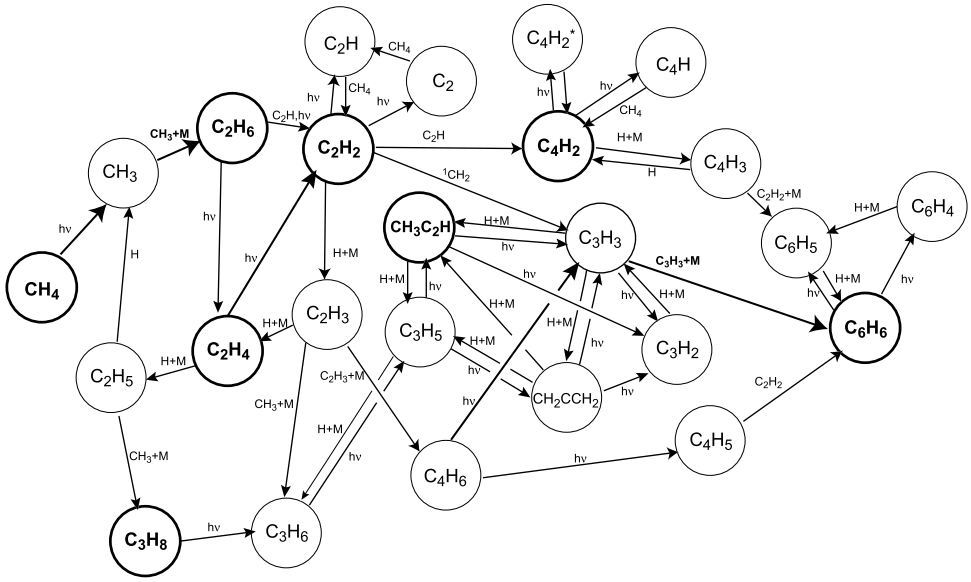

Figure 7. Schematic of Titan hydrocarbon chemistry. Stable species and primary reactions are shown in bold.

and undergoes reactions with hydrogen to reform ethylene:

$$\begin{array}{c} C_2H_2 + H \xrightarrow{M} C_2H_3 \\ \underline{C_2H_3 + H \xrightarrow{M} C_2H_4} \\ C_2H_2 + 2H \rightarrow C_2H_4 \end{array} \quad \text{(S3)}$$

The progression of this lower atmosphere hydrocarbon chemistry is demonstrated in Figure 7.

[33] Methyl radicals are produced mainly through methane photolysis (J4a) above 700 km, while the catalytic dissociation of methane

$$\begin{array}{c} C_2H_2 + h\nu \rightarrow C_2 + H_2 \\ C_2 + CH_4 \rightarrow C_2H + CH_3 \\ \underline{C_2H + CH_4 \rightarrow C_2H_2 + CH_3} \\ CH_4 \rightarrow CH_3 + H \end{array} \quad \text{(S4)}$$

$$\begin{array}{c} C_2H_2 + h\nu \rightarrow C_2H + H \\ \underline{C_2H + CH_4 \rightarrow C_2H_2 + CH_3} \\ CH_4 \rightarrow CH_3 + H \end{array} \quad \text{(S5)}$$

accounts for 80% of methyl radical production or 5.6×10^9 CH_3 molecules cm^{-3} s^{-1}. The main destination of these CH_3 radicals is the formation of ethane through the addition of (S4), (S5), or (J4a) and methyl recombination (R21),

$$\begin{array}{c} CH_4 + h\nu \rightarrow {}^1CH_2 + H_2 \\ CH_4 + {}^1CH_2 \rightarrow CH_3 + CH_3 \\ \underline{CH_3 + CH_3 \xrightarrow{M} C_2H_6} \\ 2CH_4 \rightarrow C_2H_6 + H_2 \end{array} \quad \text{(S6)}$$

Methyl radicals also combine with C_2H_5 radicals, produced from H-attachment to ethylene (R48) or C_2H-insertion-H-abstraction from ethane (R31), to produce propane in the lower stratosphere

$$\begin{array}{c} 2CH_4 \rightarrow C_2H_4 + 2H + H_2 \\ CH_4 \rightarrow CH_3 + H \\ C_2H_4 + H \xrightarrow{M} C_2H_5 \\ \underline{C_2H_5 + CH_3 \xrightarrow{M} C_3H_8} \\ 3CH_4 \rightarrow C_3H_8 + 2H + H_2 \end{array} \quad \text{(S7)}$$

$$\begin{array}{c} 2CH_4 \rightarrow C_2H_6 + 2H \\ C_2H_2 + h\nu \rightarrow C_2H + H \\ C_2H_6 + C_2H \rightarrow C_2H_5 + C_2H_2 \\ CH_4 \rightarrow CH_3 + H \\ \underline{C_2H_5 + CH_3 \xrightarrow{M} C_3H_8} \\ 3CH_4 \rightarrow C_3H_8 + 4H \end{array} \quad \text{(S8)}$$

with (S7) accounting for 61% of C_3H_8 production and (S8) producing 38% of the propane in the atmosphere.

[34] CH radical is mainly produced through (R10b) in the upper atmosphere, promoted by the formation of $^3CH_2$ radicals through both methane dissociation (J4d)–43% of $^3CH_2$ and $^1CH_2$ collisional quenching–51% of $^3CH_2$ above 600 km [*Wilson and Atreya*, 2000b]

$$CH_4 + h\nu \rightarrow {}^3CH_2 + 2H$$

and

$$\begin{array}{c} CH_4 + h\nu \rightarrow {}^1CH_2 + H_2 \\ \underline{{}^1CH_2 + N_2 \rightarrow {}^3CH_2 + N_2.} \\ CH_4 \rightarrow {}^3CH_2 + H_2 \end{array} \quad \text{(S9)}$$

Via (R10b) and (S5) CH radicals advance the production of methylacetylene and propylene. CH_3C_2H is produced in the

upper atmosphere from the direct CH-insertion-H-elimination process

$$\begin{array}{c} CH_4 \rightarrow {}^3CH_2 + 2H \\ {}^3CH_2 + H \rightarrow CH + H_2 \\ \underline{CH + C_2H_4 \rightarrow CH_3C_2H + H} \\ CH_4 + C_2H_4 \rightarrow CH_3C_2H + H_2 + 2H \end{array} \quad (S10)$$

and indirectly through collisional isomerization of allene,

$$\begin{array}{c} CH_4 \rightarrow {}^3CH_2 + 2H \\ {}^3CH_2 + H \rightarrow CH + H_2 \\ CH + C_2H_4 \rightarrow CH_2CCH_2 + H \\ \underline{CH_2CCH_2 + H \rightarrow CH_3C_2H + H} \\ CH_4 + C_2H_4 \rightarrow CH_3C_2H + H_2 + 2H \end{array} \quad (S11)$$

while propylene is formed in the upper atmosphere through the mechanism

$$\begin{array}{c} 2CH_4 \rightarrow C_2H_6 + H_2 \\ CH_4 \rightarrow {}^3CH_2 + 2H \\ {}^3CH_2 + H \rightarrow CH + H_2 \\ \underline{CH + C_2H_6 \rightarrow C_3H_6 + H} \\ 3CH_4 \rightarrow C_3H_6 + 2H_2 + 2H \end{array} \quad (S12)$$

and more prominently in the lower atmosphere through

$$\begin{array}{c} 2CH_4 \rightarrow C_2H_4 + 2H + H_2 \\ CH_4 \rightarrow CH_3 + H \\ C_2H_4 + h\nu \rightarrow C_2H_2 + H_2 \\ C_2H_2 + H \xrightarrow{M} C_2H_3 \\ \underline{C_2H_3 + CH_3 \xrightarrow{M} C_3H_6} \\ 3CH_4 \rightarrow C_3H_6 + 2H_2 + 2H \end{array} \quad (S13)$$

[35] Heavier hydrocarbons may also be formed in Titan's atmosphere - among the most prominent, benzene. *Wilson et al.* [2003] explored possible mechanisms for benzene formation, supported by the tentative detection of C_6H_6 by *Coustenis et al.* [2003]. Benzene in the lower stratosphere is primarily formed through the scheme

$$\begin{array}{c} 4(C_2H_2 + H \xrightarrow{M} C_2H_3) \\ 2(C_2H_3 + C_2H_3 \xrightarrow{M} C_4H_6) \\ 2(C_4H_6 + h\nu \rightarrow C_3H_3 + CH_3) \\ CH_3 + CH_3 \xrightarrow{M} C_2H_6 \\ C_3H_3 + C_3H_3 \xrightarrow{M} n - C_6H_6 \\ \underline{n - C_6H_6 + H \rightarrow C_6H_6 + H} \\ 4C_2H_2 + 4H \rightarrow C_6H_6 + C_2H_6 \end{array} \quad (S14)$$

with H-addition onto phenyl radical

$$\begin{array}{c} C_2H_2 + h\nu \rightarrow C_2H + H \\ C_2H_2 + C_2H \rightarrow C_4H_2 + H \\ C_4H_2 + H \xrightarrow{M} C_4H_3 \\ C_4H_3 + C_2H_2 \xrightarrow{M} C_6H_5 \\ \underline{C_6H_5 + H \xrightarrow{M} C_6H_6} \\ 3C_2H_2 \rightarrow C_6H_6 \end{array} \quad (S15)$$

providing a minor pathway.

4.2. Nitriles

[36] Nitrogen, the predominant molecule in Titan's atmosphere, is largely chemically inert. The primary manner in which nitrogen is involved in chemistry is through dissociation via both photons and electrons. Nitrogen is photodissociated mainly due to radiation in the 800–1000 Å region. *Zipf and McLaughlin* [1978] and *Zipf et al.* [1980] have determined the yields of nitrogen atoms from this process to be approximately 50% for ground-state N^{4s} and 30–40% and 10–20% for excited states N^{2d} and N^{2p}, respectively. However, *Zipf et al.* [1980] found that N^{2p} atoms are rapidly de-excited to the N^{2d} state. Therefore N^{4s} and N^{2d} are assumed to adopt a quantum yield of 0.5 each from N_2 photolysis. Nitrogen also undergoes electron-impact dissociation, with quantum yields determined by *Zipf et al.* [1980] and *Itikawa et al.* [1986].

[37] Nitrogen atoms combine with hydrocarbons to form an assortment of nitrile neutrals and ions in the upper atmosphere, as shown in Figure 8. The flux of N^{4s} atoms combines with methane photolytic product, CH_3, to form the basis of nitrile chemistry–HCN. HCN is formed through photodissociation

$$\begin{array}{c} 0.5(N_2 + h\nu \rightarrow N^{4s} + N^{4s}) \\ CH_4 + h\nu \rightarrow CH_3 + H \\ N^{4s} + CH_3 \rightarrow H_2CN + H \\ \underline{H_2CN + H \rightarrow HCN + H_2} \\ 0.5N_2 + CH_4 \rightarrow HCN + H_2 + H \end{array} \quad (S16)$$

electron impact processes

$$\begin{array}{c} N_2 + e^- \rightarrow N^+ + N^{4s,2d} + 2e^- \\ CH_4 + N^+ \rightarrow H_2CN^+ + H_2 \\ \underline{e^- + H_2CN^+ \rightarrow HCN + H} \\ N_2 + CH_4 \rightarrow HCN + N + H_2 + H \end{array} \quad (S17)$$

and photoionization

$$\begin{array}{c} N_2 + h\nu \rightarrow N^+ + N^{2d} + e^- \\ CH_4 + N^+ \rightarrow H_2CN^+ + H_2 \\ N^{2d} + C_2H_4 \rightarrow CH_3CN + H \\ \underline{CH_3CN + H_2CN^+ \rightarrow CH_3CNH^+ + HCN} \\ N_2 + CH_4 + C_2H_4 \rightarrow HCN + H_2 + H + CH_3CNH^+ + e^- \end{array} \quad (S18)$$

with (S16) accounting for 60% of non-recycled HCN in the atmosphere. HCN is then diffused down into the lower atmosphere, providing the major source of HCN in this region, evident by an HCN flux of 3.4×10^8 cm^{-2} s^{-1} at 600 km, where it undergoes recycling mechanisms, commenced through photolysis and H-addition

$$\begin{array}{c} HCN + h\nu \rightarrow CN + H \\ \underline{CN + CH_4 \rightarrow HCN + CH_3} \\ CH_4 \rightarrow CH_3 + H \end{array} \quad (S19)$$

$$\begin{array}{c} HCN + H \xrightarrow{M} H_2CN \\ \underline{H_2CN + H \rightarrow HCN + H_2} \\ H + H \rightarrow H_2 \end{array} \quad (S20)$$

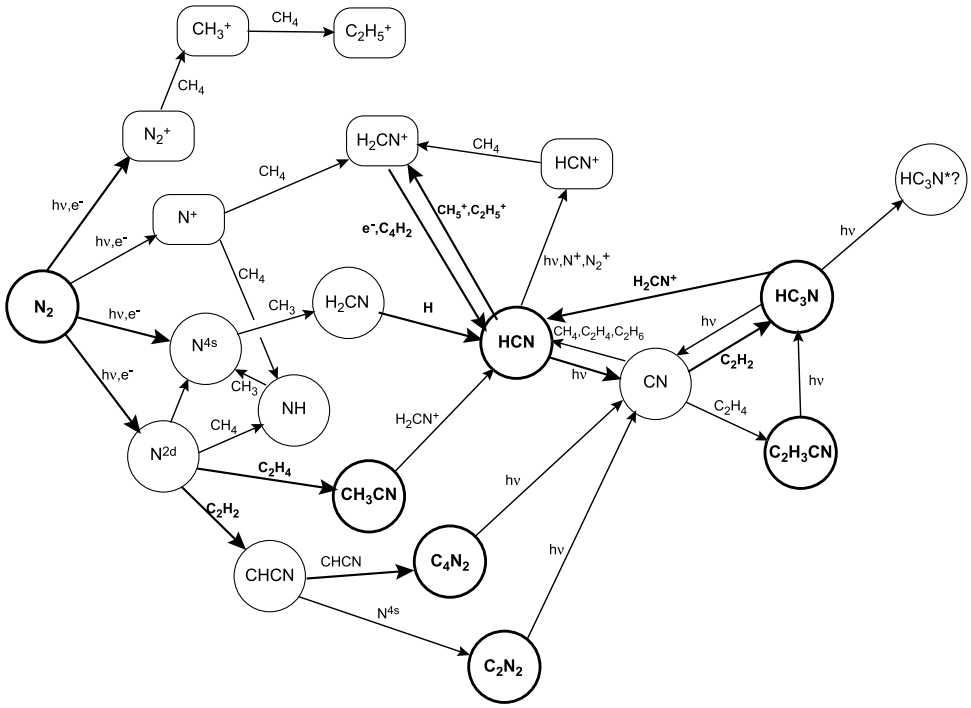

Figure 8. Schematic of Titan nitrile chemistry. Stable species and primary reactions are shown in bold, with ions shown in rounded rectangles.

[38] HC_3N is produced primarily through the addition of the photolytic product CN and acetylene

$$\begin{array}{c} \mathrm{HCN} + h\nu \rightarrow \mathrm{CN} + \mathrm{H} \\ \underline{\mathrm{CN} + \mathrm{C_2H_2} \rightarrow \mathrm{HC_3N} + \mathrm{H}} \\ \mathrm{HCN} + \mathrm{C_2H_2} \rightarrow \mathrm{HC_3N} + \mathrm{H} \end{array} . \quad \text{(S21)}$$

[39] C_4N_2 can also be formed through CN-insertion, as studied by *Halpern et al.* [1989]

$$\mathrm{CN} + \mathrm{HC_3N} \rightarrow \mathrm{C_4N_2} + \mathrm{H}. \quad \text{(R149)}$$

Yung [1987] proposed another mechanism for the formation of C_4N_2 as well as C_2N_2 through the action of the CHCN radical in the reactions

$$\mathrm{CHCN} + \mathrm{CHCN} \rightarrow \mathrm{C_4N_2} + \mathrm{H_2} \quad \text{(R161)}$$

$$\mathrm{CHCN} + \mathrm{N^{4s}} \rightarrow \mathrm{C_2N_2} + \mathrm{H}. \quad \text{(R160)}$$

Considering estimations by *Yung* [1987] for (R161), the main source of dicyanoacetylene is the scheme

$$\begin{array}{c} \mathrm{N_2} + h\nu \rightarrow 2\mathrm{N^{2d}} \\ 2\left[\mathrm{N^{2d}} + \mathrm{C_2H_2} \rightarrow \mathrm{CHCN} + \mathrm{H}\right] \\ \underline{\mathrm{CHCN} + \mathrm{CHCN} \rightarrow \mathrm{C_4N_2} + \mathrm{H_2}} \\ \mathrm{N_2} + 2\mathrm{C_2H_2} \rightarrow \mathrm{C_4N_2} + 2\mathrm{H} + \mathrm{H_2} \end{array} , \quad \text{(S22)}$$

responsible for 98% of C_4N_2 production throughout Titan's atmosphere. Likewise, C_2N_2 is produced through the scheme

$$\begin{array}{c} \mathrm{N_2} + h\nu \rightarrow \mathrm{N^{4s}} + \mathrm{N^{2d}} \\ \mathrm{N^{2d}} + \mathrm{C_2H_2} \rightarrow \mathrm{CHCN} + \mathrm{H} \\ \underline{\mathrm{N^{4s}} + \mathrm{CHCN} \rightarrow \mathrm{C_2N_2} + \mathrm{H_2}} \\ \mathrm{N_2} + \mathrm{C_2H_2} \rightarrow \mathrm{C_2N_2} + 2\mathrm{H} \end{array} , \quad \text{(S23)}$$

responsible for virtually all of C_2N_2 production. Reactions with CH_3 and H_2CN, to produce HCN, severely limit the availability of N^{4s} atoms, giving a preference for CHCN to produce C_4N_2 in the upper atmosphere.

[40] In the upper atmosphere, C_2H_3CN production follows along the same procedure as (S19),

$$\begin{array}{c} \mathrm{HCN} + h\nu \rightarrow \mathrm{CN} + \mathrm{H} \\ \underline{\mathrm{CN} + \mathrm{C_2H_4} \rightarrow \mathrm{C_2H_3CN} + \mathrm{H}} \\ \mathrm{HCN} + \mathrm{C_2H_4} \rightarrow \mathrm{C_2H_3CN} + 2\mathrm{H} \end{array} , \quad \text{(S24)}$$

while in the lower atmosphere, C_2H_3CN is produced through

$$\begin{array}{c} \mathrm{C_2H_2} + \mathrm{H} \xrightarrow{\mathrm{M}} \mathrm{C_2H_3} \\ \underline{\mathrm{HCN} + \mathrm{C_2H_3} \rightarrow \mathrm{C_2H_3CN} + \mathrm{H}} \\ \mathrm{HCN} + \mathrm{C_2H_2} \rightarrow \mathrm{C_2H_3CN} + \mathrm{H} \end{array} . \quad \text{(S25)}$$

4.3. Oxygen Species

[41] Stratospheric measurements of CO [e.g., *Gurwell and Muhleman*, 2000], CO_2 [*Coustenis et al.*, 1989], and H_2O [*Coustenis et al.*, 1998] have indicated the presence of oxygen chemistry in the atmosphere of Titan. A likely contributor to this oxygen inventory is an influx of micrometeorites into the atmosphere, providing a source of H_2O molecules. Primarily, H_2O molecules undergo UV photolysis. The formation of hydroxyl radicals through H_2O

photodissociation comprises 60% of H_2O destruction in Titan's atmosphere. Some of the OH radicals serve to recycle H_2O. In fact, 54% of H_2O destruction is recycled back to H_2O, mainly through charged-particle catalysis,

$$\begin{array}{c} N_2 + h\nu \rightarrow N_2^+ + e^- \\ N_2^+ + H_2O \rightarrow H_2O^+ + N_2 \\ H_2O^+ + CH_4 \rightarrow H_3O^+ + CH_3 \\ \underline{H_3O^+ + HCN \rightarrow H_2CN^+ + H_2O} \\ CH_4 + HCN \rightarrow H_2CN^+ + CH_3 + e^- \end{array} \quad \text{(S26)}$$

$$\begin{array}{c} N_2 + h\nu \rightarrow N_2^+ + e^- \\ N_2^+ + C_2H_2 \rightarrow N_2H^+ + C_2H \\ N_2H^+ + H_2O \rightarrow H_3O^+ + N_2 \\ \underline{H_3O^+ + HCN \rightarrow H_2CN^+ + H_2O} \\ CH_4 + HCN \rightarrow H_2CN^+ + CH_3 + e^- \end{array} , \quad \text{(S27)}$$

through the reversibility of methylene-water addition

$$^1CH_2 + H_2O \rightarrow CH_3 + OH \quad \text{(R214a)}$$

$$CH_3 + OH \rightarrow H_2O + {}^1CH_2, \quad \text{(R208a)}$$

and through

$$\begin{array}{c} H_2O + h\nu \rightarrow OH + H \\ \underline{OH + CH_4 \rightarrow H_2O + CH_3} \\ CH_4 \rightarrow CH_3 + H \end{array} . \quad \text{(S28)}$$

The main destiny of OH radicals that are not recycled back to H_2O is the formation of CO_2 through reaction with primordial CO,

$$CO + OH \rightarrow CO_2 + H. \quad \text{(R219)}$$

[42] CO is engaged in chemistry mainly in the lower atmosphere, where it produces oxygenated compounds through pressure-dependent reactions

$$CO + {}^3CH_2 \xrightarrow{M} CH_2CO \quad \text{(R217)}$$

and

$$\begin{array}{c} 2(CO + H \xrightarrow{M} HCO) \\ \underline{HCO + HCO \rightarrow H_2CO + CO} \\ CO + 2H \rightarrow H_2CO \end{array} \cdot \quad \text{(S29)}$$

However, photolysis of these compounds simply leads to CO recycling, the dominant mechanism in Titan oxygen chemistry.

4.4. Ion Chemistry

[43] Ion chemistry in Titan's atmosphere commences with the ionization of molecular nitrogen. Nitrogen is ionized by solar photons below 796 Å and by electron impact. These sources provide N_2^+ and N^+ ions that readily react with neutrals to form larger ions. Likewise, the abundance of CH_4 in the upper atmosphere makes its ionization an important early process in the formation of the ionosphere. Methane is ionized by photons and electrons producing a number of hydrocarbon and hydrogen ions.

[44] The formation of most of the ions in Titan's ionosphere begin with the mechanism

$$\begin{array}{c} N_2 + h\nu \rightarrow N_2^+ + e^- \\ N_2^+ + CH_4 \rightarrow CH_3^+ + N_2 + H \\ \underline{CH_3^+ + CH_4 \rightarrow C_2H_5^+ + H_2} \\ 2CH_4 \rightarrow C_2H_5^+ + H_2 + H + e^- \end{array} \quad \text{(S30)}$$

which serves to produce the abundant ion $C_2H_5^+$. H_2CN^+, found to be the major ion in the *Keller et al.* [1992] and *Banaszkiewicz et al.* [2000] models, is produced through

$$\begin{array}{c} 2CH_4 \rightarrow C_2H_5^+ + H_2 + H + e^- \\ \underline{C_2H_5^+ + HCN \rightarrow H_2CN^+ + C_2H_4} \\ 2CH_4 + HCN \rightarrow H_2CN^+ + C_2H_4 + H_2 + H + e^- \end{array} \quad \text{(S31)}$$

and

$$\begin{array}{c} N_2 + h\nu \rightarrow N_2^+ + e^- \\ N_2^+ + H_2 \rightarrow N_2H^+ + H \\ N_2H^+ + CH_4 \rightarrow CH_5^+ + N_2 \\ \underline{CH_5^+ + HCN \rightarrow H_2CN^+ + CH_4} \\ HCN + H_2 \rightarrow H_2CN^+ + H + e^- \end{array} , \quad \text{(S32)}$$

where (S31) is responsible for 78% of H_2CN^+ production and (S32) accounts for 10%. As indicated previously, the main function of H_2CN^+ ions is the formation of HCN through electron recombination (R349) and through reactions (R347) and scheme (S18), while $C_2H_5^+$ serves to convert nitriles to hydrocarbons through (S31).

5. Results and Discussion

5.1. Sensitivity to Eddy Diffusion and Methane Abundance

[45] A test of the accuracy of a photochemical model is comparison with observations of constituent abundances. However, exactly what is being considered when dealing with observations must be taken into account. The large error bars associated with the Vervack et al. (submitted manuscript, 2003) UVS reanalysis and the questions about the CH_4 and C_2H_2 observations that affect the retrieval of other species, as well, have been pointed out in section 3.5.2. However, the absence of other observations of constituent densities in Titan's upper atmosphere, with the exception of CH_4 and C_2H_2, and the difficulty in reconciling Titan chemistry with the *Smith et al.* [1982] >825 km C_2H_2 observation suggests the use of the Vervack non-CH_4 retrievals as a preliminary guide to how Titan's constituents might be distributed in the upper atmosphere. Furthermore, many of the existing observations in the stratosphere (e.g., IRIS) are determined assuming a uniform mole fraction profile, which is not realistic for chemically active constituents, affecting the abundances derived. For instance, *Coustenis et al.* [1989] derived a CO_2 mole fraction of $1.4^{+0.3}_{-0.5} \times 10^{-8}$ at 105 km, the altitude where the contribution function of CO_2 peaks. However, as dictated by the contribution function, the IRIS instrument received signal

contribution from layers above and below this layer. Consequently, an uncertainty of +55, −30 km is included with this result, associated with the region where the contribution function is greater than half of the peak value. The authors were able to fit the obtained spectra with a CO_2 mole fraction profile that reaches 1.4×10^{-8} at ~180 km and decreases to 5×10^{-9} at 105 km, outside the range of values indicated at the contribution peak assuming a uniform mole fraction profile. A similar case is found for H_2O as the stratospheric value of 4×10^{-10} is 20 times smaller than the value of the best-fitting H_2O mole fraction profile, provided by *Lara et al.* [1996], at the peak of the contribution function for the observation [*Coustenis et al.*, 1998]. Thus the assumption of a uniform profile must be kept in mind when comparing model results to observations.

[46] To demonstrate the effect of the eddy diffusion coefficient on the distribution of constituents, mole fraction profiles of key constituents for the eddy diffusion profiles demonstrated in Figure 6 are displayed in Figures 9 and 10. Figure 9 shows the results for CH_4 and HCN, key constituents used as guides in obtaining the eddy coefficient along with the observations referred to in section 3.5.2. The Vervack et al. (submitted manuscript, 2003) and *Vervack* [1997] UVS reanalysis observations displayed represent the extremes of both ingress and egress results, converted to mole fractions on the basis of the nominal total number density profile of this model.

[47] The nominal CH_4 profile fits the *Smith et al.* [1982] 1125 km observation along with the *Strobel et al.* [1992] 1400 km observation and the Vervack et al. (submitted manuscript, 2003) observations up to ~1000 km. SB approximates the upper limits of *Smith et al.* [1982] while HI matches Vervack et al. (submitted manuscript, 2003) up to higher levels but does not approach the *Strobel et al.* [1992] observation.

[48] For HCN the nominal profile fits the *Tanguy et al.* [1990] observations at 100 km and 200 km, as well as provides a good fit to the *Coustenis et al.* [1989] IRIS observations. Above 300 km, the nominal profile splits the divergent observations of *Tanguy et al.* [1990] and *Hidayat et al.* [1997] HI was generated to fit the *Hidayat et al.* [1997] HCN observations below 300 km as closely as possible, while simultaneously matching the CH_4Vervack et al. (submitted manuscript, 2003) observations up to 1000 km, but is unable to completely match the HCN observations below 200 km. On the other hand, SB clearly overpredicts the HCN abundance in the lower stratosphere.

[49] In the upper atmosphere, the nominal profile provides a reasonable fit to the *Vervack* [1997] reanalysis, below 800 km, in all cases with the exception of C_2H_2. The C_2H_2 nominal profile overpredicts acetylene abundance in relation to the *Vervack* [1997] results, consistent with the other photochemical models but on a lesser scale than the *Yung et al.* [1984] or *Toublanc et al.* [1995] models. Vervack et al. (submitted manuscript, 2003) provide reanalysis profiles assuming C_2H_2 to be the only absorbing species that exceeds the nominal profile. Furthermore, it is difficult to imagine a C_2H_2 profile with a shape that fits both the stratospheric and nominal upper atmosphere observations, simultaneously, absent a significant localized sink around to 10^{-1}–10^{-2} millibar region. This raises the possibility that more absorption should be ascribed to

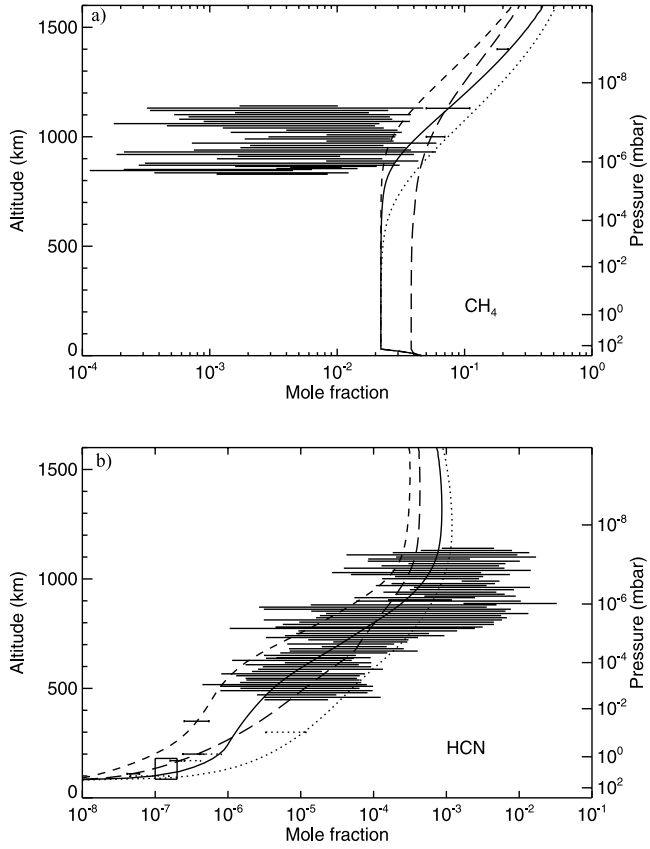

Figure 9. a) CH_4 and b) HCN profiles using the nominal eddy diffusion profile (NOM, solid line), *Steiner and Bauer* [1990] profile (SB, dotted line), the high homopause profile (HI, short dashed), and the *Lara et al.* [2002] profile (NL, long dashed line). The group of horizontal lines represent the *Vervack* [1997] reanalysis of UVS observations. In a) the horizontal bars at 1000 km and 1130 km represent the *Smith et al.* [1982] observations, while the horizontal bar at 1400 km indicates the *Strobel et al.* [1992] Voyager UVS observations. In b) the solid horizontal lines in the lower portion of the plot shows the *Hidayat et al.* [1997] observations with the dotted lines representing the *Tanguy et al.* [1990] results, and the box represents the stratospheric Voyager IRIS observations including error bars in abundance and altitude.

C_2H_2 in the UVS reanalysis than their nominal observations suggest. Above 800 km, NOM falls off with respect to the *Vervack* [1997] observations for C_4H_2 and HC_3N. However, these constituents have short lifetimes in this region of the atmosphere compared with a solar cycle and thus are sensitive to changes in the solar radiation output, as discussed in the next section, and assuming solar maximum conditions provides a better fit to this data. Furthermore, as *Vervack* [1997] points out, the uniformity in number density with respect to altitude for the C_4H_2 and HC_3N observations suggest that these species may not have been well-retrieved. Misassignment of CH_4 absorption may have understated CH_4 densities at high altitudes while overstating these species.

[50] The high homopause eddy diffusion profile limits the amount of methane in the upper atmosphere, resulting in

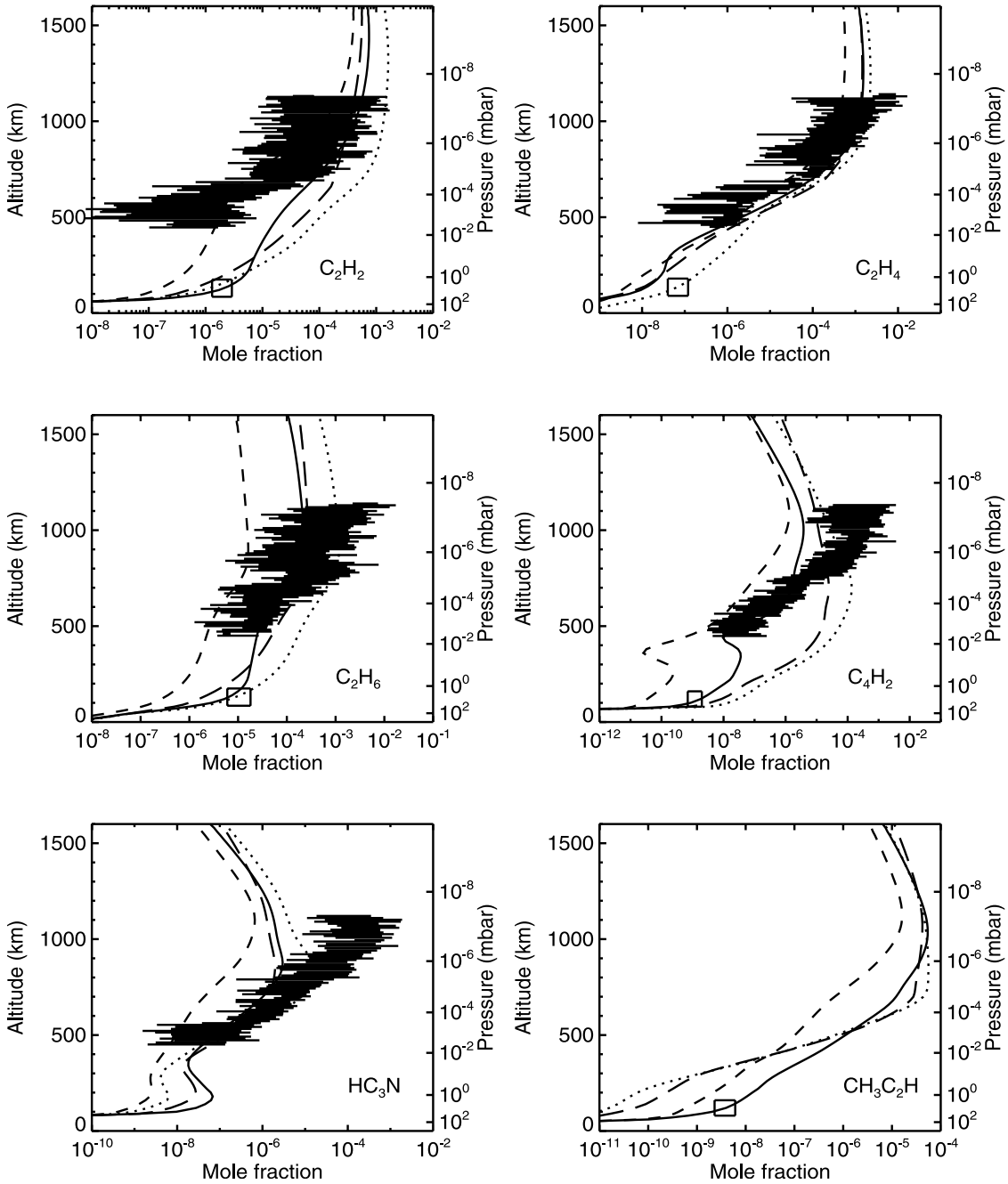

Figure 10. Constituent profiles using the nominal eddy diffusion profile (NOM, solid line), *Steiner and Bauer* [1990] profile (SB, dotted line), the high homopause profile (HI, short dashed), and the *Lara et al.* [2002] profile (NL, long dashed line). The boxes represent the stratospheric Voyager IRIS observations including error bars in abundance and altitude, while the horizontal lines represent the *Vervack* [1997] reanalysis of UVS observations.

less conversion to higher order hydrocarbons and, consequently, smaller hydrocarbon abundances. HI matches the C_2H_2 and C_2H_4 upper atmosphere observations well, but underpredicts for C_2H_6, C_4H_2 and HC_3N. SB, on the other hand, provides reasonable predictions only for HC_3N and C_2H_6 above 700 km, according to the Vervack et al. (submitted manuscript, 2003) observations. The HI profile significantly underpredicts constituent abundances in the stratosphere, while SB matches IRIS observations only for the C_2-hydrocarbons.

[51] Recently, *Lara et al.* [2002] reanalyzed this question of the eddy diffusion coefficient in relation to the methane density in the upper atmosphere. They proceeded by recalculating the methane density with an assumption of CH_4 stratospheric mole fraction at 3.8%, compared to the *Lara et al.* [1996] assumption of 1.7%. This value assumes very high methane supersaturation in the troposphere, which according to *Courtin et al.* [1995], can be as high as 230%. In contrast, the nominal model uses the results of *Samuelson et al.* [1997], which places the level of maxi-

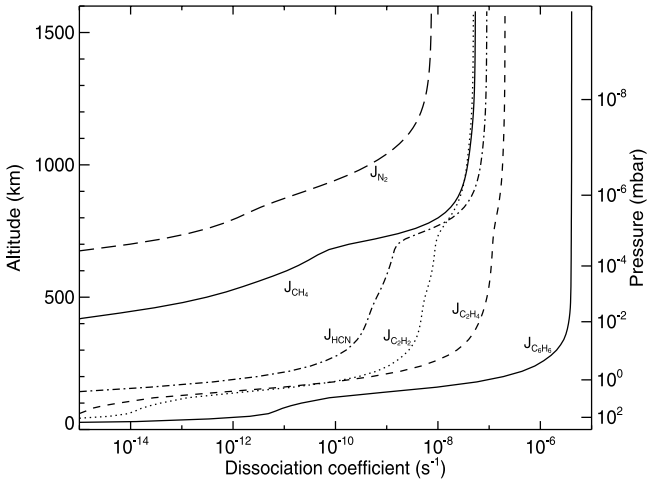

Figure 11. Photodissociation coefficients of key species.

mum methane supersaturation at 1.48 ± 0.11, using a methodology that, according to the authors, avoids some of the sources of systematic error inherent in the *Courtin et al.* [1995] study. A methane supersaturation value of 1.37 yields of CH_4 stratospheric mole fraction of 2.2%. Nevertheless, with the large methane abundance, *Lara et al.* [2002] adopt an eddy diffusion profile (NL) that increases rapidly in the stratosphere and middle atmosphere, resulting in a high homopause level around 1000 km (Figure 6b). This profile with a CH_4 stratospheric mole fraction of 3.8% was tested along with the nominal case. As Figure 9 shows, NL provides good agreement with the HCN infrared and microwave observations, which eliminates the necessity for a large sink for HCN to the haze due to polymerization, as promoted by *Lara et al.* [1999]. However, demonstrated by Figure 10, the NL case underpredicts hydrocarbons in the lower stratosphere, with the exception of C_4H_2. C_3-hydrocarbons are especially diminished in the NL case, with a CH_3C_2H profile that is two orders of magnitude smaller and a C_3H_8 profile (not shown) that is an order of magnitude smaller than IRIS observations. In the upper atmosphere, the nominal case provides profiles more consistent with the UVS reanalysis than the NL case, as well.

5.2. Sensitivity to Solar Flux and Aerosol Structure

[52] The stable constituents in Titan's atmosphere are dissociated and ionized by solar photons and electrons that are transferred through the atmosphere. A comparison of Figure 11 and absorption cross sections will yield the deposition regions of different wavelength regions. N_2, which is dissociated by EUV photons, undergoes attenuation in dissociation in the upper atmosphere, with J_{N_2} having been reduced by an order of magnitude at 1000 km. Below 900 km, electron impact dominates N_2 absorption as J_{N_2} drops off at the base of the ionosphere at 720 km. Abundant species that undergo significant absorption of photons at 1000 Å $\leq \lambda \leq$ 1450 Å experience dissociation attenuation around 800 km, as these photons are deposited through methane absorption. Deposition of UV radiation longer than 1450 Å occurs lower in the atmosphere, at 200–300 km, as a result of absorption by molecules such as HCN ($\lambda \leq$ 1800 Å) and C_2H_2 ($\lambda \leq$ 2100 Å) as well as by aerosols ($\lambda \geq$ 1800 Å).

[53] During much of the upcoming Cassini-Huygens encounter with Titan, the Sun will undergo moderate solar activity, likely resulting in a reduced solar flux compared with what took place during the Voyager flybys. In Titan's atmosphere, constituents above 500 km are typically destroyed chemically within one solar cycle, while for certain stable constituents, like C_4H_2, their relatively short lifetimes may allow changes in solar output to affect their lower stratospheric abundances, as well. With this in mind, it is constructive to analyze the effect of variations in solar flux on the distribution of various key constituents in Titan's atmosphere. Figure 12 provides such a comparison, assuming solar fluxes in the FUV and NUV obtained by SOLSTICE for average solar maximum, solar moderate, and solar minimum conditions, with the corresponding EUV calculated fluxes for (F10.7, F10.7A) = (233, 211.9), (130, 130), and (70, 70), respectively. The C_2-hydrocarbons, which are more directly affected by methane and its dependence in the upper atmosphere on transport rather than chemistry, show little dependence on solar activity. However, nitriles like HCN and HC_3N show much more sensitivity in the upper atmosphere to solar output as HCN photolysis plays a considerably larger role with respect to transport than CH_4 photolysis.

[54] In comparing the nominal dissociation coefficients with the photodissociation coefficients of *Toublanc et al.* [1995] and *Lara et al.* [1996] the most glaring differences reside in the lower 300 km. The nominal dissociation coefficients fall off much more rapidly than *Lara et al.* [1996] most likely due to differences in the treatment of aerosols. Solar radiation at wavelengths 1800 Å $\leq \lambda \leq$ 2100 Å is relatively unattenuated in the *Lara et al.* [1996] model, reaching to lower regions, while those photons are deposited above 200 km in the nominal model due to C_2H_2 absorption and aerosol opacity. The assertion of significant opacity at these wavelengths is corroborated by the analysis of UV spectra by *McGrath et al.* [1998]. The *Toublanc et al.* [1995] photodissociation rates fall off more significantly than *Lara et al.* [1996] which used the *Yung et al.* [1984] parameterization of aerosol absorption, but less than the nominal case, probably a result of consideration of Mie haze particles. For instance, $J_{C_2H_2}(100\text{ km})/J_{C_2H_2}(500\text{ km}) = 1.0 \times 10^{-5}$ in the nominal model while *Toublanc et al.* [1995] and *Lara et al.* [1996] yield 4.8×10^{-2} and 8.2×10^{-3}, respectively. Fractal particles are more opaque than Mie particles at short wavelengths [*Rannou et al.*, 1995], limiting the penetration of radiation at deeper levels. However, aerosol opacities amount to a significant uncertainty affecting photodissociation coefficients, as Titan aerosol densities and optical constants are still not well understood. The effect of the type of aerosol particle considered is shown in Figure 13, which compares constituent mole fraction profiles from the nominal case with those assuming Mie opacities derived from *Rannou et al.* [1995]. In the Mie case more radiation is allowed to penetrate into the lower atmosphere, promoting greater formation of CH_3 radical through catalytic dissociation of methane (S5) and increasing the levels of ethane and propane in the atmosphere. Furthermore, the smaller opacity provided by Mie particles longward of 1800 Å results in much larger dissociation of HC_3N and C_2H_3CN molecules which significantly absorb in that wavelength region. The IRIS HC_3N upper limit of

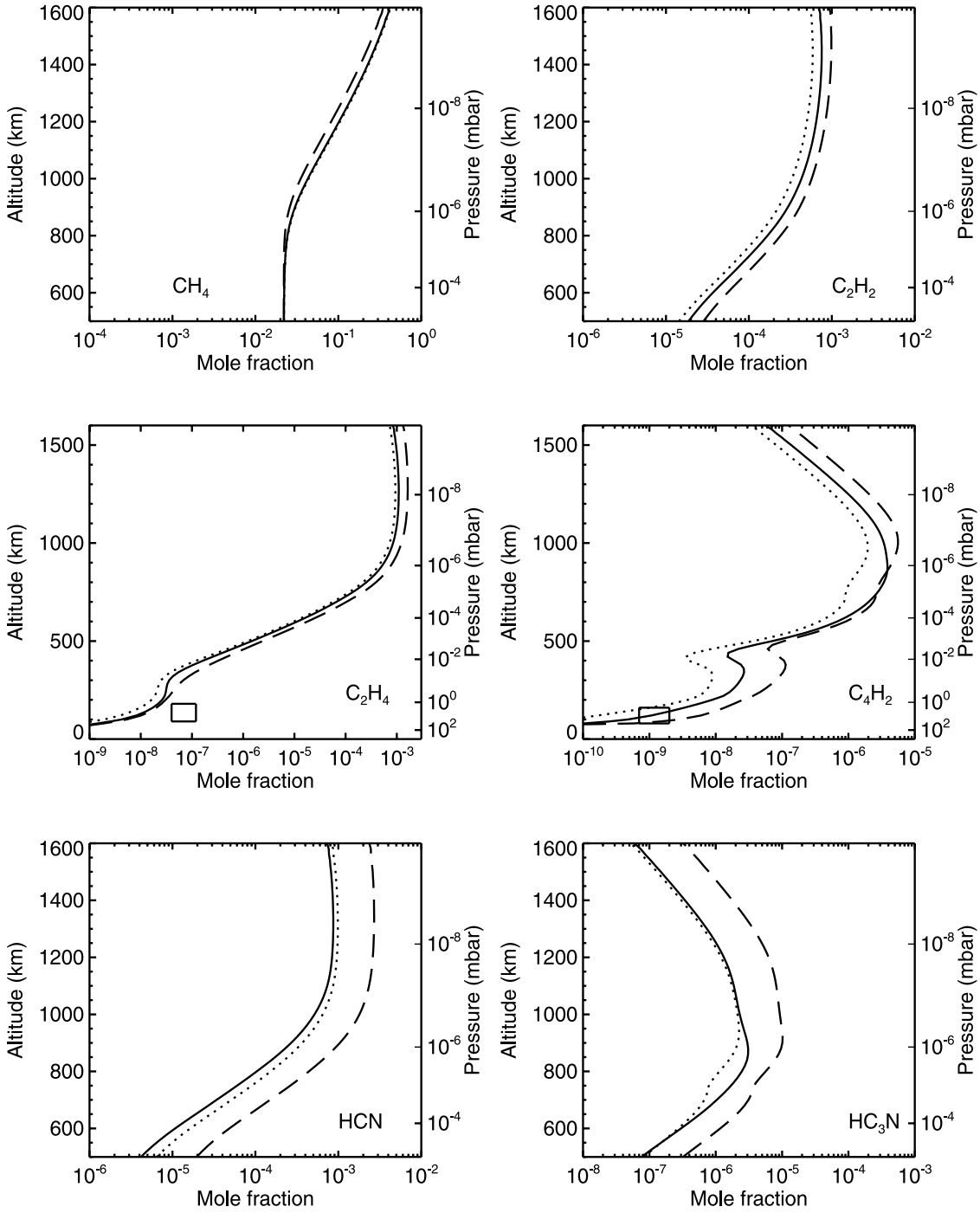

Figure 12. Constituent profiles for average solar maximum (long dashed line), solar moderate (solid line), and solar minimum conditions (dotted line).

1.5×10^{-9} and the lack of observations of C_2H_3CN suggest that more absorption of these molecules takes place in the lower atmosphere than what is determined by the nominal profile. These factors along with the C_3H_8 Mie profile hint at possibly less aerosol opacity in Titan's stratosphere than what is considered in the nominal case.

5.3. Hydrocarbons

[55] Figure 10 shows that the model slightly underpredicts ethylene density in Titan's stratosphere. This issue is a factor in the *Toublanc et al.* [1995] model, as well. *Lara et al.* [1996] assumed a boundary condition of 1.5×10^{-7} to match IRIS observations, necessitating a flux of 7.0×10^7 cm^{-2} s^{-1} from the surface, resulting from some surficial process (e.g., outgassing). The nominal model calculates a C_2H_4 net loss of 8.1×10^7 cm^{-2} s^{-1} (Table 7), requiring a corresponding flux from the surface in order to maintain steady state equilibrium. Such a flux, which would not be cold-trapped as C_2H_4 does not condense at those abundances, is a viable mechanism to account for the IRIS obser-

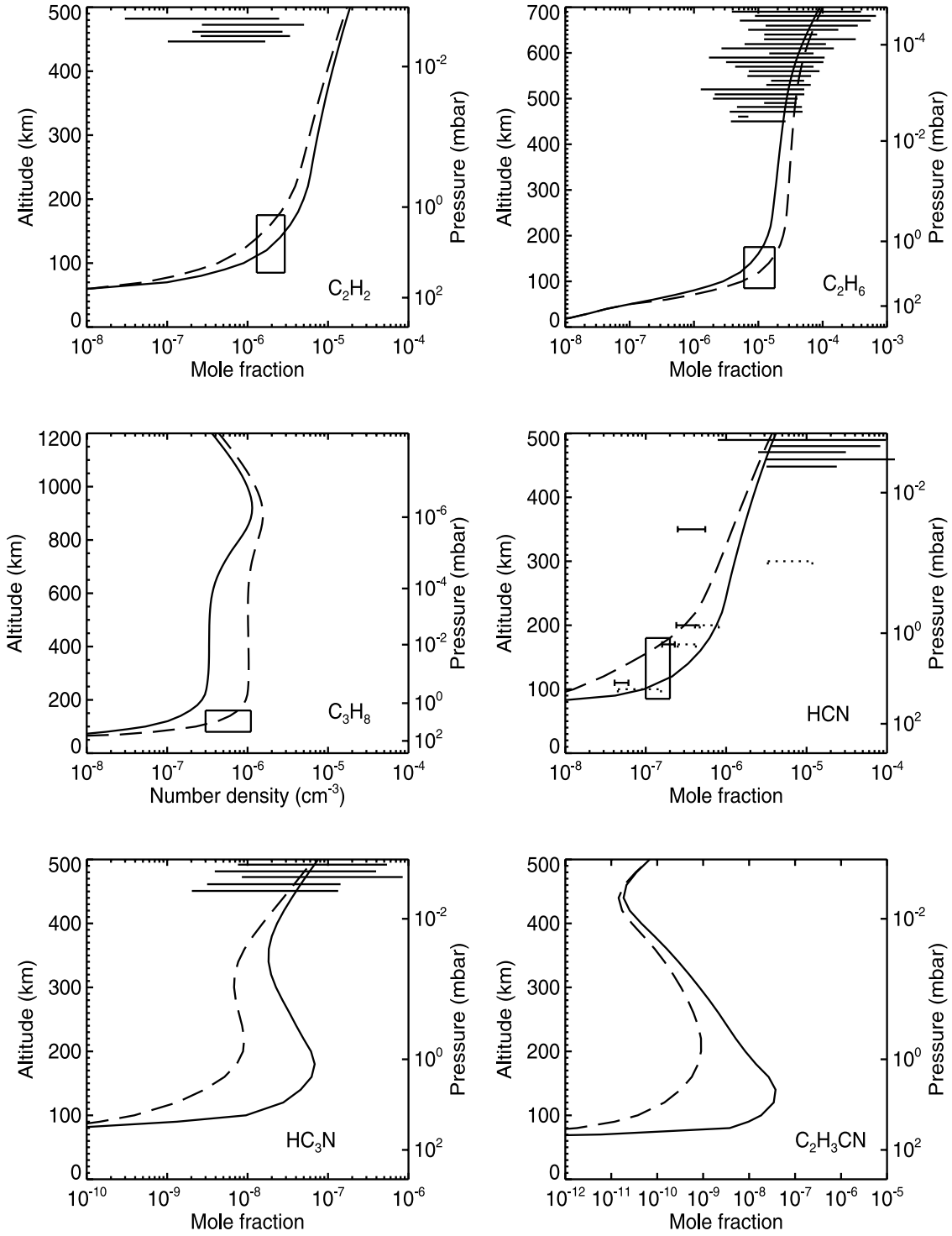

Figure 13. Constituent profiles assuming fractal haze particles (solid line) and Mie haze particles (long dashed line). The boxes represent the stratospheric Voyager IRIS observations including error bars in abundance and altitude, while the horizontal lines represent the *Vervack* [1997] reanalysis of UVS observations. For HCN, the solid horizontal bars show the *Hidayat et al.* [1997] observations with the dotted bars representing the *Tanguy et al.* [1990] observations.

vations. Possible irradiation of hydrocarbon condensates on Titan's surface may also provide a source of C_2H_4 in the stratosphere.

[56] *Canosa et al.* [1997] measured the CH + CH_4 rate coefficient in a temperature range of 23–295 K, but could not positively identify products. Thermochemical and kinetic analysis indicate, however, that H-atom elimination is the most favored process [*Canosa et al.*, 1997], yielding the C_3H_4 complex. With potential products CH_3C_2H and CH_2CCH_2 similarly exothermic, these isomers are assumed

Table 7. Production and Loss Rates and Chemical Lifetimes of Various Stable Species

Species[a]	Production (P), cm^{-2} s^{-1}	Loss (L), cm^{-2} s^{-1}	P − L, cm^{-2} s^{-1}	Chemical Lifetime at 300 km, s
N_2	1.1×10^7	2.9×10^8	-2.8×10^8	8.4×10^{15}
H_2	3.2×10^9	3.9×10^7	3.2×10^9	8.7×10^{12}
CH_4	1.1×10^8	4.9×10^9	-4.8×10^9	8.4×10^{11}
C_2H_2	3.3×10^9	2.9×10^9	3.7×10^8	3.1×10^8
C_2H_4	6.7×10^8	7.6×10^8	-9.3×10^7	3.7×10^7
C_2H_6	1.7×10^9	1.3×10^8	1.6×10^9	2.3×10^{10}
CH_3C_2H	1.9×10^8	2.0×10^8	-7.6×10^6	2.8×10^7
CH_2CCH_2	1.5×10^8	1.5×10^8	-1.1×10^6	2.5×10^6
C_3H_6	1.1×10^8	1.1×10^8	6.6×10^5	3.9×10^6
C_3H_8	3.7×10^7	4.1×10^6	3.3×10^7	1.0×10^{10}
C_4H_2	1.8×10^9	1.8×10^9	-2.2×10^6	1.4×10^6
C_4H_6	9.8×10^7	9.8×10^7	6.5×10^4	4.4×10^4
C_4H_8	2.7×10^6	2.6×10^6	9.2×10^4	3.9×10^6
C_4H_{10}	3.6×10^7	6.2×10^6	3.0×10^7	5.5×10^9
C_6H_2	3.7×10^6	3.7×10^6	2.5×10^4	3.4×10^6
C_6H_6	2.0×10^8	2.0×10^8	4.6×10^5	4.8×10^5
C_8H_2	5.7×10^4	5.8×10^4	-1.0×10^3	3.4×10^6
CO	1.8×10^7	2.2×10^7	-4.1×10^6	7.8×10^{11}
CO_2	3.3×10^6	2.0×10^5	3.1×10^6	2.2×10^{10}
H_2O	3.9×10^6	7.3×10^6	-3.4×10^6	1.3×10^8
H_2CO	1.3×10^6	3.7×10^5	9.1×10^5	7.7×10^7
CH_3OH	4.3×10^3	4.6×10^3	-2.6×10^2	1.0×10^8
CH_2CO	4.6×10^6	4.6×10^6	9.3×10^3	1.9×10^6
HCN	4.1×10^8	4.0×10^8	2.1×10^6	1.4×10^9
CH_3CN	8.5×10^6	8.5×10^6	-3.4×10^4	1.3×10^9
C_2N_2	2.4×10^6	3.5×10^5	2.0×10^6	8.0×10^6
HC_3N	2.0×10^8	1.9×10^8	1.3×10^7	2.5×10^7
C_2H_3CN	2.5×10^8	2.3×10^8	1.6×10^7	1.6×10^6
C_4N_2	7.3×10^6	6.4×10^6	9.7×10^5	3.7×10^6
N^+	4.7×10^7	4.7×10^7		
N_2^+	1.6×10^8	1.6×10^8		
CH_3^+	1.5×10^8	1.5×10^8		
CH_4^+	1.0×10^7	1.0×10^7		
$C_2H_5^+$	9.3×10^7	9.3×10^7		
H_2CN^+	1.5×10^8	1.5×10^8		
e^-	1.8×10^8	1.8×10^8		

[a]Species that have long lifetimes compared to a solar cycle are italicized.

in this model to have a branching ratio of 0.5 for this reaction. This mechanism for forming methylacetylene and allene is not considered in other Titan photochemical models. With this assumption, the CH_3C_2H profile shown in Figure 10 agrees well with observations as opposed to *Toublanc et al.* [1995], which is a factor of six too large or *Lara et al.* [1996], which is two orders of magnitude too small (Table 8).

[57] Notwithstanding the effect of aerosol opacity, the model-generated propane profile has a similar uniform shape in the homosphere as the *Yung et al.* [1984], *Lara et al.* [1996], and *Lebonnois et al.* [2001]. The *Toublanc et al.* [1995] C_3H_8 profile shape differs with propane peaking at 500 km, mainly a product of their chemical scheme which results in a C_3H_8 net production rate 15 times larger than the *Lara et al.* [1996] or our nominal rate. In our model, the C_3H_8 abundance is governed by the synthesis of ethyl and methyl radicals (R51b) above 140 km, and the self-reaction of C_3H_7 radicals (R81) below 140 km, which facilitates the recycling of propane in the stratosphere, via H_2-elimination in propane photolysis (J15a) and subsequent hydrogen attachment (R72). The omission of this recycling mechanism in the *Lara et al.* [1996] scheme is responsible for their C_3H_8 fall-off above 100 km. 89% of propane created is lost to condensation below 50 km.

[58] The diacetylene profile compares well with the IRIS observations while both *Toublanc et al.* [1995] and *Lara et al.* [1996] overpredict C_4H_2 abundance, by a factor of three and two, respectively, due to smaller eddy mixing in the stratosphere. The C_4H_2 profile shape compares similarly to the *Lebonnois et al.* [2001] C_4H_2 equatorial profile shape, although the nominal profile exhibits larger diacetylene densities in the stratosphere as a result of larger acetylene mixing ratios, compared to the *Lebonnois et al.* [2001] C_2H_2 equatorial profile. Diacetylene reacts with the photo-

Table 8. A Comparison of Model-Generated Species Abundances Along With Available Observations[a]

Species	Altitude, km	Observational Limits	Y84	T95	La96/B00	Le01/Le02	Nominal With Fractal/Mie Haze
C_2H_2	125	1.3–2.9(−6) (IRIS)	4.3(−5)	2.2(−6)	3.0(−6)[b]	1.9(−6)	1.9(−6)/1.1(−6)
C_2H_4	125	0.4–1.2(−7) (IRIS)	3.1(−7)	3.2(−9)	8.3(−8)	2.1(−8)	9.4(−9)/1.5(−8)
C_2H_6	125	0.6–1.8(−5) (IRIS)	2.0(−4)	1.2(−5)	8.7(−6)	2.7(−6)	5.8(−6)/1.2(−5)
CH_3C_2H	105	2.3–6.1(−9) (IRIS)	9.5(−7)	1.4(−8)	2.3(−11)/<1.0(−11)	9.8(−10)	1.8(−9)/6.6(−10)
C_3H_8	105	0.3–1.1(−6) (IRIS)	4.2(−6)	2.8(−7)	1.0(−7)[c]	2.4(−7)	6.3(−8)/2.8(−7)
C_4H_2	105	0.7–2.0(−9) (IRIS)	1.6(−10)	6.8(−9)	4.7(−9)[d]	3.9(−9)	6.2(−10)/1.9(−9)
C_6H_6	110	1.0–7.0(−10) (ISO)	–	–	–	<1.0(−13)	6.1(−10)/5.8(−11)
CO_2	105	0.9–1.7(−8) (IRIS)	5.7(−9)	4.6(−13)	5.5(−9)	–	6.2(−9)/5.8(−9)
H_2O	400	0.4–1.4(−8) (ISO)	1.2(−9)	3.1(−9)	1.9(−8)	–	1.1(−8)/1.0(−8)
HCN	110	0.5–1.6(−7) (IRAM)	3.8(−6)	1.6(−7)	1.2(−7)/4.0(−8)	1.3(−7)	1.4(−7)/3.2(−7)
	300	0.03–1.2(−5) (IRAM)	9.7(−6)	2.2(−6)	6.4(−6)/2.3(−6)	7.9(−7)	1.3(−6)/2.0(−6)
CH_3CN	450	2.2–6.2(−8) (IRAM)	–	1.2(−7)	7.3(−9)[e]	7.8(−7)	9.6(−9)/8.0(−9)
HC_3N	105	1.5–8.5(−10) (ISO)	3.3(−7)	<1.0(−12)	2.4(−8)/1.4(−8)	3.2(−8)	1.2(−8)/1.2(−10)
	450	2.2–6.2(−8) (IRAM)	3.1(−6)	4.1(−6)	3.9(−6)/3.1(−6)	1.3(−6)	4.0(−8)/3.7(−8)
C_2N_2	105	≤1.0(−9) (IRIS)	1.1(−7)	<1.0(−12)	4.5(−12)/1.6(−11)	1.5(−9)	1.1(−9)/1.6(−13)
C_2H_3CN[f]	105	–	–	–	–	6.6(−9)	2.1(−8)/8.8(−12)
C_4N_2[f]	105	–	–	–	1.2(−11)/1.7(−12)	–	1.4(−9)/6.2(−12)
H_2CO[f]	120	–	<1.0(−11)	9.1(−12)	–	–	1.0(−9)/4.1(−9)
CH_3OH[f]	120	–	–	1.6(−9)	–	–	4.5(−13)/1.0(−14)
CH_2CO[f]	120	–	<1.0(−11)	3.2(−9)	–	–	2.4(−11)/2.2(−11)

[a]Read 1.0(−9) as 1.0×10^{-9}. Y84 = *Yung et al.* [1984]; T95 = *Toublanc et al.* [1995]; La96 = *Lara et al.* [1996]; B00 = *Banaszkiewicz et al.* [2000]; Le01/Le02 = *Lebonnois et al.* [2001] (equator), *Lebonnois et al.* [2002].
[b]Mixing ratio at 130 km.
[c]Mixing ratio at 110 km.
[d]Mixing ratio at 125 km.
[e]Mixing ratio at 400 km.
[f]This species has not yet been observed in Titan's atmosphere.

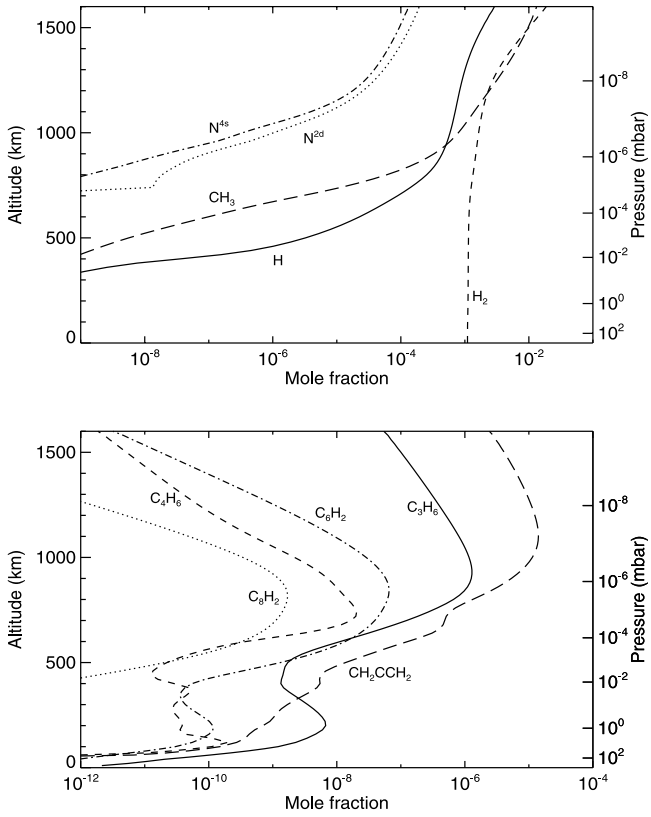

Figure 14. Nominal constituent profiles for various hydrocarbon species along with atomic nitrogen, atomic hydrogen, and molecular hydrogen.

lytic products of C_2H_2 and C_4H_2 to form C_6H_2 and C_8H_2, whose profiles are shown in Figure 14. These processes may have implications in the formation of Titan haze between 500–800 km.

[59] *Wilson et al.* [2003] suggested the possibility of benzene formation in Titan's atmosphere, corroborated by the tentative detection of benzene by the Infrared Space Observatory (ISO) [*Coustenis et al.*, 2003]. The observation fit by a uniform mole fraction profile of $4 \pm 3 \times 10^{-10}$ was matched by a vertical profile of benzene from *Wilson et al.* [2003], multiplied by 3.0 ± 0.5, an upper-limit profile calculated assuming reaction rates for aromatic compounds that correspond to a temperature of 300 K. However, aerosol opacity was not considered in that calculation. Haze particles act to shield benzene from photodissociation, which extends as far as 2700 Å [*Pantos et al.*, 1978]. Figure 15 compares the nominal benzene profile from *Wilson et al.* [2003] with the present nominal profiles including aerosols and calculated with the nominal temperature profile, taken from *Yelle et al.* [1997], which ranges from 71 K at the tropopause to 175 K in the thermosphere. The present profile matches the ISO observation with a column density of 2.4×10^{15} cm^{-2} s^{-1} above 30 mbar, with a benzene mole fraction of 6.1×10^{-10} at 110 km. The only other modeling study that covers benzene abundance on Titan is *Lebonnois et al.* [2002], which calculates a benzene mole fraction at least three orders of magnitude smaller at the observation altitude. Figure 15 also demonstrates the large dependence on solar flux for benzene abundance in the upper atmosphere. *Wilson and Atreya* [2003] explored possible mechanisms for haze formation and suggested that aromatic compounds like benzene could be a source of Titan haze. Assuming this nominal benzene profile and that the mechanism for haze formation begins with the reactions

(R115) $C_6H_6 + C_2H \rightarrow haze$

(R112) $C_6H_5 + C_2H_2 \rightarrow haze,$

the aromatic pathway provides a haze production rate of 9.5×10^6 cm^{-2} s^{-1} or 3.2×10^{-14} g cm^{-2} s^{-1}, assuming a nucleation mass of 2000 amu [*Richter and Howard*, 2000], compared with $0.5–2 \times 10^{-14}$ g cm^{-2} s^{-1} derived by microphysical models [*McKay et al.*, 2001].

[60] An important uncertainty in modeling chemistry in outer planetary atmospheres is the methyl recombination rate. Methyl recombination serves as the primary loss mechanism for the chemically important methyl radical as well as the source of ethane production. However, until recently, rate measurements have only been taken as low as room temperature, with extrapolations down to lower temperatures yielding widely varying results [*Atreya et al.*, 1999]. ISO observations of CH_3 seem to indicate that the more widely used *Slagle et al.* [1988] rate expression is too low, perhaps by an order of magnitude. For this reason, we use a methyl recombination rate that is ten times that obtained with the *Slagle et al.* [1988] expression. Studies comparing hydrocarbon mixing ratio profiles using both the *Slagle et al.* [1988] rate and our rate indicate little difference in the ethane stratospheric profile and a factor a two increase in ethane density in the upper atmosphere with our rate [*Wilson and Atreya*, 2000a]. Recently, *Cody et al.* [2003] have measured methyl recombination at lower temperatures, obtaining results at as low as 155 K. These results find

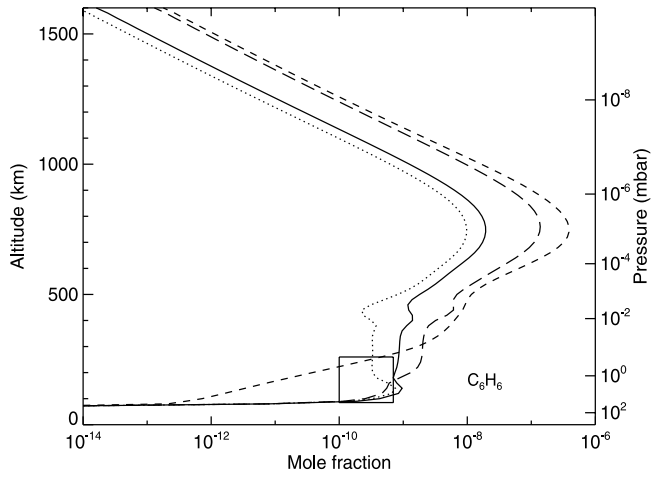

Figure 15. Benzene profiles for average solar maximum (long dashed line), solar moderate (solid line), and solar minimum conditions (dotted line), along with the *Wilson et al.* [2003] nominal benzene profile (short dashed line). The box represents the ISO benzene observations including error bars in abundance and altitude.

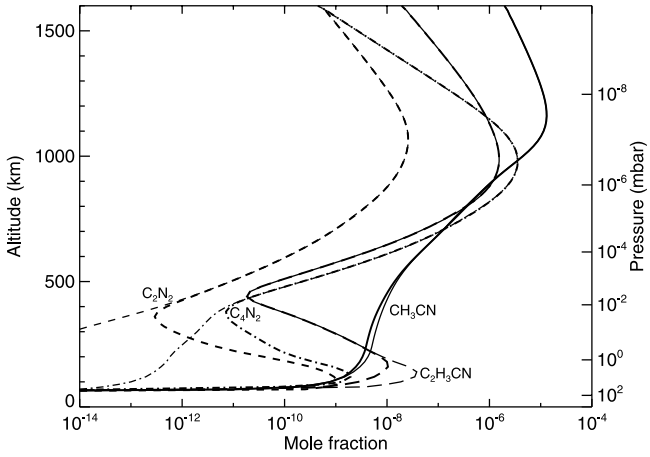

Figure 16. Constituent profiles of various nitrile species including cosmic ray deposition (thick line) and no cosmic ray deposition (thin line).

methyl recombination to proceed at roughly 1.6 times the *Slagle et al.* [1988] rate at high pressures. However, these experiments were conducted with He as a bath gas, and the reaction may proceed faster with N_2 as the background atmosphere as exhibited by the hydrogen atom recombination reaction, which proceeds 60% faster at 150 K with the *Tsang and Hampson* [1986] rate which uses an N_2 bath gas, as opposed to the *Baulch et al.* [1992] rate which uses an H_2 bath gas. Using the *Cody et al.* [2003] rate, the nominal ethane density in the upper atmosphere is reduced by 55% at 1100 km and reduced by 6% at 200 km, while the CH_3 density is increased by 145% and 35%, respectively, at those altitudes.

5.4. Nitriles

[61] Cosmic rays can play a substantial role in the formation of nitriles. Cosmic rays penetrate the atmosphere and dissociate nitrogen molecules (Figure 4b), producing N atoms that serve as a source for stratospheric nitriles, in particular, nitriles that are formed directly from N-atom addition. In addition, *Molina-Cuberos et al.* [2002] demonstrated that the possible formation of ion clusters in this region through high pressure reactions may be a source of stratospheric nitriles. The kinetics and identification of products of these reactions, however, are still to be determined. Figure 16 shows the profiles of several nitrile compounds with and without the inclusion of galactic cosmic rays. In particular, the stratospheric abundances of C_2N_2 and C_4N_2 are highly dependent on cosmic ray dissociation of nitrogen, through the schemes (S20) and (S21). Treatment of cosmic ray interaction through particle cascade, illustrated by *Capone et al.* [1983], may increase C_2N_2 and C_4N_2 densities in the lower atmosphere further.

[62] *Lara et al.* [1996] in order to explain the CH_3CN observations announced by *Bézard et al.* [1993] propose a source provided by CH_4 + CN and C_2H_6 + CN. Previous studies [*Hess et al.*, 1989; *Yang et al.*, 1992b; *Sims et al.*, 1993], however, give no indication of an acetonitrile channel, while *Balla et al.* [1991] point out that though the CH_3CN channel is thermodynamically possible, their measurements only indicate traces of CH_3CN. Nevertheless, *Lara et al.* assume a quantum yield for the production of 0.05 for CH_4 + CN and 0.035 for C_2H_6 + CN. The reaction $N^{2d} + C_2H_4$ was taken to proceed at a rate of 1.2×10^{-12} cm^{-3} s^{-1} by *Lellouch et al.* [1994] in their Neptune model, on the basis of N^{2d} quenching coefficients by *Black et al.* [1969]. They predicted the reaction to proceed in an insertion/abstraction manner, producing products NH and C_2H_3. This reaction was included in the *Lara et al.* model, while *Toublanc et al.* [1995] and *Yung* [1987] did not include this reaction. However, *Sato et al.* [1999] measured $N^{2d} + C_2H_4$ down to 230 K and obtained a rate of 2.6×10^{-11} cm^{-3} s^{-1}, a rate over 20 times that assumed by *Lellouch et al.* [1994] and *Lara et al.* [1996]. Furthermore, crossed-beam experiments conducted by *Balucani et al.* [2000] indicate CH_3CN to be the likely product

$$\text{(R127)} \qquad N^{2d} + C_2H_4 \rightarrow CH_3CN + H.$$

Including (R127) with the *Sato et al.* [1999] rate produces a profile (Figure 16) that matches observations reasonably well, producing acetonitrile primarily in the upper atmosphere through the scheme

$$\text{(S33)} \qquad \begin{array}{c} 0.5(N_2 + h\nu \rightarrow 2N^{2d}) \\ N^{2d} + C_2H_4 \rightarrow CH_3CN + H \\ \hline 0.5N_2 + C_2H_4 \rightarrow CH_3CN + H \end{array}.$$

[63] Notwithstanding the nominal C_2H_3CN profile (Figure 16), which presents a stratospheric mixing ratio as high as 3.8×10^{-8}, observations suggest the lack of significant abundance of acrylonitrile in this region of the atmosphere. C_2H_3CN has not been identified in the atmosphere of Titan by IRIS or ISO observations. Furthermore, Voyager infrared spectra analysis do not seem to advocate the presence of acrylonitrile condensates in larger abundances than say C_2N_2 or C_4N_2. In the nominal model, acrylonitrile stratospheric production, despite the low rate coefficient for (R156), is clearly dominated by (S23) over (S22). *Monks et al.* [1993] assume an addition-decomposition process as the favored mechanism of (R156) through analogy with (R155) and (R29). However, a definitive yield for acrylonitrile production was not given as only trace amounts of C_2H_3CN were identified in the experiment. Thus an excessively large reaction rate for acrylonitrile production through (R156), as well as excessive aerosol opacity in the NUV as discussed in section 5.2, are possible explanations for the large stratospheric abundance of C_2H_3CN calculated by the model.

5.5. Will Ammonia Be Detected?

[64] Ammonia has not been detected in Titan's atmosphere but does serve prominently in Saturn's atmosphere and may have played a significant role in the formation of Titan's present nitrogen inventory [*Atreya et al.*, 1978; *Atreya and Wilson*, 2001]. *Bernard et al.* [2003] detected ammonia in their electron discharge simulations of Titan's atmosphere. They correctly point out that the source of ammonia molecules would likely arise through charged-particle chemistry. Apart from a supply of primordial NH_3 from the interior, any ammonia in Titan's strato-

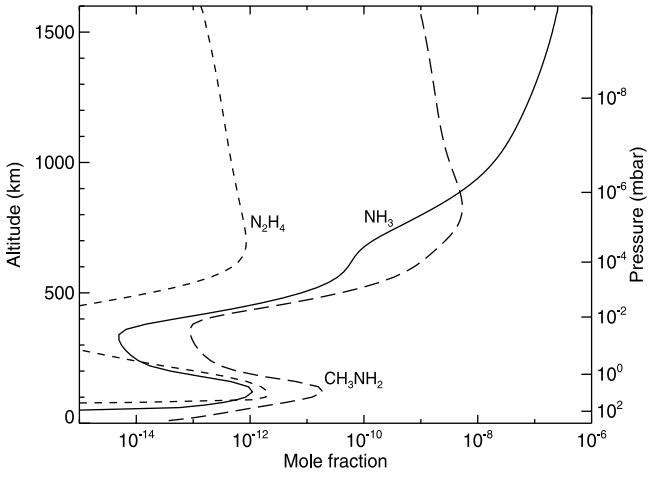

Figure 17. Constituent profiles for various amine species.

sphere will be the result of cosmic-ray ionization of N_2, through the mechanism

$$\begin{array}{c} N_2 + GCR \rightarrow N^+ + N + e^- \\ CH_4 + N^+ \rightarrow HCN^+ + H_2 + H \\ CH_4 + HCN^+ \rightarrow C_2H_3^+ + NH_2 \\ NH_2 + H \xrightarrow{M} NH_3 \\ \hline N_2 + 2CH_4 \rightarrow NH_3 + N + H_2 + C_2H_3^+ + e^- \end{array} \quad \text{(S34)}$$

[65] However, this mechanism results in an ammonia mole fraction of only 9.6×10^{-13} at 120 km (Figure 17). The profile of NH_3 indicates a decrease in mole fraction above this level as a result of smaller cosmic ray precipitation, followed by an increasing profile with altitude at higher levels due to the greater influence of precipitating electrons in the upper atmosphere. In this region, electron recombination of ammonium ions, as suggested by *Atreya* [1986], is the most likely ammonia source. The larger estimate for NH_3 by *Bernard et al.* [2003] is most likely a result of the use of electron discharge as the primary energy source.

[66] The amino radical (NH_2), produced through (R336a), is responsible for the formation of other amine species, such as N_2H_4(R174b) and CH_3NH_2(R175). Figure 17 shows methylamine (CH_3NH_2) as the most abundant of the amine species in the stratosphere. However, barring a significant source of primordial ammonia, the low densitites of ammonia may preclude detection by Cassini-Huygens.

5.6. Oxygen Species

[67] Buoyed by the recent detection of H_2O on the giant planets, *Feuchtgruber et al.* [1997] estimate a water influx of $3–50 \times 10^5$ cm^{-2} s^{-1}. With the recent detection of H_2O in Titan's atmosphere, it is evident that this applies to Titan as well. CO is the most abundant oxygen-bearing molecule in Titan's atmosphere. Sensitive millimeter observations have found a uniformly mixed carbon monoxide profile at $\sim 5 \times 10^{-5}$ [*Muhleman et al.*, 1984; *Gurwell and Muhleman*, 1995], although further millimeter observations [*Hidayat et al.*, 1998] and near infrared observations [*Noll et al.*, 1996] have suggested lower abundances with stratospheric depletion. Using a surface CO mole fraction of 5×10^{-5} from the *Gurwell and Muhleman* [1995] finding of $5 \pm 1 \times 10^{-5}$ and an external H_2O influx of 5×10^6 cm^{-2} s^{-1} [*Feuchtgruber et al.*, 1997], abundances are calculated for oxygen-bearing species, shown in Figure 18.

[68] ISO confirmed the existence of water vapor in Titan's atmosphere as *Coustenis et al.* [1998] found a uniform H_2O profile at 4×10^{-10} consistent with the obtained H_2O spectrum. However, scaling the *Lara et al.* [1996] H_2O model profile by a factor of 0.4 yielded a profile with an H_2O mole fraction of $8^{+6}_{-4} \times 10^{-9}$ at 400 km to fit the ISO data. The nominal model finds agreement with this observation as shown in Figure 18.

[69] With (R219) as the primary source of CO_2, the IRIS carbon dioxide observations argue for an external source of water. *Coustenis et al.* [1989] found a uniform mole fraction profile of $1.4^{+0.3}_{-0.5} \times 10^{-8}$ to fit IRIS observations, although a linear scaling of a altitude-dependent CO_2 profile of *Samuelson et al.* [1983], yielding a CO_2 mole fraction of 1.4×10^{-8} at 1.5 mbar where the value of the CO_2 contribution function was about 35% of the peak value at 4 mbar, provided a decent fit. The nominal profile of CO_2 is consistent with the IRIS observations, rendering a CO_2 mole fraction of 1.4×10^{-8} at 4 mbar.

[70] The nominal model predicts much lower abundances for CH_2CO and CH_3OH in the stratosphere than *Toublanc et al.* [1995] as a result of including photolysis which provides

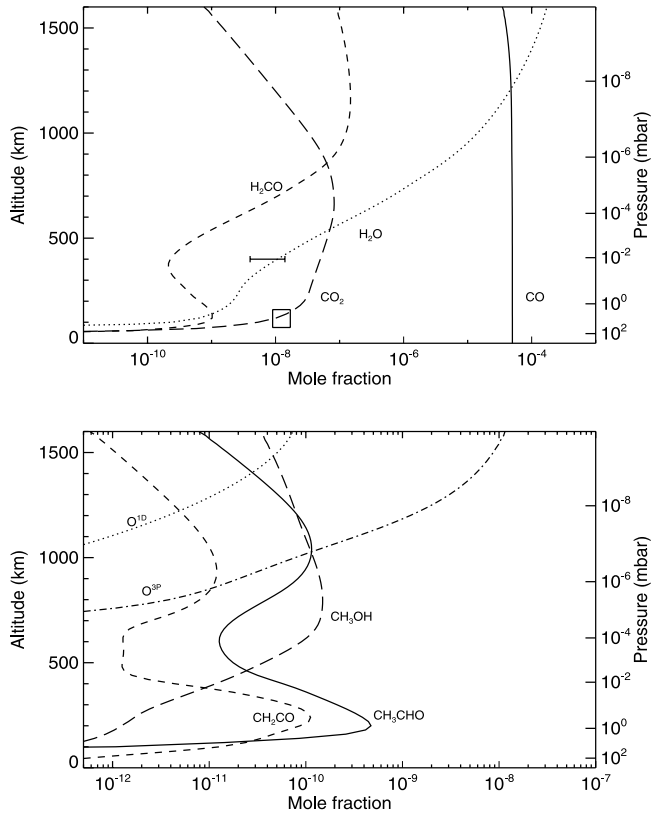

Figure 18. Constituent profiles for various oxygen-bearing species with the horizontal bar representing the ISO H_2O observations based on the *Lara et al.* [1996] profile, and the box representing the Voyager IRIS CO_2 observations.

the main sink for these compounds. *Toublanc et al.* [1995] refer the absorption cross section of ketene to that of H_2O, although the absorption cross section for CH_2CO extends past 3000 Å [*Rabalais et al.*, 1971], much further than that of H_2O (2000 Å). Furthermore, the nominal model includes the measurement of the CH_3OH cross section [*Wodtke and Lee*, 1987], not included in previous models.

[71] However, formaldehyde is predicted to be in greater abundance than in previous models, perhaps near the levels of detection in the stratosphere. H_2CO is formed through self-reaction of formic acid (HCO), which is produced via pressure-dependent H-attachment to CO, demonstrated in (S29). The calculated H_2CO mole fraction of 1.0×10^{-9} at 4 mbar and the corresponding condensation at the tropopause indicate the possibility of detection of H_2CO gas and condensate by the GCMS, CIRS, and ACP instruments during the upcoming Cassini-Huygens exploration.

[72] The significant abundance of formaldehyde also suggests the possibility of detection of ethylene oxide (C_2H_4O) in Titan's stratosphere. Ethylene oxide was detected in the Titan simulations of *Bernard et al.* [2003], although they did not detect formaldehyde, presumably a result of the lack of water in their experiments. The isomer of ethylene oxide, acetaldehyde (CH_3CHO) is largely produced through the synthesis of methyl radicals and formic acid at higher pressures (R223) and it is redistributed in the oxygen family via reaction with N atoms (R283), released by cosmic rays, and through photolysis. This balance results in a calculated peak CH_3CHO mole fraction of 4.7×10^{-10} at 1 mbar, suggesting possible identification by Cassini-Huygens. Ethylene oxide, on the other hand, is formed less efficiently in Titan's atmosphere, produced by the synthesis of ethylene and oxygen atoms [*Gaedtke et al.*, 1973]. Considering this synthesis and the photodissociation of C_2H_4O [*Fleming et al.*, 1959], ethylene oxide is expected to be present in Titan's atmosphere in abundances of 1–2 orders of magnitude less than acetaldehyde.

[73] A major question involving the distribution of these oxygen-bearing molecules is what the source of carbon monoxide is. *Samuelson et al.* [1983] suggested a source from the water influx through the mechanism $OH + CH_3 \rightarrow CO + 2H_2$. However, this was an overall reaction mechanism that was measured by *Fenimore* [1969]. No laboratory studies [e.g., *De Avillez Pereira et al.*, 1997; *Fagerström et al.*, 1993] have detected CO as a product of this reaction, and no mechanism involving the products of $CH_3 + OH$ forming CO is evident. *Lara et al.* [1996] calculated an upward flux from the surface of 1.6×10^6 cm^{-2} s^{-1} necessary to maintain an mole fraction of 5×10^{-5} in equilibrium, which they deem to be unlikely over the course of Titan evolution. Consequently, they have suggested that CO may be provided directly from the influx of micrometeorites, although a typical cometary inventory of CO does not provide enough influx to achieve equilibrium.

[74] Primordial CO remains the most likely source. *Bézard et al.* [2002] report the likelihood that CO is primordial on Jupiter, on the basis of the CO abundance in the troposphere. The Titan nominal model calculates an upward CO flux of 3.9×10^6 cm^{-2} s^{-1} necessary to maintain photochemical equilibrium. Oxygen is lost from the atmosphere through condensation of CO_2 and H_2CO, which combines for an upper limit condensation flux of 4.0×10^6 cm^{-2} s^{-1} as determined by the net production rate shown in Table 7. Surficial processes such as outgassing from the interior or irradiation of CO_2 and H_2CO condensates may balance this oxygen loss to the surface, providing a source for CO. Another possibility is that CO is not in equilibrium and was more abundant in Titan's past. *Wong et al.* [2002] postulate that CO may have been as much as 14 times more abundant after the initial escape stage in Titan's early evolution.

5.7. Charged Particles

[75] As shown in section 4.4, ions produced through N_2 and CH_4 ionization, in particular N_2^+, N^+, CH_4^+, and CH_3^+ begin the chemical processes that furnish Titan's ionosphere. Figure 19 shows the relative importance of photoionization and photoelectron-impact ionization in the formation of these ions. Electron impact becomes important only below 1000 km, providing an important source in the lower part of this ionospheric region. Five times more N_2^+ than N^+ is produced at the peak of ion production through N_2 ionization, facilitating the formation of abundant ions $C_2H_5^+$ and H_2CN^+ through (S28) and (S29). Comparing these production rates with previous Titan ionosphere models show that the *Keller et al.* [1992] model provides an N_2^+ production rate peak due to photoionization about three times larger than the nominal profile and about twice as large for CH_4^+, while *Banaszkiewicz et al.* [2000] exceeds the nominal rates by 3.5 and 3 times, respectively. The reason for this discrepancy is not evident, but the fact that *Banaszkiewicz et al.* [2000] consider photoionization at a solar zenith angle of 30° would certainly be a factor in enhancing their photoionization rates with respect to the nominal model.

[76] The *Banaszkiewicz et al.* [2000] model shows a significant decrease in the CH_4 ionospheric density due to the inclusion of ion chemistry. However, our results indicate that loss of CH_4 through chemistry, which is larger than determined by *Lara et al.* [1999], peaking at 13 cm^{-3} s^{-1} at 1040 km for solar maximum conditions, is more than replenished by the transport of methane from lower altitudes. An increase in the electron flux by a factor of 10 would be necessary to deplete methane whereby the mole fraction decreases with altitude in this region (Figure 20a), but such an increase would result in a peak electron density of 9740 cm^{-3} (Figure 20b), 2–4 times larger than observations.

[77] With the influence of EUV radiation on the formation of electrons, the electron density has a strong dependence on solar conditions, as exhibited in Figure 21a. For solar maximum conditions, consistent with those which took place during the Voyager flyby, the nominal model calculates an electron density profile which peaks at a density of 4200 cm^{-3} at 1060 km, 20% larger than the upper limit of the *Bird et al.* [1997] radio occultation observations. Considering the differences in production rates, it is not surprising that electron densities of *Keller et al.* [1992] and *Banaszkiewicz et al.* [2000] are larger by about 40% than the nominal model. Assuming electron-impact processes to be scaled for solar minimum and solar moderate conditions, Figure 21a shows a 24% decrease in the peak electron concentration from solar maximum

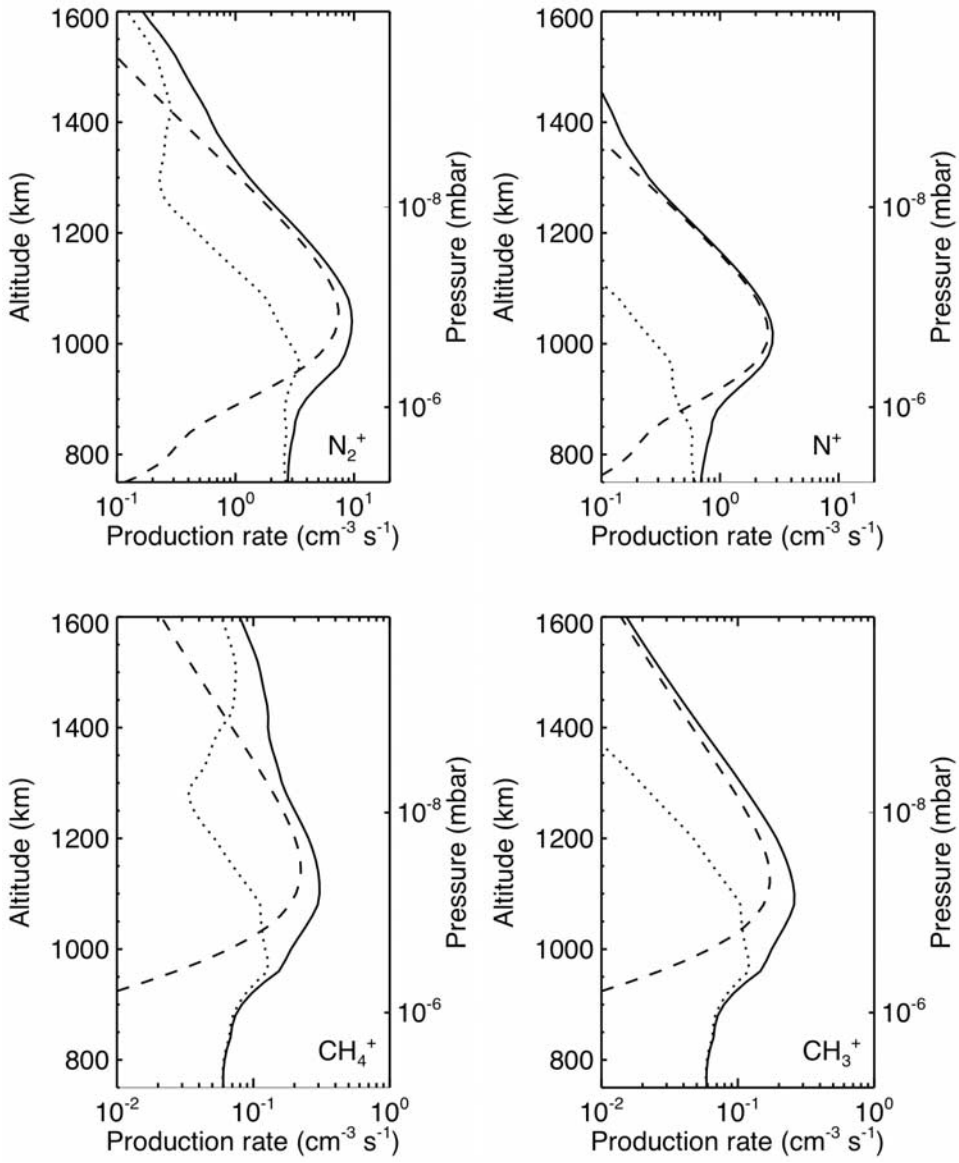

Figure 19. Production rates of N_2^+, N^+, CH_4^+, and CH_3^+ ions from photoionization (dashed line), electron impact (dotted line), and the sum of the two processes (solid line).

conditions for moderate solar activity, which should have implications in the INMS observations from the upcoming Cassini-Huygens mission.

[78] Nominal ion densities, calculated for solar maximum conditions, are shown in Figures 21b and 21c. In agreement with *Banaszkiewicz et al.* [2000] and *Keller et al.* [1992] the nominal model finds H_2CN^+ as the major ion above 1000 km. Below this level, a pseudoion representing the collection of larger ions not considered separately in the model is found to dominate, necessitating the kinetic study and modeling of higher order ions.

[79] The most abundant oxidized ion is H_3O^+, formed by

$$\begin{array}{c} 2CH_4 \rightarrow C_2H_5^+ + H_2 + H + e^- \\ C_2H_5^+ + H_2O \rightarrow H_3O^+ + C_2H_4 \\ \hline 2CH_4 + H_2O \rightarrow H_3O^+ + C_2H_4 + H_2 + H + e^- \end{array} \quad \text{(S35)}$$

However, the primary function of H_3O^+ is recycling back to H_2O, through

$$H_3O^+ + HCN \rightarrow H_2CN^+ + H_2O, \quad \text{(R494)}$$

as shown in (S23).

[80] In the stratosphere, an ionosphere develops as well, as a result of cosmic ray ionization of nitrogen. Methane cosmic ray destruction, which is shielded by nitrogen, occurs at a much lesser extent. This cosmic ray deposition, which plays a significant role in nitrile chemistry in the stratosphere as shown previously, results in an electron peak of 1410 cm^{-3} at 120 km for maximum solar conditions. This value increases to 2010 cm^{-3} (Figure 4b) with a moderate sun, as cosmic rays diffuse more efficiently during periods of reduced solar activity [*Jokipii and Kopriva*, 1979]. As products of reactions with larger stable molecules

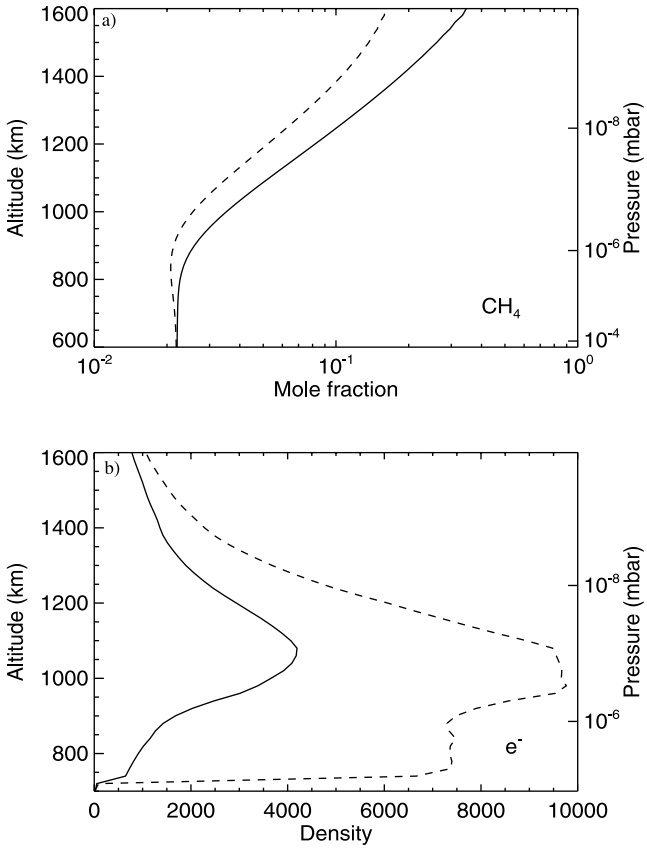

Figure 20. a) CH_4 mole fraction and b) electron density profiles for maximum solar conditions with nominal electron fluxes (solid line) and 10 × nominal electron fluxes (dashed line).

like ethane and acetonitrile, ions like $C_4H_7^+$(R413b), $C_2H_7^+$(R376b), HCO^+(R379), CH_3CNH^+(R347), and $C_5H_5^+$(R430), serve as the gateway to the formation of the large ions which populate Titan's lower ionosphere, as demonstrated by *Molina-Cuberos et al.* [1999]. Ion clusters, as stated before, may also play a significant role in the lower ionosphere.

6. Conclusions

[81] The results of a one-dimensional photochemical model of Titan's neutral constituents and charged particles have been reported. This model contains updated chemistry and an extensive treatment of dissociation processes from solar photons at 50–3000 Å and electrons at 15–1000 eV, as well as parameterization of processes including galactic cosmic rays, magnetospheric electrons, and opacity provided by fractal haze particles.

[82] A test of various eddy diffusion profiles has revealed a profile with a homopause level of 850 km to provide the best fit to IRIS and ISO stratospheric observations as well as UVS observations in the upper atmosphere. With such a profile, fitted with the assumption of methane supersaturation near the tropopause, as analyzed by the *Samuelson et al.* [1997] study, the nominal model provides a good fit for the bulk of Titan stratospheric observations and provides a reasonable fit for most of the Voyager UVS reanalysis observations, an improvement over previous models. In this model, loss of HCN due to polymerization to Titan haze is not required to match observations. The profile of *Lara et al.* [2002], derived with a more extreme scenario of tropospheric methane supersaturation suggested by *Courtin et al.* [1995], was also tested. This profile, although providing a good fit of CH_4 and HCN observations, significantly underestimates stratospheric CH_3C_2H and overestimates C_4H_2 in the lower and middle atmosphere. The nominal profile, assuming opacity provided by fractal haze particles from *Lebonnois et al.* [2001], underpredicts the C_3H_8 stratospheric mole fraction by about a factor of two, while rendering profiles for HC_3N and C_2H_3CN that are not consistent with the lack of firm detection by the IRIS equatorial observations. Assuming Mie haze opacities, these profiles fall much more in line with what has and has not been observed, suggesting that the opacities for the fractal case used in the model may be too large.

[83] Dynamics is certain to play an important role in the distribution of Titan's constituents and the effect of dynamical processes should certainly be explored. However,

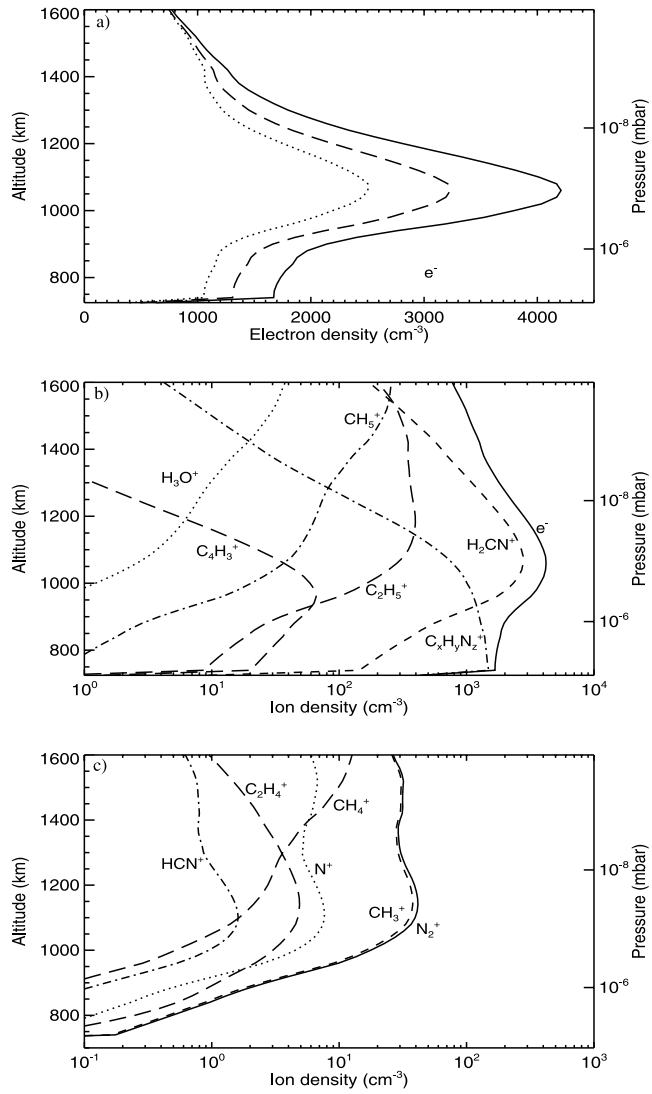

Figure 21. Density distribution of ions in Titan's upper ionosphere.

considering the limitations of existing observations, the uncertainties in other parameters such as aerosol opacity, and the results of the model, it is not possible to rule out the possibility that the globally averaged distribution of Titan's constituents can be accurately and simultaneously described with a single eddy-diffusion profile.

[84] Considering the differences in the expected solar flux during the upcoming Cassini-Huygens mission and the more enhanced solar flux during the Voyager flyby of Titan, sensitivity to variations in solar flux during the course of solar cycle has been explored. With the large chemical lifetimes of most of the stable constituents in Titan's atmosphere, only C_4H_2 demonstrated significant sensitivity among likely observed species, with stratospheric densities for moderate solar conditions reduced by about 60% from solar maximum conditions and a variation of a factor of three from solar maximum to solar minimum.

[85] The profile of C_6H_6 is improved on the basis of ISO observations [*Coustenis et al.*, 2003], compared with previous studies by the authors [*Wilson et al.*, 2003]. The inclusion of haze opacity sharply reduces the amount of benzene photolysis, the primary sink for C_6H_6 in the stratosphere. With this inclusion, the profile of C_6H_6 under nominal Titan temperature dependency matches the ISO observations and suggests a mechanism for haze production peaking at 180 km.

[86] A mechanism for the formation of CH_3C_2H is proposed with the aid of the kinetic measurements of *Canosa et al.* [1997]. Assuming a branching ratio of 0.5 for methylacetylene production through CH + C_2H_4, the profile of CH_3C_2H finds good agreement with observations, over the results of previous models. In agreement with previous models exploring Titan's ionosphere, the dominant ion at the electron peak is found to be H_2CN^+, with larger ions making up the bulk of Titan's ionosphere below 1000 km. The peak of electron density is found to be 4200 cm^{-3}, a 20% enhancement over the observations of *Bird et al.* [1997]. The electron peak density is expected to be reduced by about 24% for moderate solar conditions. Cassini-Huygens will encounter variations in the magnetospheric input into the ionosphere. Any major enhancement of magnetospheric electrons over what was found by Voyager should affect the electron density above 1150 km, with no major effect on atmospheric neutrals.

[87] The Cassini-Huygens mission will seek to answer many of the questions explored in this study, among many others. Results from this model indicate the possible detection of H_2CO and C_2H_3CN by the Composite Infrared Spectrometer (CIRS) and the Gas Chromatograph Mass Spectrometer (GCMS), although acrylonitrile abundances may be overpredicted due to chemistry or opacity assumptions. Benzene, already tentatively detected by ISO [*Coustenis et al.*, 2003] is predicted to be observed by these instruments, and the analysis of aerosols by the Aerosol Collector Pyrolyser (ACP) will enhance what we know about the composition and formation processes of Titan's aerosols. Furthermore, observations of constituents like C_2H_2 and CH_3C_2H by the Ultraviolet Imaging Spectrograph (UVIS) and the Ion and Neutral Mass Spectrometer (INMS) will further increase our understanding of the chemical and diffusive processes in the upper atmosphere. This model in conjunction with data can be used as a helpful tool in furthering the understanding of Titan's atmosphere.

Appendix A: Finite Differencing and Matrix Solver

[88] The photochemical model solves the continuity-diffusion equation in spherical coordinates, accounting for condensation,

$$P_i - L_i - \gamma_i = \frac{1}{r^2}\frac{\partial(r^2\Phi_i)}{\partial r}$$

where Φ_i is taken to be the flux of species i in the radial direction. Multiplying both sides by r^2 and integrating over the interval $[\tilde{r}_1,\tilde{r}_2]$ yields

$$\int_{\tilde{r}_2}^{\tilde{r}_1} \frac{\partial(r^2\Phi_i)}{\partial r}\,dr = \int_{\tilde{r}_2}^{\tilde{r}_1} r^2[P_i - L_i - \gamma_i]dr$$

or

$$\tilde{r}_1^2\Phi_i(\tilde{r}_1) - \tilde{r}_2^2\Phi_i(\tilde{r}_2) = \frac{1}{3}\tilde{r}_1^3[P_i(r) - L_i(r) - \gamma_i(r)] - \frac{1}{3}\tilde{r}_2^3[P_i(r) - L_i(r) - \gamma_i(r)]$$

assuming $P_i - L_i - \gamma_i$ constant over the interval $[\tilde{r}_1,\tilde{r}_2]$. Equations (2) and (4) indicate that $n = n(\xi_1^A, \ldots, \xi_S^A)$ where the $\xi_1^A, \ldots, \xi_S^A$ are the S abundant species which affect the mean molecular weight, defined as species with a mole fraction greater than 10^{-3} for a particular level r. So, $\Phi_i = \Phi_i(n(\xi_1^A, \ldots, \xi_S^A), \xi_i)$ and the P_i, L_i, and γ_i are functions of $n(\xi_1^A, \ldots, \xi_S^A)$ and the $\xi_1, \ldots, \xi_N$ for M species and N atmospheric levels. Charged particles are assumed to be governed solely by chemistry, with $\Phi_i = 0$, and the assumption of charge neutrality

$$n_e = \sum_i n_i$$

where n_e is the electron density and n_i is the density of each ion i.

[89] This system of equations is set up through finite differencing on a grid where the fluxes are expressed in terms of its values at $\tilde{r}_1 = r_{i+1/2}$ and $\tilde{r}_2 = r_{i-1/2}$, assuming that they are linear in the intervals $[i - 1, i]$ and $[i, i + 1]$, while the chemical terms are expressed at $r = r_i$. Thus for a quantity Q,

$$Q(\tilde{r}_1) = \frac{Q(r_{i+1}) + Q(r_i)}{2}, Q(\tilde{r}_2) = \frac{Q(r_i) + Q(r_{i-1})}{2}$$

while

$$\frac{\partial Q(\tilde{r}_1)}{\partial z} = \frac{Q(r_{i+1}) - Q(r_i)}{r_{i+1} - r_i}, \frac{\partial Q(\tilde{r}_2)}{\partial z} = \frac{Q(r_i) - Q(r_{i-1})}{r_i - r_{i-1}}.$$

At the lower boundary, the mixing ratios $\xi_1, \ldots, \xi_N$ and number density n are set to zero or their lower boundary

conditions, shown in Table 5, where n is described by equation (5). At the upper boundary, the flux equations are finite differenced where, using equation (2),

$$\begin{aligned}\Phi_i(\tilde{r}_N) = &-[D_i(\tilde{r}_N)+K(\tilde{r}_N)]n(\tilde{r}_N)\frac{\partial \xi_i(\tilde{r}_N)}{\partial z}\\ &-D_i(\tilde{r}_N)\xi(\tilde{r}_N)\left[\frac{\partial n(\tilde{r}_N)}{\partial z}+n(\tilde{r}_N)\left(\frac{1}{T(\tilde{r}_N)}\frac{\partial T(\tilde{r}_N)}{\partial z}\right.\right.\\ &\left.\left.+\frac{1}{H_i(\tilde{r}_N)}\right)\right]\\ &=\beta_i^{\Phi}\end{aligned}$$

where for quantity Q,

$$Q(\tilde{r}_N)=\frac{Q(r_N)+Q(r_{N-1})}{2},\frac{\partial Q(\tilde{r}_N)}{\partial z}=\frac{Q(r_N)-Q(r_{N-1})}{r_N-r_{N-1}}$$

and β_i^{Φ} = flux boundary condition for species i. For species H and H_2, the velocity equations at the boundary from equation (15) are expressed as

$$\begin{aligned}w_i(\tilde{r}_N) = &-[D_i(\tilde{r}_N)+K(\tilde{r}_N)]\frac{\partial \ln(\xi_i(\tilde{r}_N))}{\partial z}\\ &-D_i(\tilde{r}_N)\left[\frac{\partial \ln(n(\tilde{r}_N))}{\partial z}+\left((1+\alpha_i(\tilde{r}_N))\frac{1}{T(\tilde{r}_N)}\frac{\partial T(\tilde{r}_N)}{\partial z}\right.\right.\\ &\left.\left.+\frac{1}{H_i(\tilde{r}_N)}\right)\right]\\ &=\beta_i^{w}\end{aligned}$$

where for quantity Q,

$$\frac{\partial \ln(Q_i(\tilde{r}_N))}{\partial z}=\frac{1}{Q_i(\tilde{r}_N)}\frac{\partial Q_i(\tilde{r}_N)}{\partial z}=\frac{\ln(Q_i(r_N))-\ln(Q_i(r_{N-1}))}{r_N-r_{N-1}}$$

and β_i^{w} = velocity boundary condition for species i.

[90] Meanwhile, equations (3) and (4) can be combined with expression (1) and expressed in terms of r_{i-1}, r_i, and r_{i+1} to calculate the total density

$$r^2\nabla_r p=-r^2 nmg$$

$$\int_{\tilde{r}_2}^{\tilde{r}_1}\frac{\partial}{\partial r}(r^2p)dr=-GM\int_{\tilde{r}_2}^{\tilde{r}_1}\frac{r^2 nm}{r^2}dr$$

$$\tilde{r}_1^2p(\tilde{r}_1)-\tilde{r}_2^2p(\tilde{r}_2)=-GMn(r)m(r)[\tilde{r}_1-\tilde{r}_2] \qquad \text{(A1)}$$

or, taking condensation into account,

$$\tilde{r}_1^2p(\tilde{r}_1)-\tilde{r}_2^2p(\tilde{r}_2)=-GM[n(r)m(r)-\gamma^c][\tilde{r}_1-\tilde{r}_2]$$

where

$$p(\tilde{r}_1)=\frac{n(\tilde{r}_1)kT(\tilde{r}_1)}{f(\tilde{r}_1)},p(\tilde{r}_2)=\frac{n(\tilde{r}_2)kT(\tilde{r}_2)}{f(\tilde{r}_2)},$$

$$\gamma^c=\begin{cases}[nm(r)-nm^{sat}(r)]^p, m(r)m^{sat}(r)\\ -[nm^{sat}(r)-nm(r)]^p, m^{sat}(r)m(r)\end{cases},$$

and

$$m(r)=\sum_j^S \xi_j^A(r)m\left(\xi_j^A(r)\right).$$

At the boundary ($r=r_N$), since $\tilde{r}_1=R_0+z-\frac{1}{2}\Delta z$ and $\tilde{r}_2=R_0+z+\frac{1}{2}\Delta z$, one can write in equation (A1) $\tilde{r}_2=2(R_0+z)-\tilde{r}_1$ or $\tilde{r}_2=2r_N-\tilde{r}_1$, where $\tilde{r}_1=\frac{r_N+r_{N-1}}{2}$, and as follows, $n(\tilde{r}_2)=2n(r_N)-n(\tilde{r}_1)$, $T(\tilde{r}_2)=2T(r_N)-T(\tilde{r}_1)$, and $f(\tilde{r}_2)=2f(r_N)$ $2f(r_N)-f(\tilde{r}_1)$.

[91] To solve this set of $T=(N)\times(M+1)$ nonlinear equations, the set can be linearized by expressing the equations as

$$f_i(\xi_1,\ldots,\xi_M,n)=0,$$

expanding f_i in a Taylor series expansion, and dropping the higher order terms,

$$\begin{aligned}&f_i(\xi_1+\Delta\xi_1,\ldots,\xi_M+\Delta\xi_M,\ldots,n+\Delta n)\\ &\quad=0\\ &\quad=f_i(\xi_1,\ldots,\xi_M,n)\\ &\qquad+\sum_j^M\frac{\partial f(\xi_1,\ldots,\xi_M,n)}{\partial\xi_j}\Delta\xi_j+\frac{\partial f(\xi_1,\ldots,\xi_M,n)}{\partial n}\Delta n\end{aligned}$$

This results in the formation of a Jacobian matrix

$$\mathbf{J}=\begin{bmatrix}\frac{\partial f_1}{\partial\xi_1} & \cdots & \frac{\partial f_1}{\partial\xi_M} & \frac{\partial f_1}{\partial n}\\ \vdots & & \vdots & \vdots\\ \cdot & \cdot & \cdot & \cdot\\ \frac{\partial f_T}{\partial\xi_1} & \cdots & \frac{\partial f_T}{\partial\xi_M} & \frac{\partial f_T}{\partial n}\end{bmatrix},\Delta\mathbf{x}=\begin{bmatrix}\Delta\xi_1\\ \cdot\\ \cdot\\ \cdot\\ \Delta\xi_M\\ \Delta n\end{bmatrix}$$

such that

$$\mathbf{J}\bullet\Delta\mathbf{x}=-\mathbf{f}.$$

The Jacobian can then be inverted to solve for the $\Delta\mathbf{x}=(\Delta\xi_1,\ldots,\Delta\xi_M,\Delta n)$, which is then added to the $\mathbf{x}=(\xi_1,\ldots,\xi_M,n)$ and the following equation is solved iteratively

$$\mathbf{x}^{(k+1)}=\mathbf{x}^{(k)}-\left[\mathbf{J}^{(k)}\right]^{-1}\mathbf{f}^{(k)}$$

until $\Delta\mathbf{x}=\mathbf{x}^{(k+1)}-\mathbf{x}^{(k)}$ falls below the tolerance level. The Jacobian matrix is solved by the Crout-LU decomposition method with scaled partial pivoting [*Yakowitz and Szidarovszky*, 1989], optimized for banded matrices.

[92] **Acknowledgments.** SKA acknowledges support received from NASA's Planetary Atmospheres Program, and the Cassini-Huygens GCMS and ACP projects. EHW acknowledges support received from the National Research Council Research Associateship Program. The authors thank Scott Edgington for useful discussions and Tom Cravens for pertinent electron fluxes.

References

Adachi, H., N. Basco, and D. G. L. James (1979), A quantitative study of alkyl radical reactions by kinetic spectroscopy. III. Absorption spectrum and rate constants of mutual interaction for the ethyl radical, *Int. J. Chem. Kinet.*, *11*, 995–1005.

Adachi, H., N. Basco, and D. G. L. James (1981), The acetyl radicals $CH_3CO\bullet$ and $CD_3CO\bullet$ studied by flash photolysis and kinetic spectroscopy, *Int. J. Chem. Kinet.*, *13*, 1251–1276.

Aleksandrov, E. N., V. S. Arutyunov, I. V. Dubrovina, and S. N. Kozlov (1980), Study of the reaction of atomic hydrogen with allene, *Kinet. Catal.*, *21*, 1323–1326.

Allen, C. W. (1976), *Astrophysical Quantities*, Athelone, London.

Allen, J. E., Jr., and R. N. Nelson (1998), Low-temperature vapor pressures of some light hydrocarbons, *Bull. Am. Astron. Soc.*, *30*, 1101–1102.

Anastasi, C., and P. R. Maw (1982), Reaction kinetics in acetyl chemistry over a wide range of temperature and pressure, *J. Chem. Soc. Faraday Trans.*, *Part 1*, *78*, 2423–2433.

Andrieux, D., Y. Bénilan, E. de Vanssay, P. Paillous, M. Khlifi, F. Raulin, P. Bruston, and J.-C. Guillemin (1995), Absorption coefficient of propynenitrile in the mid-UV range for the study of Titan's atmosphere: Solution to sample constraints, *J. Geophys. Res.*, *100*, 9455–9460.

Anicich, V. G., and M. J. McEwan (1997), Ion-molecule chemistry in Titan's ionosphere, *Planet. Space Sci.*, *45*, 897–921.

Arai, H., S. Nagai, and M. Hatada (1981), Radiolysis of methane containing small amount of carbon monoxide—Formation of organic acids, *Radiat. Phys. Chem.*, *17*, 211–216.

Ashfold, M. N. R., M. A. Fullstone, G. Hancock, and G. W. Ketley (1981), Singlet methylene kinetics—Direct measurements of removal rates of ã $^1A_2$ and b $^1B_1$ CH_2 and CD_2, *Chem. Phys.*, *55*, 245–257.

Atkinson, D. B., and J. W. Hudgens (1999), Rate coefficients for the propargyl radical self-reaction and oxygen addition reaction measured using ultraviolet cavity ring-down spectroscopy, *J. Phys. Chem.*, *103*, 4242–4252.

Atkinson, R., D. L. Baulch, R. A. Cox, R. F. Hampson, J. A. Kerr, M. J. Rossi, and J. Troe (1992), Evaluated kinetic and photochemical data for atmospheric chemistry: Supplement IV. IUPAC subcommittee on gas kinetic data evaluation for atmospheric chemistry, *J. Phys. Chem. Ref. Data*, *21*, 1125–1568.

Atkinson, R., D. L. Baulch, R. A. Cox, R. F. Hampson, J. A. Kerr, M. J. Rossi, and J. Troe (1997), Evaluated kinetic and photochemical data for atmospheric chemistry: Supplement VI. IUPAC subcommittee on gas kinetic data evaluation for atmospheric chemistry, *J. Phys. Chem. Ref. Data*, *26*, 1329–1499.

Atreya, S. K. (1986), *Atmospheres and Ionospheres of the Outer Planets and Their Satellites*, Springer-Verlag, New York.

Atreya, S. K., and E. H. Wilson (2001), Evolution of Titan's nitrogen atmosphere, paper presented at the Scientific Assembly of the International Association of Meteorology and Atmospheric Sciences, Innsbruck, Austria.

Atreya, S. K., T. M. Donahue, and W. R. Kuhn (1978), Evolution of a nitrogen atmosphere on Titan, *Science*, *201*, 611–613.

Atreya, S. K., S. G. Edgington, D. Gautier, and T. C. Owen (1995), Origin of the major planet atmospheres: Clues from trace species, *Earth Moon Planets*, *67*, 71–75.

Atreya, S. K., S. G. Edgington, T. Encrenaz, and H. Feuchtgruber (1999), ISO observations of C_2H_2 on Uranus and CH_3 on Saturn: Implications for atmospheric vertical mixing in the Voyager and ISO epochs, and a call for relevant laboratory measurements, *Eur. Space Agency Spec. Publ.*, *ESA-SP 427*, 149–152.

Au, J. W., G. Cooper, G. R. Burton, T. N. Olney, and C. E. Brion (1993), The valence shell photoabsorption of the linear alkanes, C_nH_{2n+2}(n = 1–8), absolute oscillator strengths (7–220 eV), *Chem. Phys.*, *173*, 209–239.

Backx, C., G. R. Wight, and M. J. Van der Wiel (1976), Oscillator strengths (10–70 eV) for absorption, ionization and dissociation in H_2, HD and D_2, obtained by an electron-ion coincidence method, *J. Phys. B.*, *9*, 315–331.

Balla, R. J., K. H. Casleton, J. S. Adams, and L. Pasternack (1991), Absolute rate constants for the reaction of CN with CH_4, C_2H_6, and C_3H_8 from 292 to 1500 K using high-temperature photochemistry and diode laser absorption, *J. Phys. Chem.*, *95*, 8694–8701.

Balucani, N., L. Cartechini, M. Alagia, P. Casavecchia, and G. G. Volpi (2000), Observation of nitrogen-bearing organic molecules from reactions of nitrogen atoms with hydrocarbons: A crossed beam study of $N(^2D)$ + ethylene, *J. Phys. Chem.*, *104*, 5655–5659.

Banaszkiewicz, M., L. M. Lara, R. Rodrigo, J. J. Lòpez-Moreno, and G. J. Molina-Cuberos (2000), A coupled model of Titan's atmosphere and ionosphere, *Icarus*, *147*, 386–404.

Bandy, R. E., C. Lakshminarayan, R. K. Frost, and T. S. Zwier (1993), The ultraviolet photochemistry of diacetylene: Direct detection of primary products of the metastable $C_4H_2^*$ + C_4H_2 reaction, *J. Chem. Phys.*, *98*, 5362–5374.

Banks, P. M., and G. Kockarts (1973), *Aeronomy*, Academic, San Diego, Calif.

Bartels, M., J. Edelbüttel-Einhaus, and K. Hoyermann (1991), The detection of CH_3CO, C_2H_5, and CH_3CHO by REMPI/mass spectrometry and the application to the study of the reactions H + CH_3CO and O + CH_3CO, *Symp. Int. Combust. Proc.*, *23*, 131–138.

Baulch, D. L., et al. (1992), Evaluated kinetic data for combustion modelling, *J. Phys. Chem. Ref. Data*, *21*, 411–734.

Baulch, D. L., et al. (1994), Evaluated kinetic data for combustion modeling supplement I, *J. Phys. Chem. Ref. Data*, *23*, 847–1033.

Becker, K. H., B. Engelhardt, P. Wiesen, and K. D. Bayes (1989), Rate constants for $CH(X^2\Pi)$ reactions at low total pressures, *Chem. Phys. Lett.*, *154*, 342–348.

Bénilan, Y., P. Bruston, F. Raulin, C. Cossart-Magos, and J.-C. Guillemin (1994), Mid-UV spectroscopy of propynenitrile at low temperature: Consequences on expected results from observations of Titan's atmosphere, *J. Geophys. Res.*, *99*, 17,069–17,074.

Bénilan, Y., P. Bruston, F. Raulin, R. Courtin, and J.-C. Guillemin (1995), Absolute absorption of C_6H_2 in the mid-UV range at low-temperature—Implications for the interpretation of Titan atmospheric spectra, *Planet. Space Sci.*, *43*, 83–89.

Bénilan, Y., D. Andrieux, M. Khlifi, P. Bruston, F. Raulin, J.-C. Guillemin, and C. Cossart-Magos (1996), Temperature dependence of HC_3N, C_6H_2, and C_4N_2 mid-UV absorption coefficients: Application to the interpretation of Titan's atmospheric spectra, *Astrophys. Space Sci.*, *236*, 85–95.

Bergmann, K., and W. Demtröder (1968), Mass-spectrometric investigation of the primary processes in the photodissociation of 1,3-butadiene, *J. Chem. Phys.*, *48*, 18–22.

Bernard, J.-M., P. Coll, A. Coustenis, and F. Raulin (2003), Experimental simulation of Titan's atmosphere: Detection of ammonia and ethylene oxide, *Planet. Space Sci.*, *51*, 1003–1011.

Bézard, B., A. Marten, and G. Paubert (1993), Detection of acetonitrile on Titan, *Bull. Am. Astron. Soc.*, *25*, 1100.

Bézard, B., E. Lellouch, D. Strobel, J.-P. Maillard, and P. Drossart (2002), Carbon monoxide on Jupiter: Evidence for both internal and external sources, *Icarus*, *159*, 95–111.

Bird, M. K., R. Dutta-Roy, S. W. Asmar, and T. A. Rebold (1997), Detection of Titan's ionosphere from Voyager 1 radio occultation observations, *Icarus*, *130*, 426–436.

Black, G., T. G. Slanger, G. A. St. John, and R. A. Young (1969), Vacuum-ultraviolet photolysis of N_2O. IV, Deactivation of $N(^2D)$, *J. Chem. Phys.*, *51*, 116–121.

Bohland, T., F. Temps, and H. G. Wagner (1985), The contribution of intersystem crossing and reaction in the removal of CH_2(ã $^1A_1$) by hydrocarbons studied with the LMR, *Ber. Bunsen-Ges. Phys. Chem.*, *89*, 1013–1018.

Bohland, T., F. Temps, and H. G. Wagner (1986), Kinetics of the reactions of $CH_2(X^3B_1)$-radicals with C_2H_2 and C_4H_2 in the temperature range 296 K ≤ T ≤ 700 K, *Symp. Int. Combust. Proc.*, *21*, 841–850.

Bosco, S. R., D. F. Nava, W. D. Brobst, and L. J. Stief (1984), Temperature and pressure dependence of the absolute rate constant for the reactions of NH_2 radicals with acetylene and ethylene, *J. Chem. Phys.*, *81*, 3505–3511.

Braun, W., A. M. Bass, and M. Pilling (1970), Flash photolysis of ketene and diazomethane: Production and reaction kinetics of triplet and single methylene, *J. Chem. Phys.*, *52*, 5131–5143.

Broadfoot, A. L., et al. (1981), Extreme ultraviolet observations from Voyager 1 encounter with Saturn, *Science*, *212*, 206–211.

Brook, E., M. F. A. Harrison, and A. C. H. Smith (1978), Measurements of the electron impact ionisation cross sections of He, C, O and N atoms, *J. Phys. B.*, *11*, 3115–3132.

Brouard, M., M. T. MacPherson, and M. J. Pilling (1989), Experimental and RRKM modeling study of the CH_3 + H and CH_3 + D reactions, *J. Phys. Chem.*, *93*, 4047–4059.

Brownsword, R. A., S. D. Gatenby, L. B. Herbert, I. W. M. Smith, D. W. A. Stewart, and A. C. Symonds (1996), Kinetics of reactions between neutral free radicals—Rate constants for the reaction of CH radicals with N atoms between 216 and 584 K, *J. Chem. Soc. Faraday Trans.*, *92*, 723–727.

Brownsword, R. A., A. Canosa, B. R. Rowe, I. R. Sims, I. W. M. Smith, D. W. A. Stewart, A. C. Symonds, and D. Travers (1997), Kinetics over a wide range of temperature (13–744 K): Rate constants for the reactions of CH($\nu = 0$) with H_2 and D_2 and for the removal of CH($\nu = 1$) by H_2 and D_2, *J. Chem. Phys.*, *106*, 7662–7677.

Bruston, P., H. Poncet, F. Raulin, C. Cossart-Magos, and R. Courtin (1989), UV spectroscopy of Titan's atmosphere, planetary organic chemistry, and prebiological synthesis, *Icarus*, *78*, 38–53.

Butterfield, M. T., T. Yu, and M. C. Lin (1993), Kinetics of CN reactions with allene, butadiene, propylene, and acrylonitrile, *Chem. Phys.*, *169*, 129–134.

Canosa, A., I. R. Sims, D. Travers, I. W. M. Smith, and B. R. Rowe (1997), Reactions of the methylidiyne radical with CH_4, C_2H_2, C_2H_4, C_2H_6, and but-1-ene studied between 23 and 295 K with a CRESU apparatus, *Astron. Astrophys.*, *323*, 644–651.

Capone, L. A., J. Dubach, S. S. Prasad, and R. C. Whitten (1983), Galactic cosmic rays and N_2 dissociation on Titan, *Icarus*, *55*, 73–82.

Carstensen, H.-H., and H. G. Wagner (1995), Investigations of the reactions of $^1CH_2(\tilde{a}\ ^1A_1, \nu = 0,1)$ with H_2O, D_2O, and HCl, *Ber. Bunsen-Ges. Phys. Chem.*, *99*, 1539–1545.

Carty, D., V. LePage, I. R. Sims, and I. W. M. Smith (2001), Low temperature rate coefficients for the reactions of CN and C_2H radicals with allene ($CH_2 = C = CH_2$) and methylacetylene ($CH_3C = CH$), *Chem. Phys. Lett.*, *344*, 310–316.

Chan, W. F., G. Cooper, and C. E. Brion (1992), Absolute optical oscillator strengths (11–20 eV) and transition moments for the photoabsorption of molecular hydrogen in the Lyman and Werner bands, *Chem. Phys.*, *168*, 375–388.

Chan, W. F., G. Cooper, R. N. S. Sodhi, and C. E. Brion (1993), Absolute optical oscillator strengths for discrete and continuum photoabsorption of molecular nitrogen (11–200 eV), *Chem. Phys.*, *170*, 81–97.

Chang, A. H. H., A. M. Mebel, X. M. Yang, S. H. Lin, and Y. T. Lee (1998), Ab initio/RRKM approach toward the understanding of ethylene photodissociation, *J. Chem. Phys.*, *109*, 2748–2761.

Chastaing, D., P. L. James, I. R. Sims, and I. W. M. Smith (1998), Neutral-neutral reactions at the temperatures of interstellar clouds: Rate coefficients for reactions of C_2H radicals with O_2, C_2H_2, C_2H_4 and C_3H_6 down to 15 K, *Faraday Discuss. Chem. Soc.*, *109*, 165–181.

Chen, F. Z., D. L. Judge, and C. Y. R. Wu (2000), Temperature dependent photoabsorption cross sections of allene and methylacetylene in the VUV-UV region, *Chem. Phys.*, *260*, 215–223.

Cherian, M. A., P. Rhodes, R. J. Simpson, and G. Dixon-Lewis (1981), Kinetic modelling of the oxidation of carbon monoxide in flames, *Symp. Int. Combust. Proc.*, *18*, 385–393.

Clarke, D. W., and J. P. Ferris (1995), Photodissociation of cyanoacetylene: Application to the atmospheric chemistry on Titan, *Icarus*, *115*, 119–125.

Clarke, D. W., and J. P. Ferris (1996), Titan haze: Mechanism of cyanoacetylene photochemistry at 185 and 254 nm, *J. Geophys. Res.*, *101*, 7575–7584.

Cody, R. J., P. N. Romani, F. L. Nesbitt, M. A. Iannone, D. C. Tardy, and L. J. Stief (2003), Rate constant for the reaction $CH_3 + CH_3 \rightarrow C_2H_6$ at T = 155 K and model calculation of the CH_3 abundance in the atmospheres of Saturn and Neptune, *J. Geophys. Res.*, *108*(E11), 5119, doi:10.1029/2002JE002037.

Collin, G. J. (1988), Photochemistry of simple olefins: Chemistry of electronic excited states or hot ground state?, *Adv. Photochem.*, *14*, 135–176.

Collin, G. J., and A. Wieckowski (1978), Photolysis of n-butene and isobutene at 174.3–174.5 nm (7.10 eV), *J. Photochem.*, *8*, 103–116.

Connors, R. E., J. L. Roebber, and K. Weiss (1974), Vacuum ultraviolet spectroscopy of cyanogen and cyanoacetylenes, *J. Chem. Phys.*, *60*, 5011–5024.

Cooper, G., G. R. Burton, and C. E. Brion (1995), Absolute UV and soft X-ray photoabsorption of acetylene by high resolution dipole (e,e) spectroscopy, *J. Electron Spectrosc.*, *73*, 139–148.

Courtin, R., D. Gautier, and C. P. McKay (1995), Titan's thermal emission spectrum—Reanalysis of the Voyager infrared measurements, *Icarus*, *114*, 144–162.

Coustenis, A., B. Bézard, and D. Gautier (1989), Titan's atmosphere from Voyager infrared observations, I. The gas composition of Titan's equatorial region, *Icarus*, *80*, 54–76.

Coustenis, A., B. Bézard, D. Gautier, and A. Marten (1991), Titan's atmosphere from Voyager infrared observations, III. Vertical distribution of hydrocarbons and nitriles near Titan's north pole, *Icarus*, *89*, 152–167.

Coustenis, A., A. Salama, E. Lellouch, T. Encrenaz, G. L. Bjoraker, R. E. Samuelson, T. de Graauw, H. Feuchtgruber, and M. F. Kessler (1998), Evidence for water vapor in Titan's atmosphere from ISO/SWS data, *Astron. Astrophys.*, *336*, L85–L89.

Coustenis, A., A. Salama, B. Schultz, S. Ott, E. Lellouch, T. Encrenaz, D. Gautier, and H. Feuchtgruber (2003), Titan's atmosphere from ISO mid-infrared spectroscopy, *Icarus*, *161*, 383–403.

De Avillez Pereira, R., D. L. Baulch, M. J. Pilling, S. H. Robertson, and G. Zeng (1997), Temperature and pressure dependence of the multichannel rate coefficients for the CH_3 + OH system, *J. Phys. Chem.*, *101*, 9681–9693.

De More, W. B., M. J. Molina, S. P. Sander, D. M. Golden, R. F. Hampson, M. J. Kurylo, C. J. Howard, and A. R. Ravishankara (1987), Chemical kinetics and photochemical data for use in stratospheric modelling, *Eval. 8, JPL Publ. 87-41*, Jet Propul. Lab., Pasadena, Calif.

Demissy, M., and R. Lesclaux (1980), Kinetics of hydrogen abstraction by NH_2 radicals from alkanes in the gas-phase—A flash-photolysis laser resonance-absorption study, *J. Am. Chem. Soc.*, *102*, 2897–2902.

Demissy, M., and R. Lesclaux (1982), Absolute rate constants for the reactions between amino and alkyl radicals at 298 K, *Int. J. Chem. Kinet.*, *102*, 1–12.

Derecskei-Kovacs, A., and S. W. North (1999), The unimolecular dissociation of vinylcyanide: A theoretical investigation of a complex multichannel reaction, *J. Chem. Phys.*, *110*, 2862–2871.

Edgington, S. G., S. K. Atreya, L. M. Trafton, J. J. Caldwell, R. F. Beebe, A. A. Simon, R. A. West, and C. Barnet (1998), On the latitude variation of ammonia, acetylene, and phosphine altitude profiles on Jupiter from HST Faint Object Spectrograph observations, *Icarus*, *133*, 192–209.

Endo, Y., S. Tsuchiya, C. Yamada, E. Hirota, and S. Koda (1986), Microwave kinetic spectroscopy of reaction intermediates: O + ethylene reaction at low pressure, *J. Chem. Phys.*, *85*, 4446–4452.

Fagerström, K., A. Lund, G. Mahmoud, J. T. Jodkowski, and E. Ratajczak (1993), Kinetics of the cross reaction between methyl and hydroxyl radicals, *Chem. Phys. Lett.*, *204*, 226–234.

Fagerström, K., J. T. Jodkowski, A. Lund, and E. Ratajczak (1995), Kinetics of the self-reaction and the reaction with OH of the amidogen radical, *Chem. Phys. Lett.*, *236*, 103–110.

Fahr, A., and A. K. Nayak (1994), Temperature dependent ultraviolet absorption cross sections of 1,3-butadiene and butadiyne, *Chem. Phys.*, *189*, 725–731.

Fahr, A., and A. Nayak (1996), Temperature dependent ultraviolet absorption cross section of propylene, methylacetylene and vinylacetylene, *Chem. Phys.*, *203*, 351–358.

Fahr, A., and A. Nayak (2000), Kinetics and products of propargyl (C_3H_3) radical self-reactions and propargyl-methyl cross-combination reactions, *Int. J. Chem. Kinet.*, *32*, 118–124.

Fahr, A., and S. E. Stein (1988), Reactions of vinyl and phenyl radicals with ethyne, ethene, and benzene, *Symp. Int. Combust. Proc.*, *22*, 1023–1029.

Fahr, A., A. Laufer, R. Klein, and W. Braun (1991), Reaction rate determinations of vinyl radical reactions with vinyl, methyl, and hydrogen atoms, *J. Phys. Chem.*, *95*, 3218–3224.

Fahr, A., P. Hassanzadeh, B. Laszlo, and R. E. Huie (1997), Ultraviolet absorption and cross sections of propargyl (C_3H_3) radicals in the 230–300 nm region, *Chem. Phys.*, *215*, 59–66.

Fahr, A., P. Hassanzadeh, and D. B. Atkinson (1998), Ultraviolet absorption spectrum and cross sections of vinyl (C_2H_3) radical in the 225–238 nm region, *Chem. Phys.*, *236*, 43–51.

Fenimore, C. P. (1969), paper presented at 12th International Symposium on Combustion, Combust. Inst., Pittsburgh, Pa.

Fennelly, J. A., and D. G. Torr (1992), Photoionization and photoabsorption cross sections of O, N_2, O_2, and N for aeronomic calculations, *At. Data Nucl. Data Tables*, *51*, 321–363.

Feuchtgruber, H., E. Lellouch, T. de Graauw, B. Bezard, T. Encrenaz, and M. Griffin (1997), External supply of oxygen to the giant planets, *Nature*, *389*, 159–162.

Fleming, G., M. M. Anderson, A. J. Harrison, and L. W. Pickett (1959), Effect of ring size on the far ultraviolet absorption and photolysis of cyclic ethers, *J. Chem. Phys.*, *30*, 351–354.

Fockenberg, C., G. E. Hall, J. M. Preses, T. J. Sears, and J. T. Muckerman (1999), Kinetics and product study of the reaction of CH_3 radicals with $O(^3P)$ atoms using time resolved time-of-flight spectrometry, *J. Phys. Chem.*, *103*, 5722–5731.

Ford, A. L., K. K. Docken, and A. Dalgarno (1975), Photoionization and dissociative photoionization of H_2, HD, and D_2, *Astrophys. J.*, *195*, 819–824.

Fox, J. L., and R. V. Yelle (1997), Hydrocarbon ions in the ionosphere of Titan, *Geophys. Res. Lett.*, *24*, 2179–2182.

Frost, R. K., G. S. Zavarin, and T. S. Zwier (1995), Ultraviolet photochemistry of diacetylene: Metastable $C_4H_2^*$ + C_2H_2 reaction in helium and nitrogen, *J. Phys. Chem.*, *95*, 9408–9415.

Frost, R. K., C. A. Arrington, C. Ramos, and T. S. Zwier (1996), Ultraviolet photochemistry of diacetylene: The metastable $C_4H_2^*$ reaction with ethene, propene, and propyne, *J. Am. Chem. Soc.*, *118*, 4451–4461.

Gaedtke, H., K. Glaenzer, H. Hippler, K. Luther, and J. Troe (1973), Addition reactions of oxygen atoms at high pressures, *Symp. Int. Combust. Proc.*, *14*, 295.

Galand, M., J. Lilenstein, D. Toublanc, and S. Maurice (1999), The ionosphere of Titan: Ideal diurnal and nocturnal cases, *Icarus*, *140*, 92–105.

Gallagher, J. W., C. E. Brion, J. A. R. Samson, and P. W. Langhoff (1988), Absolute cross sections for molecular photoabsorption, partial photoionization, and ionic photofragmentation processes, *J. Phys. Chem. Ref. Data*, *17*, 9–153.

Gan, L., C. N. Keller, and T. E. Cravens (1992), Electrons in the ionosphere of Titan, *J. Geophys. Res.*, *97*, 12,137–12,151.

Gentieu, E. P., and J. E. Mentall (1970), Formaldehyde absorption coefficients in vacuum ultraviolet (650 to 1850 angstroms), *Science*, *169*, 681–683.

Gierczak, T., J. Gawlowski, and J. Niedzielski (1988), Reactions of excited C_3H_5 radicals: Implications for the photolysis of propylene at 8.4 eV, *J. Photochem. Photobiol.*, *43*, 1–9.

Gierczak, T., R. K. Talukdar, S. C. Herndon, G. L. Vaghjiani, and A. R. Ravishankara (1997), Rate coefficients for the reactions of hydroxyl radicals with methane and deuterated methanes, *J. Phys. Chem.*, *101*, 3125–3134.

Gladstone, G. R. (1983), Radiative transfer and photochemistry in the upper atmosphere of Jupiter, Ph.D. thesis, Calif. Inst. of Technol., Pasadena.

Gladstone, G. R., M. Allen, and Y. L. Yung (1996), Hydrocarbon photochemistry in the upper atmosphere of Jupiter, *Icarus*, *119*, 1–52.

Glicker, S., and H. Okabe (1987), Photochemistry of diacetylene, *J. Phys. Chem.*, *91*, 437–440.

Glicker, S., and L. J. Stief (1971), Photolysis of formaldehyde at 1470 and 1236 Å, *J. Chem. Phys.*, *54*, 2852–2857.

Gorden, S., W. Mulac, and P. Nangia (1971), Pulse radiolysis of ammonia gas, II. Rate of disappearance of the $NH(X^2B_1)$ radical, *J. Phys. Chem.*, *78*, 2087–2093.

Gray, P., and J. C. J. Thynne (1965), Arrhenius parameters for elementary combustion reactions: H-atom abstraction from N-H bonds, *Symp. Int. Combust. Proc.*, *10*, 435.

Guadagnini, R., G. C. Schatz, and S. P. Walch (1998), Ab initio and RRKM studies of the reactions of C, CH, and $^1CH_2$ with acetylene, *J. Phys. Chem.*, *102*, 5857–5866.

Gurwell, M. A., and D. O. Muhleman (1995), CO on Titan—Evidence for a well-mixed vertical profile, *Icarus*, *117*, 375–382.

Gurwell, M. A., and D. O. Muhleman (2000), CO on Titan: More evidence for a well-mixed vertical profile, *Icarus*, *145*, 653–656.

Haddad, G. N., and J. A. R. Samson (1986), Total absorption and photoionization cross sections of water vapor between 100 and 1000 Å, *J. Chem. Phys.*, *84*, 6623–6626.

Halpern, J. B., G. E. Miller, H. Okabe, and W. Nottingham (1988), The UV photochemistry of cyanoacetylene, *J. Photochem. Photobiol. A*, *42*, 63–72.

Halpern, J. B., G. E. Miller, and H. Okabe (1989), The reaction of CN radicals with cyanoacetylene, *Chem. Phys. Lett.*, *155*, 347–350.

Ham, D. I., D. W. Trainor, and F. Kaufman (1970), Gas phase kinetics of $H + H + H_2 \rightarrow 2\ H_2$, *J. Chem. Phys.*, *53*, 4395–4396.

Hanel, R., et al. (1981), Infrared observations of the Saturnian system from Voyager 1, *Science*, *212*, 192–200.

Hanning-Lee, M. A., and M. J. Pilling (1992), Kinetics of the reaction between H atoms and allyl radicals, *Int. J. Chem. Kinet.*, *24*, 271–278.

Harich, S., J. J. Lin, Y. T. Lee, and X. Yang (1999), Photodissociation dynamics of methanol at 157 nm, *J. Phys. Chem.*, *103*, 10,324–10,332.

Hassinen, E., K. Kalliorinne, and J. Koskikallio (1990), Kinetics of reactions between methyl and acetyl radicals in gas phase produced by flash photolysis of acetic anhydride, *Int. J. Chem. Kinet.*, *22*, 741–745.

Herbert, L., I. W. M. Smith, and R. D. Spencer (1992), Rate constants for the elementary reactions between CN radicals and CH_4, C_2H_6, C_2H_4, C_3H_6, and C_2H_2 in the range $295 \leq T/K \leq 700$, *Int. J. Chem. Kinet.*, *24*, 791–802.

Hess, W. P., J. L. Durant Jr., and F. P. Tully (1989), Kinetic study of the reactions of CN with ethane and propane, *J. Phys. Chem.*, *93*, 6402–6407.

Hidayat, T., A. Marten, B. Bézard, D. Gautier, T. Owen, H. E. Matthews, and G. Paubert (1997), Millimeter and submillimeter heterodyne observations of Titan: Retrieval of the vertical profile of HCN and the $^{12}C/^{13}C$ ratio, *Icarus*, *126*, 170–182.

Hidayat, T., A. Marten, B. Bézard, D. Gautier, T. Owen, H. E. Matthews, and G. Paubert (1998), Millimeter and submillimeter heterodyne observations of Titan: The vertical profile of carbon monoxide in its stratosphere, *Icarus*, *133*, 109–133.

Ho, G. H., M. S. Lin, Y. L. Wang, and T. W. Chang (1998), Photoabsorption and photoionization of propyne, *J. Chem. Phys.*, *109*, 5868–5879.

Holland, D. M. P., D. A. Shaw, M. A. Hayes, L. G. Shpinkova, E. E. Rennie, L. Karlsson, P. Baltzer, and B. Wannberg (1997), A photoabsorption, photodissociation and photoelectron spectroscopy study of C_2H_4 and C_2D_4, *Chem. Phys.*, *219*, 91–116.

Homann, K. H., and H. Schweinfurth (1981), Kinetics and mechanism of hydrocarbon formation in the system C_2H_2/O/H, *Ber. Bunsenges. Phys. Chem.*, *85*, 569–577.

Homann, K. H., and C. Wellmann (1983), Kinetics and mechanism of hydrocarbon formation in the system C_2H_2/O/H at temperatures up to 1300 K, *Ber. Bunsenges. Phys. Chem.*, *87*, 609–616.

Hoobler, R. J., and S. R. Leone (1997), Rate coefficients for reactions of ethynyl radical (C_2H) with HCN and CH_3CN: Implications for the formation of complex nitriles on Titan, *J. Geophys. Res.*, *102*, 28,717–28,723.

Hoobler, R. J., and S. R. Leone (1999), Low temperature rate coefficients for reactions of the ethynyl radical (C_2H) with C_3H_4 isomers methylacetylene and allene, *J. Phys. Chem.*, *103*, 1342–1346.

Hoobler, R. J., B. J. Opansky, and S. R. Leone (1997), Low-temperature rate coefficients for reactions of ethynyl radical (C_2H) with propane, isobutane, n-butane, and neopentane, *J. Phys. Chem.*, *101*, 1338–1342.

Huang, L. C. L., Y. T. Lee, and R. I. Kaiser (1999), Crossed beam reaction of the cyanogen radical, $CN(X^2\Sigma^+)$, with acetylene, $C_2H_2(X^1\Sigma_g^+)$: Observation of cyanoacetylene, $HCCCN(X^1\Sigma^+)$, *J. Chem. Phys.*, *110*, 7119–7122.

Itikawa, Y., M. Hayashi, A. Ichimura, K. Onda, K. Sakimoto, K. Takayanagi, M. Nakamyura, H. Nishimura, and T. Takayanagi (1986), Cross sections for collisions of electrons and photons with nitrogen molecules, *J. Phys. Chem. Ref. Data*, *15*, 985–1010.

Jackson, W. M., D. S. Anex, R. E. Continetti, B. A. Balko, and Y. T. Lee (1991), Molecular beam studies of the photolysis of allene and the secondary photodissociation of the C_3H_x fragments, *J. Chem. Phys.*, *95*, 7327–7336.

Jenkin, M. E., T. P. Murrells, S. J. Shalliker, and G. D. Hayman (1993), Kinetics and product study of the self-reactions of allyl and allyl peroxy radicals at 296 K, *J. Chem. Soc. Faraday Trans.*, *89*, 433–446.

Jodkowski, J. T., E. Ratajczak, K. Fagerström, A. Lund, N. D. Stothard, R. Humpfer, and H.-H. Grotheer (1995), Kinetics of the cross reaction between amidogen and methyl radicals, *Chem. Phys. Lett.*, *240*, 63–71.

Johnston, G. R., D. R. A. Cuff, and D. Price (1978), Mechanisms for the photochemical production of hydrocarbons in gaseous hydrocarbon systems, *Prog. React. Kinet.*, *8*, 231–291.

Jokipii, J. R., and D. A. Kopriva (1979), Effects of particle drift on the transport of cosmic rays. III. Numerical models of galactic cosmic-ray modulation, *Astrophys. J.*, *234*, 384–392.

Kameta, K., S. Machida, M. Kitajima, M. Ukai, N. Kouchi, Y. Hatano, and K. Ito (1996), Photoabsorption, photoionization, and neutral-dissociation cross sections of C_2H_6 and C_3H_8 in the extreme-uv region, *J. Electron Spectrosc.*, *79*, 391–393.

Keller, C. N., T. E. Cravens, and L. Gan (1992), A model of the ionosphere of Titan, *J. Geophys. Res.*, *97*, 12,117–12,135.

Keller, C. N., V. G. Anicich, and T. E. Cravens (1998), Model of Titan's ionosphere with detailed hydrocarbon ion chemistry, *Planet. Space Sci.*, *46*, 1157–1174.

Kerr, J. A., and M. J. Parsonage (1972), *Evaluated Kinetic Data on Gas-Phase Addition Reactions: Reactions of Atoms and Radicals with Alkenes, Alkynes, and Aromatic Compounds*, Butterworth, London.

Kiefer, J. H., and W. A. von Drasek (1990), The mechanism of the homogeneous pyrolysis of acetylene, *Int. J. Chem. Kinet.*, *22*, 747–786.

Kloster-Jensen, E., H.-J. Haink, and H. Christen (1974), The electronic spectra of unsubstituted mono- to penta-acetylene in the gas phase and in solution in the range 1100 to 4000 Å, *Helv. Chim. Acta*, *57*, 1731–1744.

Koch, E. E., and M. Skibowski (1971), Optical absorption of gaseous methane, ethane, propane and butane and reflection of solid methane and ethane in vacuum ultraviolet, *Chem. Phys. Lett.*, *9*, 429–432.

Kreile, J., A. Schweig, and W. Thiel (1982), Experimental and theoretical investigation of the photoionization of hydrogen cyanide, *Chem. Phys. Lett.*, *87*, 473–476.

Kunde, V. G., A. C. Aikin, R. A. Hanel, D. E. Jennings, W. C. Maguire, and R. E. Samuelson (1981), C_4H_2, HC_3N and C_2H_2 in Titan's atmosphere, *Nature*, *292*, 686–688.

Langford, A. O., H. Petek, and C. B. Moore (1983), Collisional removal of $CH_2(^1A_1)$: Absolute rate constants for atomic and molecular collisional partners at 295 K, *J. Chem. Phys.*, *78*(11), 6650–6659.

Lara, L. M., E. Lellouch, J. Lopez-Moreno, and R. Rodrigo (1996), Vertical distribution of Titan's atmospheric neutral constituents, *J. Geophys. Res.*, *101*, 23,261–23,283.

Lara, L. M., E. Lellouch, and V. Shematovich (1999), Titan's atmospheric haze: The case for HCN incorporation, *Astron. Astrophys.*, *341*, 312–317.

Lara, L. M., M. Banaszkiewicz, R. Rodrigo, and J. J. López-Moreno (2002), The CH_4 density in the upper atmosphere of Titan, *Icarus*, *158*, 191–198.

Larson, C. W., P. H. Stewart, and D. M. Golden (1988), Pressure and temperature-dependence of reactions proceeding via a bound complex—An approach for combustion and atmospheric chemistry modelers—Application to $HO + CO \rightarrow [HOCO] \rightarrow H + CO_2$, *Int. J. Chem. Kinet.*, *20*, 27–40.

Laufer, A. H. (1981), Kinetics of gas phase reactions of methylene, *Rev. Chem. Intermed.*, *4*, 225–257.

Laufer, A. H., E. P. Gardner, T. L. Kwok, and Y. L. Yung (1983), Computations and estimates of rate coefficients for hydrocarbon reactions of interest in the atmospheres of the outer solar system, *Icarus*, *56*, 560–567.

Lebonnois, S., D. Toublanc, F. Hourdin, and P. Rannou (2001), Seasonal variations of Titan's atmospheric composition, *Icarus*, *152*, 384–406.

Lebonnois, S., E. L. O. Bakes, and C. P. McKay (2002), Transition from gaseous compounds to aerosols in Titan's atmosphere, *Icarus*, *159*, 505–517.

Lee, J. H., J. V. Michael, W. A. Payne, and L. J. Stief (1978), Absolute rate of reaction of atomic hydrogen with ethylene from 198 to 320 K at high pressure, *J. Chem. Phys.*, *68*, 1817–1820.

Lellouch, E., P. N. Romani, and J. Rosenqvist (1994), The vertical distribution and origin of HCN in Neptune's atmosphere, *Icarus*, *108*, 112–136.

Lewis, B. R., and J. H. Carver (1983), Temperature dependence of the carbon dioxide photoabsorption cross section between 1200 Å and 1970 Å, *J. Quant. Spec. Radiat. Trans.*, *30*, 297–309.

Lightfoot, P. D., and M. J. Pilling (1987), Temperature and pressure dependence of the rate constant for the addition of H to C_2H_4, *J. Phys. Chem.*, *91*, 3373–3379.

Lin, C. L., and F. Kaufman (1971), Reactions of metastable nitrogen atoms, *J. Chem. Phys.*, *55*, 3760–3770.

Lin, J. J., Y. T. Lee, and X. Yang (1998), Crossed molecular beam studies of the $O(^1D)$ + CH_4 reaction: Evidences for the CH_2OH + H channel, *J. Chem. Phys.*, *109*, 2975–2978.

Lindal, G. F., G. E. Wood, H. B. Hotz, D. N. Sweetnam, V. R. Eshleman, and G. L. Tyler (1983), The atmosphere of Titan: An analysis of the Voyager 1 radio occultation measurements, *Icarus*, *53*, 348–363.

Linder, D. P., X. Duan, and M. Page (1996), Thermal rate constants for R + N_2H_2 → RH + N_2H(R = H, OH, NH_2) determined from multireference configuration interaction and variational transition state theory calculations, *J. Chem. Phys.*, *104*, 6298–6306.

Livengood, T. A., T. Hewagama, T. Kostiuk, K. E. Fast, and J. J. Goldstein (2002), Improved determination of ethane (C_2H_6) abundance in Titan's stratosphere, *Icarus*, *157*, 249–253.

Maguire, W. C., R. A. Hanel, D. E. Jennings, V. G. Kunde, and R. E. Samuelson (1981), C_3H_8 and C_3H_4 in Titan's atmosphere, *Nature*, *292*, 683–686.

Marston, G., F. L. Nesbitt, D. F. Nava, W. A. Payne, and L. J. Stief (1989), Temperature dependence of the reaction of nitrogen atoms with methyl radicals, *J. Phys. Chem.*, *93*, 5769–5774.

Marten, A., T. Hidayat, Y. Biraud, and R. Moreno (2002), New millimeter heterodyne observations of Titan: Vertical distributions of HCN HC_3N, CH_3CN, and the isotopic ratio $^{15}N/^{14}N$ in its atmosphere, *Icarus*, *158*, 532–544.

Mason, E. A., and T. R. Marrero (1970), The diffusion of atoms and molecules, in *Advances in Atomic and Molecular Physics*, edited by D. R. Bates and I. Esterman, pp. 155–232, Academic, San Diego, Calif.

Massman, W. J. (1998), A review of the molecular diffusivities of H_2O, CO_2, CH_4, CO, O_3, SO_2, NH_3, N_2O, NO, and NO_2 in air, O_2, and N_2 near STP, *Atmos. Environ.*, *32*, 1111–1127.

McEwan, M. J., A. B. Denison, W. T. Huntress Jr., V. G. Anicich, J. Snodgrass, and M. T. Bowers (1989), Association reactions at low pressure. 2. The CH_3^+/CH_3CN system, *J. Phys. Chem.*, *93*, 4064–4068.

McEwan, M. J., G. B. I. Scott, N. G. Adams, L. M. Babcock, R. Terzieva, and E. Herbst (1999), New H and H_2 reactions with small hydrocarbon ions and their roles in benzene synthesis in dense interstellar clouds, *Astrophys. J.*, *513*, 287–293.

McGrath, M. A., R. Courtin, T. E. Smith, P. D. Feldman, and D. F. Strobel (1998), The ultraviolet albedo of Titan, *Icarus*, *131*, 382–392.

McKay, C. P., A. Coustenis, R. E. Samuelson, M. T. Lemmon, R. D. Lorenz, M. Cabane, P. Rannou, and P. Drossart (2001), Physical properties of the organic aerosols and clouds on Titan, *Planet. Space Sci.*, *49*, 79–99.

McNutt, R. L., Jr., and J. D. Richardson (1988), Constraints on Titan's ionosphere, *Geophys. Res. Lett.*, *15*, 709–712.

Mebel, A. M., and M. C. Lin (1999), Prediction of absolute rate constants for the reactions of NH_2 with alkanes from ab initio G2M/TST calculations, *J. Phys. Chem.*, *103*, 2088–2096.

Mebel, A. M., M. C. Lin, T. Yu, and K. Morokuma (1997), Theoretical study of potential energy surface and thermal rate constants for the C_6H_5 + H_2 and C_6H_6 + H reactions, *J. Phys. Chem.*, *101*, 3189–3196.

Miyoshi, A., H. Matsui, and N. Washida (1989), Reaction of acetaldehyde and acetyl radical with atomic and molecular oxygen, *J. Phys. Chem.*, *93*, 5813–5818.

Miyoshi, A., K. Ohmori, K. Tsuchiya, and H. Matsui (1993), Reaction rates of atomic oxygen with straight chain alkanes and fluoromethanes at high temperatures, *Chem. Phys. Lett.*, *204*, 241–247.

Molina-Cuberos, G. J., J. J. López-Moreno, R. Rodrigo, L. M. Lara, and K. O'Brien (1999), Ionization by cosmic rays of the atmosphere of Titan, *Planet. Space Sci.*, *47*, 1347–1354.

Molina-Cuberos, G. J., K. Schwingenschuh, J. J. López-Moreno, R. Rodrigo, L. M. Lara, and V. Anicich (2002), Nitriles produced by ion chemistry in the lower ionosphere of Titan, *J. Geophys. Res.*, *107*(E11), 5099, doi:10.1029/2000JE001480.

Monks, P. S., P. N. Romani, F. L. Nesbitt, M. Scanlon, and L. J. Stief (1993), The kinetics of the formation of nitrile compounds in the atmospheres of Titan and Neptune, *J. Geophys. Res.*, *98*, 17,115–17,122.

Monks, P. S., F. L. Nesbitt, W. A. Payne, M. Scanlon, L. J. Stief, and D. E. Shallcross (1995), Absolute rate constants and product branching ratios for the reaction between H and C_2H_3 at T = 213 and 298 K, *J. Phys. Chem.*, *99*, 17,151–17,159.

Moortgat, G. K., W. Seiler, and P. Warneck (1983), Photodissociation of HCHO in air—CO and H_2 quantum yields at 220 K and 300 K, *J. Chem. Phys.*, *78*, 1185–1190.

Mordaunt, D. H., I. R. Lambert, G. P. Morley, N. R. Ashfold, R. N. Dixon, C. M. Western, L. Schnieder, and K. H. Welge (1993), Primary product channels in the photodissociation of methane at 121.6 nm, *J. Chem. Phys.*, *98*, 2054–2065.

Mordaunt, D. H., M. N. R. Ashfold, and R. N. Dixon (1994), Dissociation dynamics of $H_2O(D_2O)$ following photoexcitation at the Lyman-α wavelength (121.6 nm), *J. Chem. Phys.*, *100*, 7360–7375.

Moses, J. I., M. Allen, and Y. L. Yung (1992), Hydrocarbon nucleation and aerosol formation in Neptune's atmosphere, *Icarus*, *99*, 318–346.

Mount, G. H., and H. W. Moos (1978), Photoabsorption cross sections of methane and ethane 1380–1600 Å, at T = 295 K and T = 200 K, *Astrophys. J.*, *224*, L35–L38.

Mount, G. H., E. S. Warden, and H. W. Moos (1977), Photoabsorption cross sections of methane from 1400 to 1850 Å, *Astrophys. J.*, *214*, L47–L49.

Muhleman, D. O., G. L. Berge, and R. T. Clancy (1984), Microwave measurements of carbon monoxide on Titan, *Science*, *223*, 393–396.

Nakata, R. S., K. Watanabe, and F. M. Matsunaga (1965), Absorption and photoionization coefficients of CO_2 in the region 580–1670 Å, *Sci. Light*, *14*, 54–71.

Nava, D. F., M. B. Mitchell, and L. J. Stief (1986), The reaction H + C_4H_2: Absolute rate constant measurement and implication for atmospheric modeling of Titan, *J. Geophys. Res.*, *91*, 4585–4589.

Nesbitt, F. L., G. Marston, and L. J. Stief (1990), Kinetic studies of the reactions of H_2CN and D_2CN radicals with N and H, *J. Phys. Chem.*, *94*, 4946–4951.

Neubauer, F. M., D. A. Gurnett, J. D. Scudder, and R. E. Hartle (1984), Titan's magnetospheric interaction, in *Saturn*, edited by T. Gehrels, and M. S. Matthews, pp. 760–787, Univ. of Ariz. Press, Tucson.

Niedzielski, J. P., W. Makulski, and J. Gawlowski (1978), Gas phase photolysis of 1-butene at 147 nm (8.4 eV), *J. Photochem.*, *9*, 519–528.

Niedzielski, J. P., P. Geblewicz, and J. Gawlowski (1979), Gas phase photolysis of 1-butene at 123.7 nm (10.0 eV), *J. Photochem.*, *10*, 287–295.

Noll, K. S., T. R. Geballe, R. F. Knacke, and Y. J. Pendleton (1996), Titan's 5 μm spectral window: Carbon monoxide and the albedo of the surface, *Icarus*, *124*, 625–631.

Nuth, J. A., and S. Glicker (1982), The vacuum ultraviolet spectra of HCN, C_2N_2, and CH_3CN, *J. Quant. Spectrosc. Radiat. Transfer*, *28*, 223–231.

Obi, K., H. Akimoto, Y. Ogata, and I. Tanaka (1971), Photolyses of propane, n-butane, and cyclobutane at Xe and Kr resonance lines, *J. Chem. Phys.*, *55*, 3822–3828.

Ogawa, M. (1971), Absorption cross sections of O_2 and CO_2 continua in the Schumann and far-UV regions, *J. Chem. Phys.*, *54*, 2550–2556.

Ohmori, K., A. Miyoshi, H. Matsui, and N. Washida (1990), Studies on the reaction of acetaldehyde and acetyl radicals with atomic hydrogen, *J. Phys. Chem.*, *94*, 3253–3255.

Okabe, H. (1978), *Photochemistry of Small Molecules*, Wiley-Intersci., New York.

Okabe, H. (1981), Photochemistry of acetylene at 1470 Å, *J. Chem. Phys.*, *75*, 2772–2778.

Okabe, H. (1983), Photochemistry of acetylene at 1849 Å, *J. Chem. Phys.*, *78*, 1312–1317.

Okabe, H., and D. A. Becker (1963), Vacuum ultraviolet photochemistry. VII. Photolysis of n-butane, *J. Chem. Phys.*, *39*, 2549–2555.

Opansky, B. J., and S. R. Leone (1996a), Low-temperature rate coefficients of C_2H with CH_4 and CD_4 from 154 to 359 K, *J. Phys. Chem.*, *100*, 4888–4892.

Opansky, B. J., and S. R. Leone (1996b), Rate coefficients of C_2H with C_2H_4, C_2H_6, and H2 from 150 to 359 K, *J. Phys. Chem.*, *100*, 19,904–19,910.

Orient, O. J., and S. K. Srivastava (1987), Electron impact ionisation of H_2O, CO, CO_2, and CH_4, *J. Phys. B.*, *20*, 3923–3936.

Palenius, H. P., J. L. Kohl, and W. H. Parkinson (1976), Absolute measurement of photoionization cross section of atomic hydrogen with a shock tube for extreme ultraviolet, *Phys. Rev. A*, *13*, 1805–1816.

Pantos, E., J. Philis, and A. Bolovinos (1978), The extinction coefficient of benzene vapor in the region 4.6 to 36 eV, *J. Mol. Spectrosc.*, *72*, 36–43.

Park, J., S. Burova, A. S. Rodgers, and M. C. Lin (1999), Experimental and theoretical studies of the C_6H_5 + C_6H_6 reaction, *J. Phys. Chem.*, *103*, 9036–9041.

Parkes, D. A., D. M. Paul, C. P. Quinn, and R. C. Robson (1973), The ultraviolet absorption by alkylperoxy radicals and their mutual reactions, *Chem. Phys. Lett.*, *23*, 425–429.

Payne, W. A., P. S. Monks, F. L. Nesbitt, and L. J. Stief (1996), The reaction between N(^{4}S) and C_2H_3: Rate constant and primary reaction channels, *J. Chem. Phys.*, *104*, 9808–9815.

Petrie, S., C. G. Freeman, and M. J. McEwan (1992), The ion-molecule chemistry of acrylonitrile: Astrochemical implications, *Mon. Not. R. Astron. Soc.*, *257*, 438–444.

Phillips, L. J. (1978), Reaction of H with C_2N_2 at pressures near 1-torr, *Int. J. Chem. Kinet.*, *10*, 899–904.

Piper, L. G., M. E. Donahue, and W. T. Rawlins (1987), Rate coefficients for N(^{2}D) reactions, *J. Phys. Chem.*, *97*, 3883–3888.

Pitts, W. M., L. Pasternack, and J. R. McDonald (1982), Temperature dependence of the C_2($X\ ^1\Sigma_g^+$ and $a\ ^3\Pi_u$ equlibrated states) with O_2, *Chem. Phys.*, *68*, 417–422.

Pratt, G. L., and S. W. Wood (1984), Kinetics of the reaction of methyl radicals with oxygen, *J. Chem. Soc. Faraday Trans. 1*, *80*, 3419–3427.

Rabalais, J. W., J. M. McDonald, V. Scherr, and S. P. McGlynn (1971), Electronic spectroscopy of isoelectronic molecules, *Chem. Rev.*, *71*, 94–95.

Rages, K., and J. B. Pollack (1983), Vertical distribution of scattering hazes in Titan's upper atmosphere, *Icarus*, *55*, 50–62.

Rannou, P., M. Cabane, E. Chassefiere, R. Botet, C. P. McKay, and R. Courtin (1995), Titan's geometric albedo: Role of the fractal structure of the aerosols, *Icarus*, *118*, 355–372.

Rao, M. V. V. S., I. Iga, and S. K. Srivastava (1995), Ionization cross-sections for the production of positive ions from H_2O by electron impact, *J. Geophys. Res.*, *100*, 26,421–26,425.

Reid, R. C., J. M. Prausnitz, and B. E. Poling (1987), *The Properties of Gases and Liquids*, McGraw-Hill, New York.

Rennie, E. E., C. A. F. Johnson, J. E. Parker, D. M. P. Holland, D. A. Shaw, and M. A. Hayes (1998), A photoabsorption, photodissociation and photoelectron spectroscopy study of C_6H_6 and C_6D_6, *Chem. Phys.*, *229*, 107–123.

Richards, P. G., J. A. Fennelly, and D. G. Torr (1994), EUVAC: A solar EUV flux model for aeronomic calculations, *J. Geophys. Res.*, *99*, 8981–8992.

Richter, H., and J. B. Howard (2000), Formation of polycyclic aromatic hydrocarbons and their growth to soot—A review of chemical reaction pathways, *Prog. Energy Combust. Sci.*, *26*, 565–608.

Roe, H. G., T. K. Greathouse, M. J. Richter, and J. H. Lacy (2003), Propane (C_3H_8) on Titan, *Astrophys. J. Lett.*, *597*, L65–L68.

Romani, P. N. (1996), Recent rate constant and product measurements of the reactions C_2H_3 + H_2 and C_2H_3 + H—Importance for the photochemical modeling of hydrocarbons on Jupiter, *Icarus*, *122*, 233–241.

Sagan, C., and W. R. Thompson (1984), Production and condensation of organic gases in the atmosphere of Titan, *Icarus*, *59*, 133–161.

Samson, J. A. R., and G. N. Haddad (1994), Total photoabsorption cross sections of H_2 from 18 to 113 eV, *J. Opt. Soc. Am. B Opt. Phys.*, *11*, 277–279.

Samson, J. A. R., F. F. Marmo, and K. Watanabe (1962), Absorption and photoionization coefficients of propylene and butene-1 in the vacuum ultraviolet, *J. Chem. Phys.*, *36*, 783–786.

Samson, J. A. R., G. N. Haddad, T. Masuoka, P. N. Pareek, and D. A. L. Kilcoyne (1989), Ionization yields, total absorption, and dissociative photoionization cross sections of CH_4 from 110–950 Å, *J. Chem. Phys.*, *90*, 6925–6932.

Samuelson, R. E., W. C. Maguire, R. A. Hanel, V. G. Kunde, D. E. Jennings, Y. L. Yung, and A. C. Aikin (1983), CO_2 on Titan, *J. Geophys. Res.*, *88*, 8709–8715.

Samuelson, R., R. A. Nath, and A. Borysow (1997), Gaseous abundances and methane supersaturation in Titan's troposphere, *Planet. Space Sci.*, *45*, 959–980.

Sandilands, J. W., and J. C. McConnell (1997), Evaluation of a reduced Jacobian chemical solver, *J. Geophys. Res.*, *102*, 19,073–19,087.

Sato, K., K. Misawa, Y. Kobayashi, M. Matsui, S. Tsunashima, Y. Kurosaki, and T. Takayanagi (1999), Measurements of thermal rate constants for the reactions of N(^{2}D, ^{2}P) with C_2H_4 and C_2D_4 between 225 and 292 K, *J. Phys. Chem.*, *103*, 8650–8656.

Satyapal, S., J. Park, R. Bersohn, and B. Katz (1989), Dissociation of methanol and ethanol activated by a chemical reaction or by light, *J. Chem. Phys.*, *91*, 6873–6879.

Schmitt, R. G., and R. K. Brehm (1966), Double beam spectrophotometry in the far ultraviolet. 1: 1150 Å to 3600 Å, *Appl. Opt.*, *5*, 1111–1116.

Schwanebeck, W., and J. Warnatz (1975), Reactions of butadiene. I. Reaction with hydrogen atoms, *Ber. Bunsen-Ges. Phys. Chem.*, *79*, 530–535.

Scott, G. B. I., D. A. Fairley, C. G. Freeman, M. J. McEwan, and V. G. Anicich (1998), Gas-phase reactions of some positive ions with atomic and molecular nitrogen, *J. Chem. Phys.*, *109*, 9010–9014.

Seki, K., and H. Okabe (1993), Photochemistry of acetylene at 193.3 nm, *J. Phys. Chem.*, *97*, 5284–5290.

Seki, K., M. Yagi, M. Q. He, J. B. Halpern, and H. Okabe (1996), Reaction rates of the CN radical with diacetylene and dicyanoacetylene, *Chem. Phys. Lett.*, *258*, 657–662.

Shah, M. B., D. S. Elliott, and H. B. Gilbody (1987), Pulsed crossed-beam study of the ionisation of atomic hydrogen, *J. Phys. B*, *20*, 3501–3514.

Shaw, D. A., D. M. P. Holland, M. A. MacDonald, A. Hopkirk, M. A. Hayes, and S. M. McSweeney (1992), A study of the absolute photoabsorption cross section and the photoionization quantum efficiency of nitrogen from the ionization threshold to 485 Å, *Chem. Phys.*, *166*, 379–391.

Sillesen, A., E. Ratajczak, and P. Pagsberg (1993), Kinetics of the reaction H + C_2H_4 → C_2H_5, H + C_2H_5 → $2CH_3$, CH_3 + C_2H_5→products studied by pulse radiolysis combined with infrared diode lase spectroscopy, *Chem. Phys. Lett.*, *201*, 171–177.

Simonaitis, R., and J. Heicklen (1972), Kinetics and mechanism of the reaction of O(^{3}P) with carbon monoxide, *J. Chem. Phys.*, *56*, 2004–2011.

Sims, I. R., J.-L. Queffelec, D. Travers, B. R. Rowe, L. B. Herbert, J. Karthäuser, and I. W. M. Smith (1993), Rate constants for the reactions of CN with hydrocarbons at low and ultra-low temperatures, *Chem. Phys. Lett.*, *211*, 461–468.

Slagle, I. R., D. Gutman, J. W. Davies, and M. Pilling (1988), Study of the recombination reaction CH_3 + CH_3 → C_2H_6. I. Experiment, *J. Phys. Chem.*, *92*, 2455–2462.

Slagle, I. R., J. R. Bernhardt, D. Gutman, M. A. Hanning-Lee, and M. J. Pilling (1990), Kinetics of the reaction between oxygen atoms and allyl radicals, *J. Phys. Chem.*, *94*, 3652–3656.

Smith, G. R., D. F. Strobel, A. L. Broadfoot, B. R. Sandel, D. E. Shemansky, and J. B. Holdberg (1982), Titan's upper atmosphere: Composition and temperature from the EUV solar occultation results, *J. Geophys. Res.*, *87*, 1351–1359.

Smith, N. S., and F. Raulin (1999), Modeling of methane photolysis in the reducing atmospheres of the outer solar system, *J. Geophys. Res.*, *104*, 1873–1876.

Smith, N. S., Y. Bénilan, and P. Bruston (1998), The temperature dependent absorption cross sections of C_4H_2 at mid ultraviolet wavelengths, *Planet. Space Sci.*, *46*, 1215–1220.

Steiner, G., and S. J. Bauer (1990), Molecular and eddy diffusion in the atmosphere of Titan, *Ann. Geophys.*, *8*, 473–476.

Stief, L. J., and W. A. Payne (1976), Absolute rate parameter for the reaction of hydrogen with hydrazine, *J. Chem. Phys.*, *64*, 4892–4897.

Stief, L. J., W. A. Payne, and R. B. Klemm (1975), A flash photolysis-resonance fluorescence study of the formation of O(^{1}D) in the photolysis of water and the reaction of O(^{1}D) with H_2, Ar, and He, *J. Chem. Phys.*, *62*, 4000–4008.

Stief, L. J., F. L. Nesbitt, W. A. Payne, S. C. Kuo, W. Tao, and R. B. Klemm (1995), Rate constant and reaction channels for the reaction of atomic nitrogen with the ethyl radical, *J. Chem. Phys.*, *102*, 5309–5316.

Stothard, N., R. Humpfer, and H.-H. Grotheer (1995), The multichannel reaction NH_2 + NH_2 at ambient temperature and low pressures, *Chem. Phys. Lett.*, *240*, 474–480.

Strobel, D. F., M. E. Summers, and X. Zhu (1992), Titan's upper atmosphere: Structure and ultraviolet emissions, *Icarus*, *100*, 512–526.

Sun, Q., D. L. Yang, N. S. Wang, J. M. Bowman, and M. C. Lin (1990), Experimental and reduced dimensionality quantum rate coefficients for H_2(D_2) + CN → H(D)CN + H(D), *J. Chem. Phys.*, *93*, 4730–4739.

Sun, W., K. Yokoyama, J. C. Robinson, A. G. Suits, and D. M. Neumark (1999), Discrimination of products isomers in the photodissociation of propyne and allene at 193 nm, *J. Chem. Phys.*, *110*, 4363–4368.

Suto, M., and L. C. Lee (1985), Photoabsorption cross section of CH_3CN: Photodissociation rates by solar flux and interstellar radiation, *J. Geophys. Res.*, *90*, 13,037–13,040.

Suto, M., X. Wang, and L. C. Lee (1985), Fluorescence from VUV excitation of formaldehyde, *J. Chem. Phys.*, *85*, 4228–4233.

Suzuki, T., Y. Shihira, T. Sato, H. Umemoto, and S. Tsunashima (1993), Reactions of N(2 ^{2}D) and N(2 ^{2}P) with H_2 and D_2, *J. Chem. Soc. Faraday Trans.*, *89*, 995–999.

Takayanagi, T., Y. Kurosaki, K. Misawa, M. Sugiura, Y. Kobayashi, K. Sato, and S. Tsunashima (1998), Measurements of thermal rate constants and theoretical calculations for the $N^{2d,\ 2p}$ + C_2H_2 and C_2D_2 reactions, *J. Phys. Chem.*, *102*, 6251–6258.

Takayanagi, T., Y. Kurosaki, K. Sato, K. Misawa, Y. Kobayashi, and S. Tsunashima (1999), Kinetic studies on the N(^{2}D, ^{2}P) + CH_4 and CD_4 reactions: The role of nonadiabatic transitions on thermal rate constants, *J. Phys. Chem.*, *103*, 250–255.

Tanguy, L., B. Bézard, A. Marten, D. Gautier, E. Gérard, G. Paubert, and A. Lecacheux (1990), Stratospheric profile of HCN on Titan from millimeter observations, *Icarus*, *85*, 43–57.

Teng, L., and W. E. Jones (1972), Kinetics of the reactions of hydrogen atoms with ethylene and vinyl fluoride, *J. Chem. Soc. Faraday Trans. 1*, *68*, 1267–1277.

Thompson, B. A., P. Hartreck, and R. R. Reeves Jr. (1963), Ultraviolet absorption coefficients of CO_2, CO, O_2, H_2O, N_2O, NH_3, NO, SO_2, and CH_4, between 850 and 4000 Å, *J. Geophys. Res.*, *68*, 6431–6436.

Tian, C., and C. R. Vidal (1998a), Cross sections of electron impact ionization of ethylene, *Chem. Phys. Lett.*, *288*, 499–503.

Tian, C., and C. R. Vidal (1998b), Electron impact dissociative ionization of ethane: Cross sections, appearance potentials, and dissociative pathways, *J. Chem. Phys.*, *109*, 1704–1712.

Toublanc, D., J. P. Parisot, J. Brillet, D. Gautier, F. Raulin, and C. P. McKay (1995), Photochemical modeling of Titan's atmosphere, *Icarus*, *113*, 2–26.

Tsang, W. (1987), Chemical kinetic data base for combustion chemistry. 3. Methanol, *J. Phys. Chem. Ref. Data*, *16*, 471–508.

Tsang, W. (1988), Chemical kinetic data base for combustion chemistry. III. Propane, *J. Phys. Chem. Ref. Data*, *17*, 887–951.

Tsang, W. (1991), Chemical kinetic data base for combustion chemistry. V. Propene, *J. Phys. Chem. Ref. Data*, *20*, 221–274.

Tsang, W., and R. F. Hampson (1986), Chemical kinetic data base for combustion chemistry. Part 1. Methane and related compounds, *J. Phys. Chem. Ref. Data*, *15*, 1087–1279.

Umemoto, H., T. Nakae, H. Hashimoto, and K. Kongo (1998), Reactions of N(2 ^{2}D) with methane and deuterated methanes, *J. Chem. Phys.*, *109*, 5844–5848.

Upadhyaya, H. P., P. D. Naik, U. B. Pavanaja, A. Kumar, R. K. Vatsa, A. V. Sapre, and J. P. Mittal (1997), Reaction kinetics of O^{3p} with acrylonitrile and crotonitrile, *Chem. Phys. Lett.*, *274*, 383–389.

Vervack, R. J. (1997), Titan's upper atmosphere structure derived from Voyager ultraviolet spectrometer observations, Ph.D. thesis, Univ. of Ariz., Tuscon.

Veyret, B., P. Roussel, and R. Lesclaux (1984), Absolute rate constant for the disproportionation reaction of formyl radicals from 295 K to 475 K, *Chem. Phys. Lett.*, *103*, 389–392.

Wagner, H. G., and R. Zellner (1972), Reactions of hydrogen atoms with unsaturated C_3 hydrocarbons. II. Reaction of H atoms with methylacetylene, *Ber. Bunsen-Ges. Phys. Chem.*, *76*, 518–525.

Wakeham, W. A., and D. H. Slater (1973), Diffusion coefficients for n-alkanes in binary gaseous mixtures with nitrogen, *J. Phys. B. At. Mol. Phys.*, *6*, 886–896.

Wang, H., and M. Frenklach (1994), Calculations of rate coefficients for the chemically activated reactions of acetylene with vinylic and aromatic radicals, *J. Phys. Chem.*, *98*, 1465–1489.

Wang, H., and M. Frenklach (1997), A detailed kinetic modeling study of aromatics formation in laminar premixed acetylene and ethylene flames, *Combust. Flame*, *110*, 173–221.

Warnatz, J. (1984), Rate coefficients in the C/H/O system, in *Combustion Chemistry*, edited by W. C. Gardiner Jr., pp. 197–360, Springer-Verlag, New York.

Washburn, E. W. (1924), The vapor pressure of ice and of water below the freezing point, *Mon. Weather*, 488–490.

Watanabe, K., and A. S. Jursa (1964), Absorption and photoionization cross sections of H_2O and H_2S, *J. Chem. Phys.*, *41*, 1650–1653.

Watanabe, K., M. Zelikoff, and E. C. Y. Inn (1953), Absorption coefficients of several atmospheric gases, *Air Force Cambridge Res. Cent. Tech. Rep. 53-23*, Boston, Mass.

Watkins, K. W., and W. W. Word (1974), Addition of methyl radicals to carbon monoxide: Chemically and thermally activated decomposition of acetyl radicals, *Int. J. Chem. Kinet.*, *6*, 855–873.

Weast, R. C., M. J. Astle, and W. H. Beyer (1987), *Handbook of Chemistry and Physics*, 67th ed., CRC Press, Boca Raton, Fla.

Weissman, M. A., and S. W. Benson (1988), Rate parameters for the reactions of C_2H_3 and C_4H_5 with H_2 and C_2H_2, *J. Phys. Chem.*, *92*, 4080–4084.

Wendt, H. R., H. Hippler, and H. E. Hunziker (1979), Triplet acetylene: Near infrared electronic absorption spectrum of the cis isomer, and formation from methylene, *J. Chem. Phys.*, *70*, 4044–4048.

Westmoreland, P. R., A. M. Dean, J. B. Howard, and J. P. Longwell (1989), Forming benzene in flames by chemically activated isomerization, *J. Phys. Chem.*, *93*, 8171–8180.

Whytock, D. A., W. A. Payne, and L. J. Stief (1976), Rate of reaction of atomic hydrogen with propyne over an extended pressure and temperature range, *J. Chem. Phys.*, *65*, 191–195.

Wight, G. R., M. J. Van der Wiel, and C. E. Brion (1976), Dipole excitation, ionization and fragmentation of N_2 and CO in the 10–60 eV region, *J. Phys. B*, *9*, 675–689.

Wilke, C. R. (1950), Diffusional properties of multicomponent gases, *Chem. Eng. Prog.*, *46*, 95–104.

Wilson, E. H., and S. K. Atreya (2000a), On the significance of atmospheric parameters on the abundances of hydrocarbons in the atmosphere of Titan, *Geophys. Res. Abstr.*, *74*, 255.

Wilson, E. H., and S. K. Atreya (2000b), Sensitivity studies of methane photolysis and its impact on hydrocarbon chemistry in the atmosphere of Titan, *J. Geophys. Res.*, *105*, 20,263–20,273.

Wilson, E. H., and S. K. Atreya (2003), Chemical sources of haze formation in Titan's atmosphere, *Planet. Space Sci.*, *51*, 1017–1033.

Wilson, E. H., S. K. Atreya, and A. Coustenis (2003), Mechanisms for the formation of benzene in the atmosphere of Titan, *J. Geophys. Res.*, *108*(E2), 5014, doi:10.1029/2002JE001896.

Wodtke, A. M., and Y. T. Lee (1987), High-resolution photofragmentation—Translational spectroscopy, in *Advances in Gas-Phase Photochemistry and Kinetics*, edited by M. N. R. Ashfold and J. E. Baggott, pp. 31–59, R. Soc. of Chem., London.

Wong, A.-S., C. G. Morgan, Y. L. Yung, and T. Owen (2002), Evolution of CO on Titan, *Icarus*, *155*, 382–392.

Woods, T. N., et al. (1996), Validation of the UARS solar ultraviolet irradiances: Comparison with the ATLAS 1 and 2 measurements, *J. Geophys. Res.*, *101*, 9541–9569.

Wu, C. Y. R., and D. L. Judge (1985), Photoabsorption cross section of acetylene in the EUV region, *J. Chem. Phys.*, *82*, 4495–4499.

Wu, C. Y. R., F. Z. Chen, and D. L. Judge (2001), Measurements of temperature-dependent absorption cross sections of C_2H_2 in the VUV-UV region, *J. Geophys. Res.*, *106*, 7629–7636.

Yakowitz, S., and F. Szidarovszky (1989), *An Introduction to Numerical Computations*, Macmillan, Old Tappan, N. J.

Yang, D. L., T. Yu, M. C. Lin, and C. F. Melius (1992a), CN radical reactions with hydrogen cyanide and cyanogen: Comparison of theory and experiment, *J. Chem. Phys.*, *97*, 222–226.

Yang, D. L., T. Yu, N. S. Wang, and M. C. Lin (1992b), Temperature dependence of cyanogen radical reactions with selected alkanes: CN reactivities towards primary, secondary and tertiary C-H bonds, *Chem. Phys.*, *160*, 307–315.

Yelle, R. V., D. F. Strobel, E. Lellouch, and D. Gautier (1997), Engineering models for Titan's atmosphere, *Eur. Space Agency Spec. Publ., ESA-SP*, *1177*, 243–256.

Yokoyama, A., X. Zhao, E. J. Hintsa, R. E. Continetti, and Y. T. Lee (1990), Molecular beam studies of the photodissociation of benzene at 193 and 248 nm, *J. Chem. Phys.*, *92*, 4222–4233.

Yu, Y. X., S. M. Li, Z. F. Xu, Z. S. Li, and C. C. Sun (1998), An ab initio study on the reaction $NH_2 + CH_4 \rightarrow NH_3 + CH_3$, *Chem. Phys. Lett.*, *296*, 131–136.

Yung, Y. L. (1987), An update of nitrile photochemistry, *Icarus*, *72*, 468–472.

Yung, Y. L., M. Allen, and J. P. Pinto (1984), Photochemistry of the atmosphere of Titan: Comparison between model and observations, *Astrophys. J. Suppl.*, *55*, 465–506.

Zabarnick, S., and M. C. Lin (1989), Kinetics of CN($X^2\Sigma^+$) radical reactions with HCN, BrCN, and CH_3CN, *Chem. Phys.*, *134*, 185–191.

Zabarnick, S., J. W. Fleming, and M. C. Lin (1986), Kinetic study of the reaction CH($X^2\Pi$) + $H_2 \leftrightarrow CH_2(X^3B_1)$ + H in the temperature range 372 to 675 K, *J. Chem. Phys.*, *85*, 4373–4376.

Zabarnick, S., J. W. Fleming, and M. C. Lin (1989), Kinetics of methylidyne (CH $X^2\Pi$) radical reactions with ammonia and methylamines, *Chem. Phys.*, *132*, 407–411.

Zelikoff, M., and K. Watanabe (1953), Absorption coefficients of ethylene in the vacuum ultraviolet, *J. Opt. Soc. Am.*, *43*, 756–759.

Zheng, S.-H., and S. K. Srivastava (1996), Electron impact ionization and dissociative ionization of acetylene, *J. Phys. B*, *29*, 3235–3244.

Zipf, E. C., and R. W. McLaughlin (1978), On the dissociation of nitrogen by electron impact and by EUV photo-absorption, *Planet. Space Sci.*, *26*, 449–462.

Zipf, E. C., P. S. Espy, and C. F. Boyle (1980), The excitation and collisional deactivation of metastable N(^{2}P) atoms in auroras, *J. Geophys. Res.*, *85*, 687–696.

Zwier, T. S., and M. Allen (1996), Metastable diacetylene reactions as routes to large hydrocarbons in Titan's atmosphere, *Icarus*, *123*, 578–583.

S. K. Atreya, Department of Atmospheric, Oceanic, and Space Sciences, University of Michigan at Ann Arbor, 2455 Hayward Street, Ann Arbor, MI 48109-2143, USA.

E. H. Wilson, NASA/Jet Propulsion Laboratory, 4800 Oak Grove Drive, M/S 169-237, Pasadena, CA 91109-8099, USA. (eric.wilson@jpl.nasa.gov)